MECHANICAL CHARACTERIZATION OF HYBRID AND FUNCTIONALLY-GRADED ALUMINUM OPEN-CELL FOAMS WITH NANOCRYSTALLINE-COPPER COATINGS

By

Yi Sun

A DISSERTATION

Submitted to
Michigan State University
in partial fulfillment of the requirements
for the degree of

Civil Engineering—Doctor of Philosophy

2015

ABSTRACT

MECHANICAL CHARACTERIZATION OF HYBRID AND FUNCTIONALLY-GRADED ALUMINUM OPEN-CELL FOAMS WITH NANOCRYSTALLINE-COPPER COATINGS

By

Yi Sun

Cellular/foam materials found in nature such as bone, wood, and bamboo are usually functionally graded by having a non-uniform density distribution and inhomogenous composition that optimizes their global mechanical performance. Inspired by such naturally engineered products, the current study was conducted towards the development of functionally graded hybrid metal foams (FGHMF) with electrodeposited (ED) nanocrystalline coatings. First, the deformation and failure mechanisms of aluminum/copper (Al/Cu) hybrid foams were investigated using finite element analyses at different scales. The micro-scale behavior was studied based on single ligament models discretized using continuum elements and the macro-scale behavior was investigated using beam-element based finite element models of representative unit volumes consisting of multiple foam cells. With a detailed constitutive material behavior and material failure considered for both the aluminum ligament and the nano-copper coating, the numerical models were able to capture the unique behavior of Al/Cu hybrid foams, such as the typically observed sudden load drop after yielding. The numerical models indicate that such load drop is caused by the fracture of foam ligaments initiated from the rupture of the ED nano-copper coating due to its low ductility. This failure mode jeopardizes the global energy absorption capacity of hybrid foams, especially when a thick coating is applied. With the purpose of enhancing the performance of Al/Cu hybrid foams, an annealing process, which increased the ductility of the nanocrystalline copper coating by causing recovery,

recrystallination and grain growth, was introduced in the manufacturing of Al/Cu hybrid foams. Quasi-static experimental results indicate that when a proper amount of annealing is applied, the ductility of the ED copper can be effectively improved and the compressive and tensile behavior of Al/Cu hybrid foams can be significantly enhanced, including better energy absorption capacity. The behavior of Al/Cu hybrid foams under high-strain-rate condition was then investigated using experiments on a split Hopkinson pressure bar. It was found that the ED nano-copper coating can also effectively enhance the energy absorption capacities of aluminum open-cell foams under high strain rate. Similar to the quasi-static behavior, a large stress drop was observed in the compressive response of Al/Cu hybrid foams under high strain rate, which was accompanied by dramatic shattering of material. It is shown that a more ductile behavior and better energy absorption performance under high strain rate condition can be also obtained by introducing an annealing process. Finally, the manufacturing process of Al/Cu hybrid foams was customized to fabricate FGHMF systems with two dimensional property gradients. The performance of these FGHMFs at both quasi-static and dynamic conditions was evaluated. Under quasi-static condition, two flexural type loading conditions were considered, namely, a three point bending condition and a cantilever beam condition. The dynamic behavior of FGHMFs was investigated by conducting drop weight tower tests on a three point bending setup. It was found that the failure mechanism of hybrid metal foams can be modified and the mechanical properties, such as stiffness and strength, and energy absorption capacities of hybrid metal foams can be optimized under both quasi-static and dynamic conditions by introducing strategically designed coating patterns. The presented novel approach and findings in this study provide valuable information on the development of high performance hybrid and functionally-graded cellular materials.

This is dedicated to my parents and my wife Danna,
for their understanding and support all along;
and to my daughter Olivia,
for all the happiness she brought to my life.

ACKNOWLEDGMENTS

Firstly, I would like to dedicate my gratitude to my advisor, Dr. Rigoberto Burgueño. With his vision, enthusiasm and rigorous style of work, he showed me the key characteristics of an excellent researcher. His encouragement and sound advices helped me find the right directions during the difficult times. He has been inspired and enlightened me throughout my PhD studies and helped to make it a great and interesting journey in my life.

I would like to thank the members of my PhD committee, Dr. Alejandro Diaz, Dr. Nizar Lajnef and Dr. Srinivasan Arjun Tekalur for their valuable time and comments. Special thanks are due to Dr. Srinivasan Arjun Tekalur for his guidance and help in the dynamic testing of materials. I would like to thank Dr. Ilsoon Lee and Dr. Wei Wang for sharing with me their expertise in the manufacturing of hybrid foam with nanocrystalline coatings. Also, I would like to thank Dr. David Grummon for his guidance and help in the material processing.

I would like to thank Mr. Siavosh Ravanbakhsh and Mr. Joseph Nguyen,for their help at Civil Engineering Laboratories. I would also like to thank Mr. Michael Rich, Mr. Per Ashkeland, and Mr. Edward Drown at Composite Materials and Structures Center for their help in material characterization and testing, I would also like to thank Dr. Stanley Flegler and Ms. Abby Vandera at MSU's Center of Advanced Microscopy for their help in electron microscopy imaging.

I would like to thank Wassim Borchani, Andy Venderklok, David Gonzalez, Aishu Venkat for their help in material testing. And I would like to thank Scott Sutton and Andrew

Maximiuk for their help in material processing. I would also like to thank my colleagues for their support during my stay at MSU.

Lastly, and most importantly, I would like to thank my parents and my wife Danna, for their understanding and support. I would also like to thank my daughter Olivia for all the happiness she brought to my life. To them, I dedicate this dissertation.

This study was mainly funded by the National Science Foundation under grant NSF grant CMMI-0928835. Additional financial supports were obtained from the Department of Civil and Environmental Engineering, and the Graduate School at Michigan State University. All contributions are gratefully acknowledged.

TABLE OF CONTENTS

LIST OF TABLES

LIST OF FIGURES

CHAPTER 1 INTRODUCTION

1.1 Motivation and Vision

The effect of impact and blast loads on structures can lead to devastating damage to structures and their occupants alike. Thus it is of great interest to protect people and the enclosures that they use (vehicles, buildings) from the natural, accidental or purposeful effects of explosions and impacts. An approach towards this goal is to design materials and protective devices that mitigate the effect of impact and blast loads by through energy dissipation and energy management (i.e., reduction in magnitude and direction.) In this effort, metallic foams have attracted great interest due to the large amount of energy dissipated during their plastic deformation under compressive loading. Numerous studies have been conducted on traditional metallic foams (e.g., aluminum foams) and their mechanical behavior and performance are understood to a great extent. However, while the use of metal foams as a resisting material/structure has been recognized, the design of the material itself as well as structural components based on metal foams has been challenging. Lately, increased attention has been paid to the development of strategically engineered functionally-graded metal foam systems with enhanced energy absorption capacity or the ability to tailor the propagation of stress waves through the foam [1-3]. While methods to fabricate functionally-graded foams by changing the pore size and density distribution in the foam have been reported [4, 5], an alternative way with great potential is to create hybrid foam systems by reinforcing the conventional open-cell foam with nano-coatings through electrodeposition [6-8]. The effectiveness of manipulating the properties of open-cell metallic foams using electrodeposited nano-crystalline coating has been demonstrated and reported [6-8]. However, the unique behavior of such hybrid foams has not been fully understood. In addition, few studies have been conducted to evaluate the performance

of functionally graded hybrid foam systems manufactured using such methods, and the efficiency of these new hybrid material systems in the management of stress-waves has not been addressed.

1.2 Background

1.2.1 Impact and Blast Effects on Structures

Attention to the design of buildings and vehicles again blast and impact loads from events such as explosions has seen a recent increase due to the growing threat of terrorist activities [9-11]. The blast wind, debris and fires caused by the explosion of a bomb may cause catastrophic damage on the structural components of a building and can lead to injuries and even death of the occupants or people nearby. When an explosion occurs, a large amount of energy is rapidly released and usually generates very hot and dense gases under high pressure. The expansion of the hot gas creates a layer of compressed air called a blast wave.

A pressure profile for a blast wave after arrival to a resisting structure consists of a positive duration phase, during which the pressure is higher than ambient level, followed by a negative duration, in which the pressure is below ambient level [9, 12]. When the shock front from an explosion encounters a structural component, such as a wall, it is instantly reflected; which may significantly amplify the incident pressure level, depending on the orientation of the structure with respect to the incident wave. The impulse from the blast will cause stresses to propagate through the structural component in the form of an compressive stress wave. This compression wave is reflected as a tensile wave when it reaches the rear end of the structural member on which it is acting. When the compressive wave or tensile wave exceeds the material

capacity, the structural element may fail due to fracture. Continuation and accumulation of this phenomena may cause partial collapse in a building.

1.2.2 Energy Dissipation in Materials and Structures

Protective mechanisms can be provided to structural components in order to absorb or dissipate the imported kinetic energy from impact or blast effect, and thus minimize or mitigate damage due to impact or blast effects. An ideal energy absorber should have a yielding stress that is lower than the failure stress of the material being protected and a long and flat post-yielding stress-strain curve. This will lead to the maximum energy absorption while retaining the safety and integrity of the protected object. Metal foams, such as aluminum foam, have such desired response features and have thus been used as energy absorbers for impact resistance (usually in the form of core material in a sandwich panel). The compressive behavior of a metal foam (e.g., Al open-cell foam) can be described by three stages [13-18]: an elastic stage, a collapse stage (or stress plateau stage), and a densification stage. Due to the plastic deformation of cell ligaments, or cell walls, in metal foams after yielding, a relative constant stress level can be maintained up to a larger strain (densification strain), after which the metal foam goes into the densification region where the stress increases rapidly due to contact of cell ligaments or walls [13]. The area underneath the stress-strain curve within the plateau state is usually considered as the energy dissipation capacity of a metal foam. The mechanical properties (e.g., stiffness, plateau stress, densification strain, etc.) of a metal foam such as aluminum foam is mainly controlled by its relative density, which can be calculated as the ratio of density of the foam to the density of the solid material [13]. As a result, the mitigated pressure can be adjusted to the desired level by varying the density of the metal foam material used.

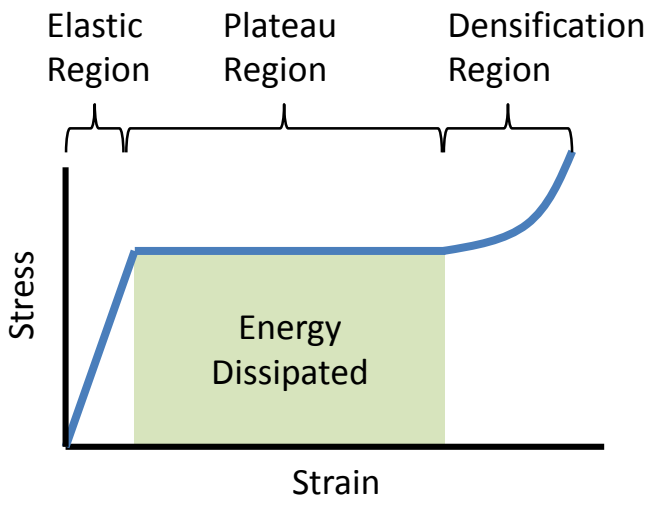

Figure 1-1 Compressive behavior of a typical metal foam

1.2.3 Nature's Functionally Graded Materials

For a structural component subjected to a given loading under a set of boundary conditions, the demand in material performance varies with location within the component. In a functionally graded material, the microstructure and composition has a gradual variation over the structure. This results in an optimized overall performance of the components while meeting the requirement of a specific function and application [19, 20]. Cellular materials found in nature such as bone, wood, and bamboo usually have a space varying density distribution that allows them to optimize intrinsic properties of the constituents that form them [21, 22].

The human bone, for example, is a naturally engineered functionally graded material. Generally, the strength of bone is highest at the surface and gradually lower towards the inside by changing its porosity. In addition, the bone structure has a sponge-like appearance at the ends (cancellous bone) while being very dense and with low porosity (cortical bone) in the middle. The gradient in mechanical properties resulting from the non-uniform structure can be used to

optimize the global mechanical performance of the structural element subjected to unevenly distributed external loads and thus lead to higher specific strength and more efficient use of the material.

1.2.4 Tailoring Energy Dissipation Mechanisms

Foam materials are widely used as energy absorbers and for impact resistance due to the large energy dissipated during the plateau region of their response [13, 23]. Many studies have been conducted to investigate the potential benefit in tailoring energy dissipation mechanisms using functionally graded foam materials. Functionally graded foam materials can be fabricated by creating a density gradient directly in the metallic porous materials through chemical or electrochemical processing [24, 25], by replication process based on graded precursors or performs [4, 5, 26, 27], or by combining layers of cellular materials with different densities to create a step-wise property gradient [28, 29].

The compressive behavior of functionally graded foams has been studied using experimental, analytical and numerical approaches under both quasi-static [2, 4, 5, 28] and dynamic conditions [1, 29-34]. These studies have shown that functionally graded foam materials can be used to control the overall stress-strain behavior of the foam and that enhanced performance in energy dissipation can be achieved. However, the experimental studies conducted thus far on functionally graded foams have been limited to those with a one-dimensional property gradient (usually the loading direction). And only few studies, those based on numerical methods, on functionally graded foams with two-dimensional property gradients have been reported [35, 36]. This may be may be partly due to the difficulty in creating properties gradients in higher dimensions using the manufacturing process of traditional cellular

materials. Thus, development in the fabrication and investigation of cellular/foam structures with two-dimensional property gradients is of great interest.

1.2.5 Electrodeposition of Metal Coatings

Electrodeposition is a electroplating process in which a metal coating is applied to a metallic or other conducting surface by an electrochemical process [37]. Electrodeposition is usually used to modify or improve the surface properties of an object, such as enhancing wear resistance, provide corrosion protection, or for aesthetic qualities [37]. During an electrodeposition process, the electrons on the surface of the cathode (part to be coated) neutralize the positive charges on the metal ions in the solution and lead to the deposition of the metal on the surface of cathode. On the other hand, electrons are removed from the anode (usually the coating material) and thus metal ions are released into the solution [37]. The electrodeposited metals, which usually have a nanocrystalline structure and high concentration of dislocations, have much higher yielding strength and are much harder compared to their bulk counterparts [37, 38]. However, this is achieved at the expense of ductility and toughness [39].

1.2.6 Hybrid Metal Foams

Lately, increased attention has been paid to the development of hybrid metal foams by coating or reinforcing conventional open-cell foams through electrodeposition to enhance or tailor their mechanical performance [6-8, 40, 41]. Different hybrid foam systems have been reported, namely, aluminum (Al) open-cell foam with nickel (Ni) based coatings [6, 7, 40] and aluminum/copper (Al/Cu) hybrid foam systems [8]. The deposited coating material (e.g., Ni or Cu), which usually has a higher modulus than the substrate, (e.g., Al) works in synergy with the substrate and leads to optimized composite behavior of the foam ligaments. It has been shown

that the stiffness and strength of open-cell hybrid metallic foams with nano-crystalline coating can be controlled by varying the coating thickness [6-8]. Thus, it is considered that such method can be adopted to create functionally graded cellular structures by introducing strategically designed coating patterns. However, the unique mechanical response features of as-deposited hybrid foams, such as their brittle failure mechanism due to its nanocrystalline coating, have not been understood.

1.2.7 Annealing of Metals

Similar to metal materials after large plastic deformations, electroplated metals in the as-deposited state usually have fine grain size and a large concentration of structural defects [37, 42-44]. These microstructure features of electrodeposited metals lead to their high strength and hardness but low ductility [37, 42-44]. The large amount of energy stored in electrodeposited or highly deformed metals due to the high concentration of structural defects may provide a great driving force for recovery and recrystallization when subjected to heat (i.e., annealing) [45-47]. When enough annealing is provided, the defects in electrodeposited or deformed metals can be removed or rearranged, and also a new microstructure with larger grain sizes can be obtained [47]. Such changes in microstructure usually result in a decrease in strength and increase in ductility of the metal.

1.3 Research Hypothesis and Objectives

1.3.1 Hypothesis

The hypothesis behind this research is that open-cell metal foams can be strategically reinforced with nanostructured coatings through electrodeposition to achieve functionally graded

hybrid foam systems with optimized performance for different loading conditions and with the ability to mitigate or redirect damaging stress waves from blast and impact loads (see Figure 1-2).

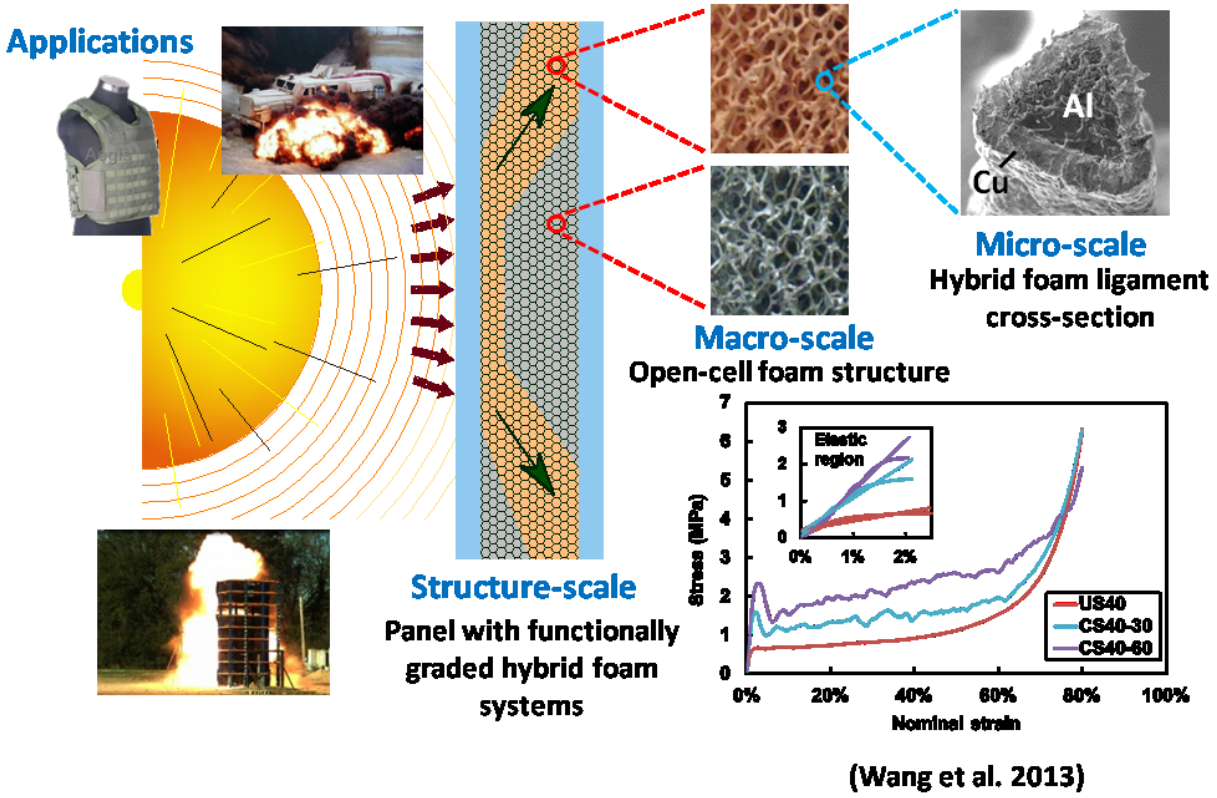

Figure 1-2 Schematic of the research motivation and the integration across scales for functionally graded hybrid foam systems

1.3.2 Objectives

The first objective of this research is to gain a comprehensive understanding of the micro- and macro-scale deformation and failure mechanisms of hybrid metal foams fabricated through electrodeposition, which have a distinct behavior compared to conventional metal foams due to their nanocrystalline coating. The second objective is to study the behavior of hybrid foams under high strain rate loading and also show that the mechanical performance of hybrid foams

can be efficiently enhanced by the nano-structured reinforcement. The third objective is to show that the mechanical performance of hybrid foam structural elements can be optimized according to the loading condition at different loading rates by means of strategically designed coating patterns. The objectives in this research were met by completing the following tasks:

1) Characterization of hybrid foam material. Finite element models at the micro- and macro-scales were established and used to investigate the unique mechanical behavior of Al/Cu hybrid foams and the effect of coating material properties. The micro-scale behavior of hybrid foams were investigated using sectional analyses combined with finite element models of single hybrid foam ligaments discretized using continuum elements. On the other hand, beam-element-based finite element models consisting of multiple foam cells were used to study the macro-scale behavior of hybrid metal foams.

2) Fabrication of material and structure. The low ductility of the nanocrystalline coating in hybrid metal foams can have a negative effect in their performance, such as localized damage and a reduction in energy dissipation capacity. Such detrimental effect can be improved by introducing annealing after the electrodeposition process in the manufacturing of hybrid metal foams. In addition, hybrid foam systems with strategically designed two dimensional (2D) coating patterns were successfully fabricated using a selective electrodeposition approach.

3) High strain rate characterization. The behavior of Al/Cu hybrid foams under high-strain-rate condition was investigated using Split Hopkinson Pressure Bar (SHPB) tests. In order to investigate the influence of the nanocrystalline coating, hybrid foams with different coating thicknesses were tested while two different strain rates were considered. The effect of coating ductility was also studied by testing annealed hybrid foams samples.

4) Structural characterization Al/Cu hybrid metal foams with strategically designed coating patterns were fabricated and tested. Two flexural type loading conditions were considered under quasi-static conditions, namely, a three point bending beam and a cantilever beam. The dynamic performance of functionally graded Al/Cu hybrid foams was investigated using drop-weight tower tests with a three point bending setup. In both conditions, different coating designs were considered to demonstrate the capability of modifying the deformation and failure mechanisms and optimizing mechanical performance by adopting functionally graded designs.

1.4 Scope

This study aims to develop a functionally graded hybrid foam systems with optimized performance responding to different loading conditions and the ability to mitigate or redirect damaging stress waves from blast and impact loads by introducing strategically designed nanocrystalline coatings onto open-cell metal foams through electrodeposition. The aim is achieved by meeting the objectives and completing the tasks discussed in Section 1.3.

While metal foams have many applications due to their unique properties (e.g., heat exchangers and sound absorbers), the current study focuses on the mechanical behavior and energy absorption capacity of hybrid and functionally-graded hybrid metal foams. The study and investigation in this research is mainly based on Al/Cu hybrid foams, which were obtained by depositing nanocrystalline copper coatings onto open-cell aluminum foams through an electrodeposition process. Copper was used as the coating material due since its electrodepostion is well-established and because of its relatively low cost. However, other types of hybrid foams have been reported (e.g., aluminum/nickel hybrid foams) [6, 7, 40]. In addition, electrodeposition processes for other metals or alloys have been established. While it is of great interest to investigate the optimized combinations of core and coating material for hybrid metal foam

systems, it is not within the scope of this study. However, as it will be shown in later chapters, some of the findings and conclusions are applicable to other types of hybrid metal foams.

1.5 Organization

This dissertation is organized into seven chapters. The remainder of this dissertation is organized as follows. Chapter 2 provides a background and literature review for open cell metal foams, electrodeposited metal coatings, hybrid metal foams, the annealing of metals, and functionally graded materials. Chapter 3 documents the investigation on micro- and macro-scale behavior on hybrid Al/Cu hybrid foams using the finite element method. Chapter 4 describes the study on the effect of ductility of electrodeposited coatings in hybrid metal foams, in which the influence of annealing was investigated. Chapter 5 reports the experimental characterization of Al/Cu hybrid foams under high strain rate loading using a Split Hopkinson Pressure Bar (SHPB). Chapter 6 describes the experimental characterization of Al/Cu hybrid foam structure elements with strategically designed coating patterns under quasi-static and dynamic loading. Finally, Chapter 7 summarizes the research by noting its significance, main conclusions and future research needs.

CHAPTER 2 BACKGROUND

2.1 General

This chapter presents the background and fundamental knowledge based on which the current work is established. The contents presented in this chapter will be used and referenced in the following chapters.

2.2 Behavior of Open Cell Metallic Foams

Metallic foams are a cellular material made of metal with polyhedral cells packed in three dimensions to fill space [13]. An open-cell foam only contains the cell edges and forms an interconnected network of solid struts (see Figure 2-1). There are many methods currently employed in the manufacturing of metallic foams, including liquid metals, powder metallurgy, electrochemical deposition, or vapor deposition techniques. [13-18]. Metallic foams excel in different kinds of mechanical properties, such as great impact energy absorption, high specific strength, and good stiffness [48]. As a result, metallic foams can have numerous applications in different fields such as energy absorption systems for impact protection and lightweight structural components [13, 23].

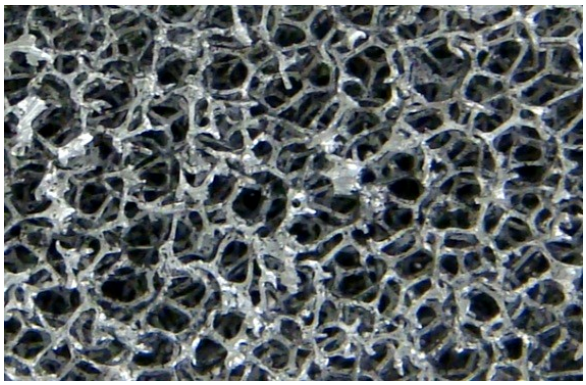

Figure 2-1 Metallic open-cell foam

The unique physical properties of open-cell foam materials can be attributed to its cell structure at the micro scale. A proper representation of the foam structure is thus usually the key to study its behavior using analytical or numerical approaches. A well-known method to resemble the foam structure is to fill the space with Kelvin's tetrakaidecahedron cell (see Figure 2-2), which has 14 faces consisting of 6 square faces and 8 hexagonal faces [49]. Such structure was believed to minimize surface area per unit volume for over a century. With the help of computer software, Weaire and Phelan identified a better structure solution consisting of six tetrakaidecahedron cells (with 2 hexagonal and 12 pentagonal faces) and two irregular dodecahedron cells (with pentagonal faces), that lead to even lower surface area per unit volume [50]. In addition, computer software has been developed to generate random soap froth micro structures, based on which an open-cell foam with random cell structures [51].

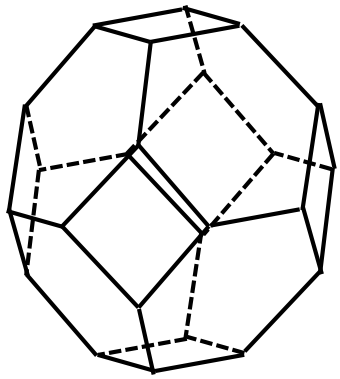

Figure 2-2 Kelvin's tetrakaidecahedron cell structure

Numerous studies have been conducted on metallic foams due to their excellent properties and wide range of applications, and their mechanical behavior has been studied extensively using experimental, analytical and numerical approaches. Deshpande and Fleck

studied the yield behavior of aluminum alloy foams by conducting tests considering a range of axisymmetric compressive stress states and proposed phenomenological isotropic constitutive models [52]. Zhu et al. [53] established elastic constants for open-cell foams based on tetrakaidecahedral cells (Figure 2-2 (a)). Finally, in what is perhaps the most well-known and followed work on the subject, Gibson and Ashby [13] derived semi-empirical equations to predict the performance of foam materials under different failure mechanisms based on simplified unit cell models.

The compressive behavior of a metal foam (e.g., Al open-cell foam) can be described by three stages [13-18]: an elastic stage, a collapse stage (or stress plateau stage), and a densification stage. Figure 2-3 shows a schematic of the compressive stress-strain curves for a typical metal (elastic-plastic) foam. Within elastic stage, the deformation mechanism of open-cell metal foam is controlled by cell wall bending and the stress-strain relationship is basically linear and can be described using a Young's modulus E^*. The plateau stage in the compressive behavior of open-cell metal foam is associated with collapse of the cells during which material yielding and the creation of plastic hinges occurs. A relatively constant stress level can be maintained within the plateau stage up to a large strain. The area underneath the stress-strain curve within the plateau stage is usually considered as the energy dissipation capacity of a metal foam. When the foam cells have completely collapsed, the deformation enters the densification stage during which the stress increases rapidly due to contact between the foam ligaments.

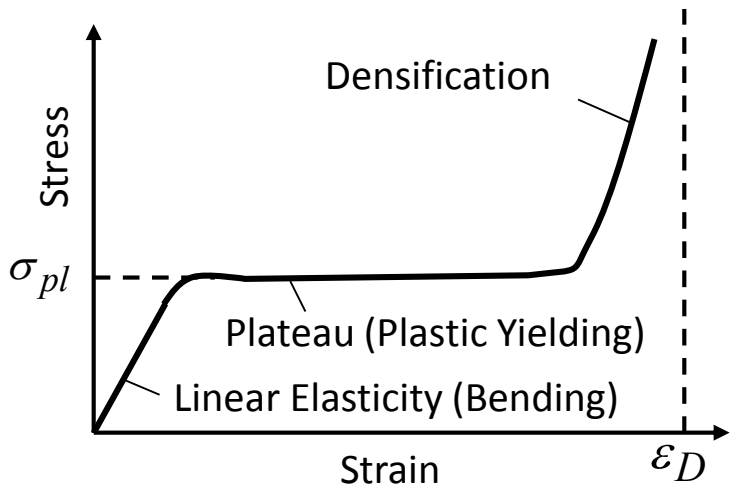

Figure 2-3 Compressive behavior of open-cell metal foams (Adapted from Gibson and Ashby [13])

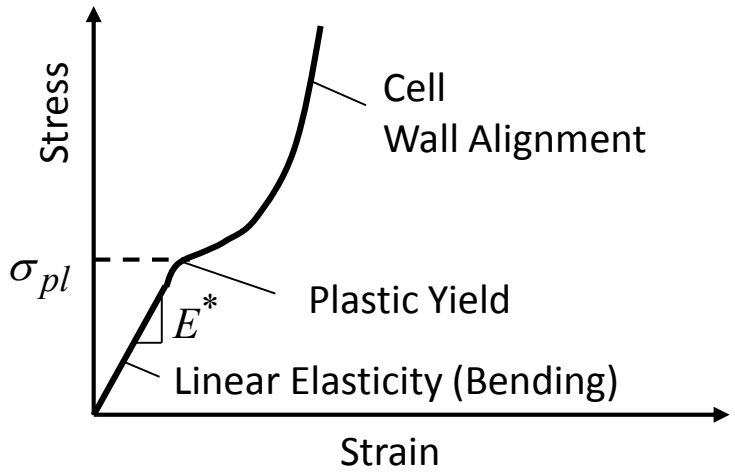

Figure 2-4 Tensile behavior of open-cell metal foams (Adapted from Gibson and Ashby [13])

The tensile behavior of open-cell metal foam is shown in Figure 2-4. Under low stress, the behavior is linear elastic, which is caused by cell wall bending. At larger strains, plastic bending occurs and the cell walls rotate towards the tensile axis, thus leading to a yield point

followed by a rising (stiffening) stress-strain curve [13]. Fracture occurs in open-cell metal foams upon reaching the material's ultimate tensile strain.

One of the most important structural properties of metallic foams is their relative density, which is usually calculated using the density of the foam ρ_{foam}, divided by that of the solid of which it is made ρ_{solid} [13]. However, the following relationship can be easily obtained considering single material foam:

$$\frac{\rho_{foam}}{\rho_{solid}} = \frac{V_{solid}}{V_{foam}} \qquad \text{Equation 2-1}$$

One of the pioneering studies on foam materials is that by Gibson and Ashby [13], in which they studied the mechanical behavior of open-cell foams based on a simplified cubic models (Figure 2-5). The unit cell model used by Gibson and Ashby for three-dimensional open-cell foams consists of a cubic array of members of length *l* and square cross-section with an edge thickness *t*. The mechanical properties of open-cell metal foams were studied by considering different deformations and failure mechanisms. The semi-empirical equations obtained by Gibson and Ashby [13] for the mechanical properties of open-cell foams are summarized in

Table 2-1. It can be seen that the mechanical properties of open-cell metal foams are related to the base material properties and the relative density of the foam. According to Gibson and Ashby, the modulus and yield stress under compress and tension are approximately the same for open-cell metal foams.

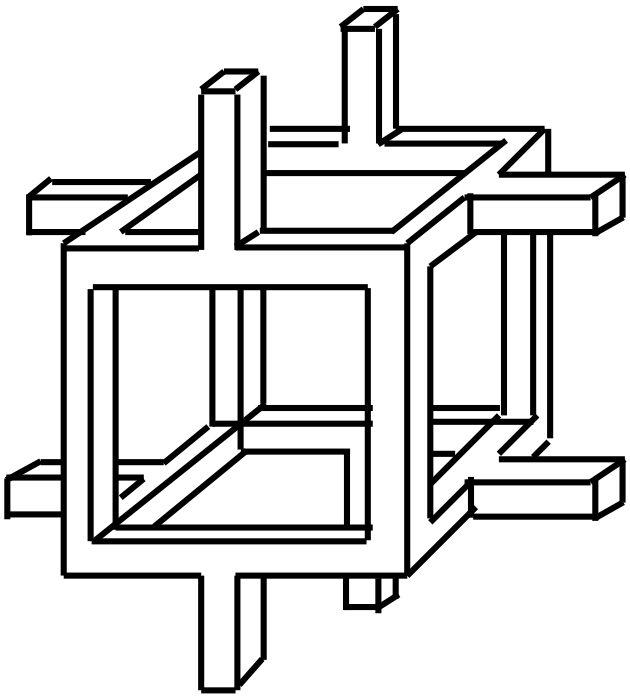

Figure 2-5 Cubic unit cell (Adapted from Gibson and Ashby [13])

In the work by Gibson and Ashby [13], the post-yield behavior of open-cell metal foam is described using Equation 2-2 and Equation 5-37, in which constants D and m are determined by fitting the curves with experimental data. Gibson and Ashby suggested m=1 $\pm$ 0.4 and D = 2.3 for elastic-plastic open-cell foams based on experimental data for polymethacrylimid foams.

$$\frac{\sigma}{\sigma_{pl}} = 1 \text{ when } \varepsilon \le \varepsilon_D\left(1-\frac{1}{D}\right) \qquad \text{Equation 2-2}$$

$$\frac{\sigma}{\sigma_{pl}} = \frac{1}{D}\left(\frac{\varepsilon_D}{\varepsilon_D-\varepsilon}\right)^m \text{ when } \varepsilon > \varepsilon_D\left(1-\frac{1}{D}\right) \qquad \text{Equation 2-3}$$

Table 2-1 Equations for the Mechanical Properties of Open-cell Metal Foams

Mechanical Properties	Formula
Relative density RD	$RD = \frac{\rho^*}{\rho_s}$
Young's Modulus	$E^* \approx E_s \left(\frac{\rho^*}{\rho_s} \right)^2$
Shear Modulus	$G^* \approx \frac{3}{8} E_s \left(\frac{\rho^*}{\rho_s} \right)^2$
Poisson's Ratio	$\nu^* \approx \frac{1}{3}$
Plastic Collapse Strength	$\sigma_{pl}^* = 0.3\sigma_{ys} \left(\frac{\rho^*}{\rho_s} \right)^{3/2}$
	$\sigma_{pl}^* = 0.23\sigma_{ys} \left(\frac{\rho^*}{\rho_s} \right)^2 \left(1 + \left(\frac{\rho^*}{\rho_s} \right)^{1/2} \right)$
Densification Strain	$\varepsilon_D = 1 - 1.4 \left(\frac{\rho^*}{\rho_s} \right)$

2.3 Electrodeposition of Metal Coatings

Electrodeposition is a electroplating process in which a metal coating is applied to a metallic or other conducting surface by an electrochemical process [37]. Hybrid metal foams can be manufactured by reinforcing a conventional single-material foam with a different coating material through electrodeposition [6, 8, 40, 54]. This section discusses the electrodeposition process, and the physical characteristics and mechanical properties of electrodeposited metals.

2.3.1 Electrodeposition Process [37, 55]

The electrolysis cell for an electrodeposition process basically consists of four parts, namely, the cathode, the anode, the electrolyte, and a power supply (i.e., rectifier). The cathode is the negative electrode which is the part being plated (coated). The anode is the positive electrode which is the source of the metal ions for the electrolyte and provides electrons for the circuit. The electrolyte, which is called "the bath", is mostly aqueous and contains metal ions. During an electrodeposition process, the electrons on the surface of the cathode neutralize the positive charges on the metal ions in the solution and lead to the deposition of the metal on the surface of cathode. On the other hand, electrons are removed from the anode and thus metal ions are formed and released into the solution. A power supply is needed to create an electric field that moves the metal ions in the solution. Equation 2-4 and Equation 2-5 show the reactions taking place at the cathode and anode.

Cathode reaction: $M^{z+}(\text{aq}) + \text{ze}^- \rightarrow M(s)$ Equation 2-4

Anode reaction: $M(s) \rightarrow M^{z+}(\text{aq}) + \text{ze}^-$ Equation 2-5

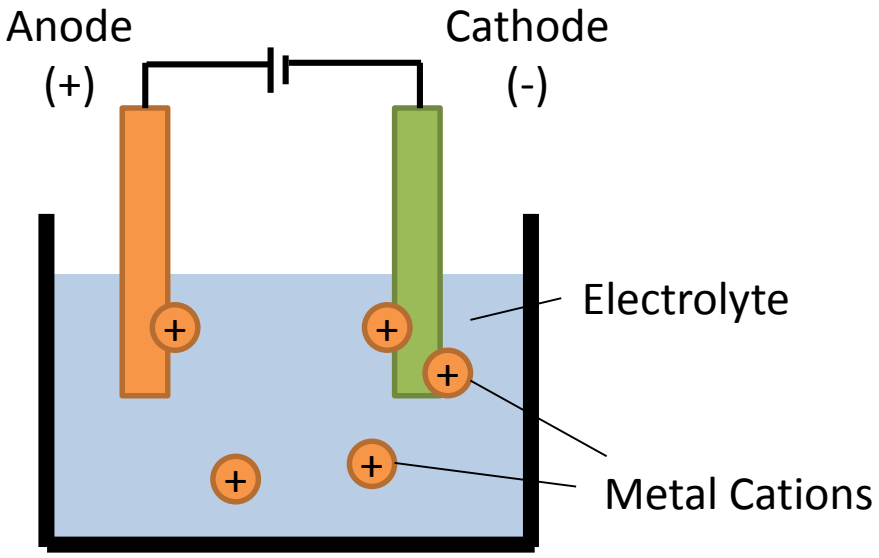

Figure 2-6 Electrolytic cell for electrodeposition of metal

The amount of metal deposited on the cathode (coating) can be estimated using Faraday's laws of electrolysis [56], which can be summarized by Equation 2-6. In the equation, m is the mass of the substance liberated at an electrode, Q is the total electric charge passed through the substance, F is the Faraday constant (96485 C mol^{-1}), M is the molar mass of the substance, and z is the valence number of ions of the substance (electrons transferred per ion). In the case of constant-current electrolysis, $Q = It$ and it leads to Equation 2-7.

$$m = \left(\frac{Q}{F}\right)\left(\frac{M}{z}\right) \qquad \text{Equation 2-6}$$

$$m = \left(\frac{It}{F}\right)\left(\frac{M}{z}\right) \qquad \text{Equation 2-7}$$

2.3.2 Structures and Properties of Electrodeposited Metals

The physical, chemical and mechanical properties of electrodeposited metals usually differ from those of their bulk counterparts. This can be mainly attributed to two factors: the microstructure of electrodeposted materials and the presence of impurities [37]. During the electrodeposition process, the diffusing atoms at the surface may not be able to achieve an equilibrium position and end up be in a metastable configuration due to the deposition rates. This phenomenon leads to a structure containing high concentration of vacancies, dislocations, twins, etc. The refinement mechanisms based on these structural defects leads to a small grain structure (usually nanocrystalline structure [8, 57]). Due to the high concentration of these structural defects and small-grained structure, the properties of the deposits are quite different from those of bulk materials.

The movement of dislocations is the cause of plastic deformation. On the other hand, due to the change in orientation, grain boundaries, twin boundaries, other dislocations act as obstacles that dislocation motion. Such resistance to dislocation motion, or plastic deformation, defines the yield strength and hardness of a metal material [58]. As a result, the electrodeposited metals, which usually have a small grain size and high concentration of dislocations, have higher yielding strength and are harder compared to their bulk counterparts [37, 38]. An electrodeposited metal can be two or three times as strong as the corresponding bulk metal [38].

Electrodeposited metals can have various impurity contents originated from additives, metal or nonmetal particles, metal complexes, hydroxides, and gas bubbles (e.g., hydrogen) [59]. The amount of impurities can noticeably influence the strength of electrodeposited metals [60, 61].

2.3.3 Properties of Electrodeposited Metals

Similar to plastically deformed (cold worked) metals, the high dislocation densities, fine grain structure found in electrodeposited metals are due to the existence of a strained condition. However, the dislocation density in electrodeposited metal is usually much higher (in the order of 10^{15}-10^{16} m^{-2}) compared with heavily deformed or quenched metals [37]. As discussed in Section 2.3.2, the dislocation densities as well as the grain size affect the mechanical properties of metals, such as strength, ductility and hardness.

A deposited metal with a small grain size can have a high strength. Petch and Hall [62, 63] proposed an expression to describe relationship between the grain size in a metal and its mechanical properties, as shown in Equation 2-8 and Figure 2-7. In this equation, H can represent the hardness or yield strength of the metal and d is the grain size. H_0 and K_H are determined through experiment for a specific metal. More specifically, H_0 is determined by dislocation blocking and K_H represents the penetrability of the moving dislocation boundary [62, 63]. This empirical expression is applicable to many electrodeposited metals and provides useful information on the relationship between mechanical properties and microstructure of deposits. It needs to be noticed that the strength of deposited metal films also depends on film thickness. Generally, the strength of a thin film is higher. However, the change in strength is only for films thinner than 10 μm, with respect to the value measured in thick films [37].

$$H=H_0+\frac{K_H}{\sqrt{d}} \qquad \text{Equation 2-8}$$

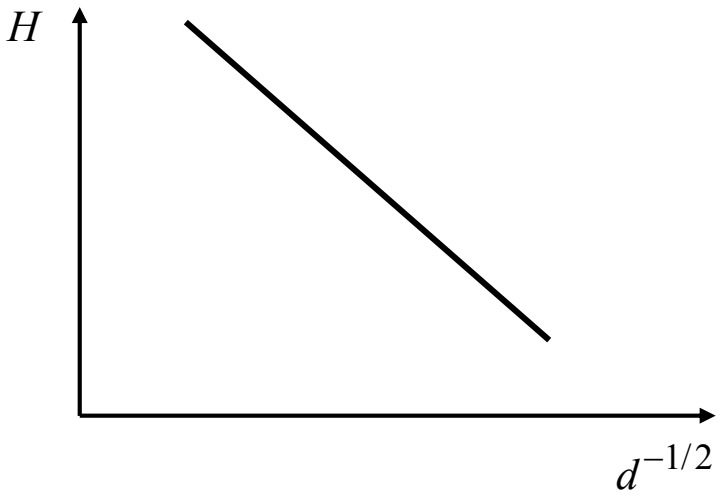

Figure 2-7 Hall-Petch relationship

An electrodeposited metal usually has a nanocrystalline structure, which leads to a high tensile strength. However, the increased strength is achieved at the expense of ductility and toughness [39]. The ductility of a metal material can be defined as the degree of plastic deformation that can occur before fracture [38]. Since plastic deformations are the result of dislocation motions, ductility is affected by the dislocation structure. As a result, the ability for dislocation motion usually leads to ductile behavior. On the other hand, fracture occurs if the higher stresses at the structural defects cannot be relieved by plastic deformation [43]. Thus, due to the small grain size and the existence of obstacles to dislocation motion, electrodeposited metals usually show low ductility and relatively brittle behavior compared to their bulk counterparts. The low ductility of electrodeposited metal films can also be caused by the precipitation of impurities at grain boundaries [37].

It also needs to be noted that the structure formation of electrodeposited metals results from the nucleation and growth of metal crystals during the electrochemical process and is

related to the particular electrodeposition condition [37]. As a result, the mechanical properties of electrodeposited metals, such as tensile strength, ductility can be affected by the variables in the electrodeposition process, including metal ion concentration, additives, current density, temperature, agitation and polarization [64].

2.4 Hybrid Metal Foams through Nanocrystalline Coatings

2.4.1 State-of-the-art Review

Increased attention has been recently paid to the development of hybrid metal foams by coating or reinforcing conventional open-cell foams through electrodeposition to enhance, or tailor, their mechanical performance [6-8, 40, 41]. Different hybrid foam systems have been reported, namely, aluminum (Al) open-cell foam with nickel (Ni) based coatings [6, 7, 40] and aluminum/copper (Al/Cu) hybrid foam systems [8]. The deposited coating material (e.g., Ni or Cu), usually has a higher modulus than the substrate, (e.g., Al) and works interactively with the substrate to create improved composite behavior of the foam ligaments. Boonyongmaneerat et al. [40], Bouwhuis et al. [6] and Jung et al. [7] investigated the quasi-static and high-strain-rate performance of open-cell aluminum (Al) foam reinforced with nanocrystalline nickel-tungsten (Ni-W) or nanocrystalline nickel (Ni) coatings and found significantly enhanced modulus, strength and energy absorption capacity. Wang et al. [8] found similar enhancements under quasi-static loading for aluminum open-cell foams reinforced with nanocrystalline copper (Cu).

The investigation of this study focuses on Al/Cu hybrid foams. One of the reasons is the well-established electrodeposition process of copper. In addition, copper has a high plating efficiency and a low cost. However, as it is shown in later chapters, the conclusions and findings

of this study are also applicable to other types of hybrid metal foam systems (e.g., Al.Ni hybrid foam).

2.4.2 Manufacture of Al/Cu Hybrid Foam

The Al/Cu hybrid foams were manufactured by applying a nanocrystalline copper coatings on an aluminum open-cell foams using electrodeposition (see Figure 2-8) [8]. The electrodeposition process was conducted in a glass container filled with an electrolyte and placed on top of a stirrer/hot plate. The temperature was monitored and controlled by a thermocouple placed into the electrolyte. A rectangular titanium basket with copper strips tied on the sides was used as the anode and the foam specimen was placed in the center of the basket without any contact with it. The copper strips were necessary to maintain the copper concentration and pH value within the electrolyte.

Copper can be electrodeposited from acid, alkaline, and neutral bath formulations [55]. In this study, copper pyrophosphate plating bath was used. A commercial electrolyte (Uyemura International Co., Ontario, CA, US), which mainly contained copper pyrophosphate as the copper source was used at 65 °C and a PH of 7.5 A stirring bar was applied throughout the entire deposition process at 180 rpm to minimize the gradient of electrolyte concentration. The electrodeposition was carried out at a constant current density of about 13 mA/cm^2. Pre-treatment according to ASTM Standard B 253 was applied to the foam specimens prior to electrodeposition to yield a better coating result. SEM images of the hybrid foam fabricated are shown in Figure 2-9. It can be seen that a uniform coating can be obtained using the setup discussed.

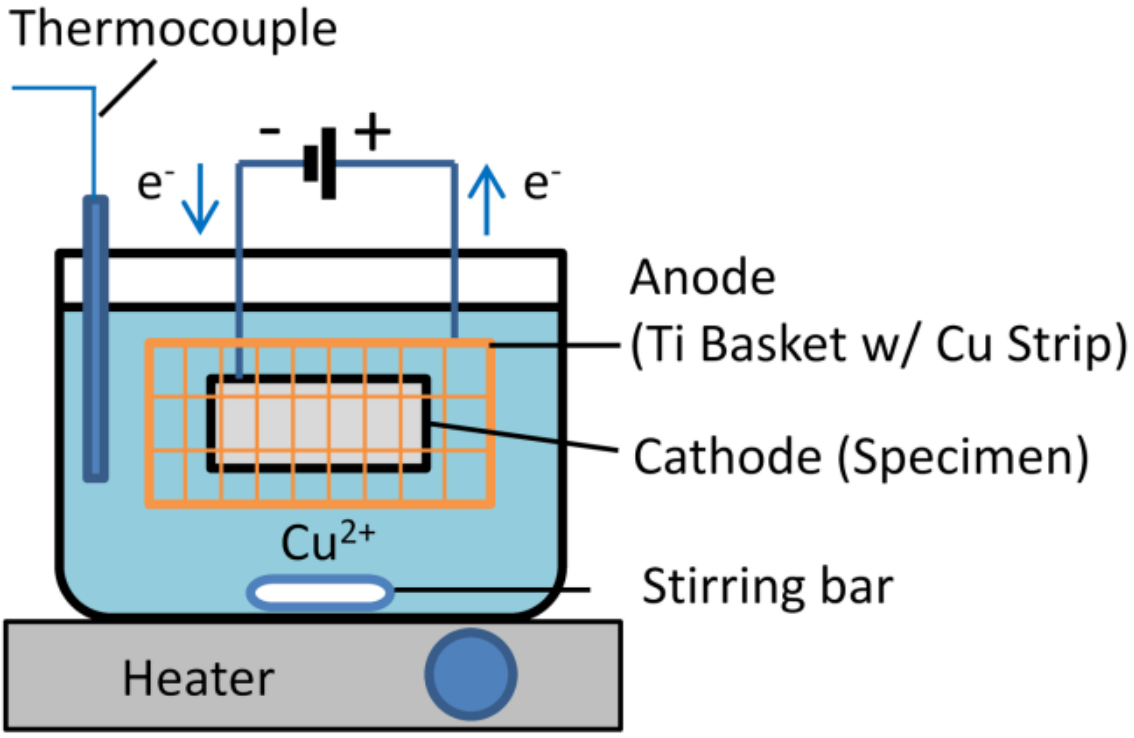

Figure 2-8 Schematic of electrodeposition setup

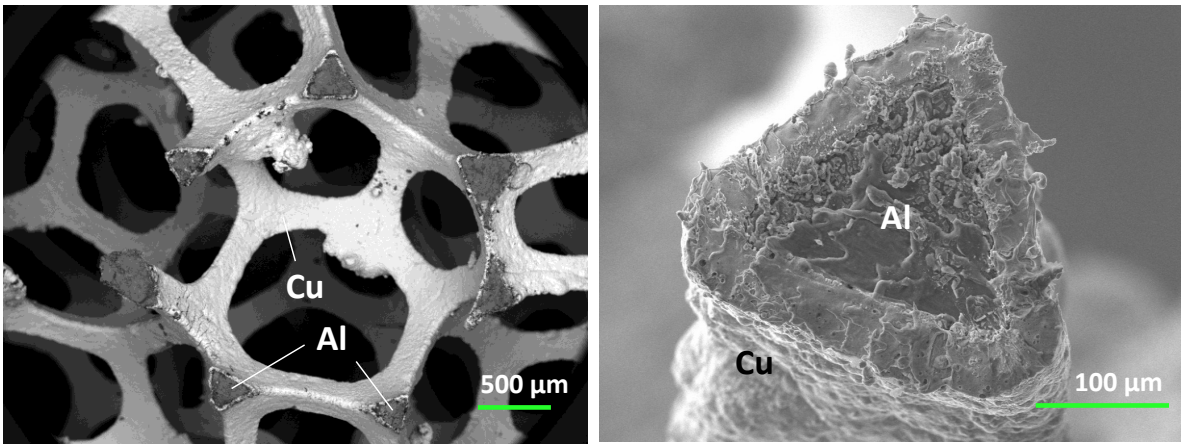

Figure 2-9 SEM images of hybrid Al/Cu foams: a) SEM image of micro-structure of hybrid Al/Cu foams with ligament cross sections exposed; b) SEM image of cross-section of a single ligament of hybrid Al/Cu foam

The nominal copper coating thicknesses on Al/Cu hybrid foam samples can be calculated based on the gained weight. Assuming that the copper coating is uniformly applied on the foam ligaments with circular cross sections of radius r, the weight of copper coating is proportional to the cross section area of the coating layer as shown in Equation 2; where W is the copper weight density (g/cm^3), C is a constant and t_c is the coating thickness (μm). The radius r was defined to be 97 μm based on measurements of ligaments on 40 PPI foams by Wang et al. [8]. The constant in Equation 2 was determined by fitting the equation with the measurements reported by Wang et al. [8] in which coated foam struts of representative samples were imaged with a scanning electron microscopy and measured coating thickness were averaged based on at least 30 measurements at different locations for each sample. Figure 2-10 shows the comparison between the coating thicknesses estimated using Equation 2 and the measured thicknesses with different weight gain.

$$W = C\left(\left(r + t_c\right)^2 - r^2\right) = C\left(t_c{}^2 + 2rt_c\right),\ C = 2.76\times10^{-5} \qquad \text{Equation 2-9}$$

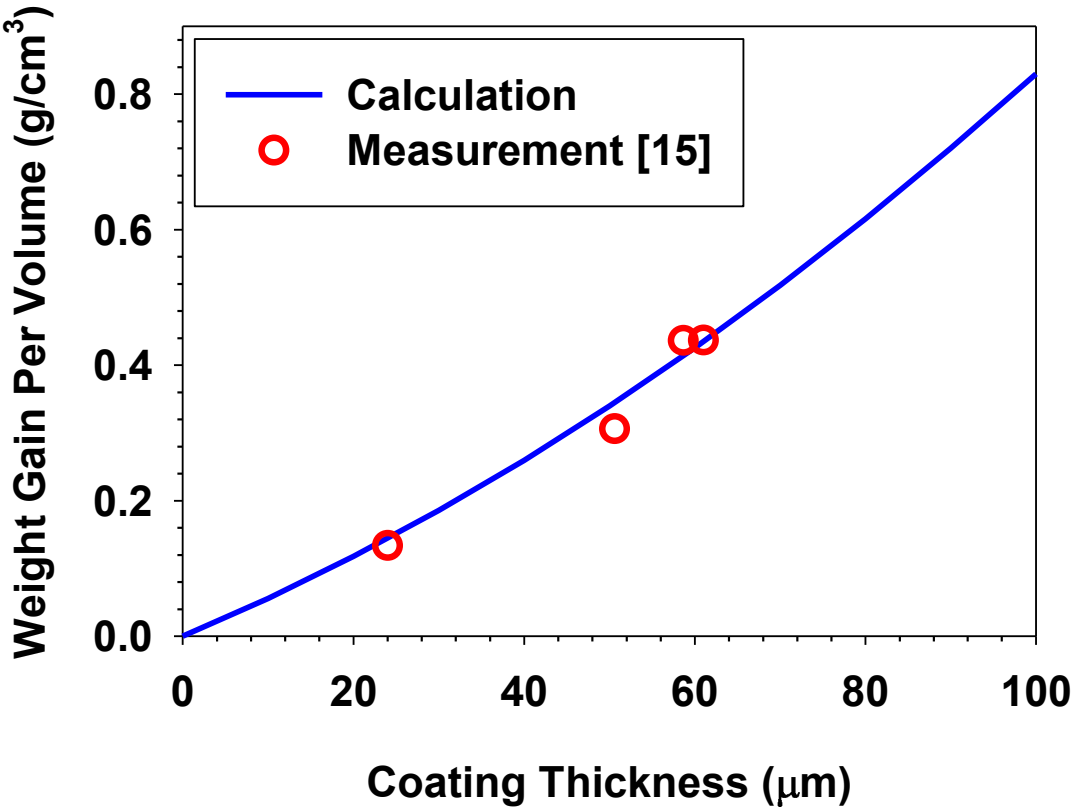

Figure 2-10 Comparison of coating thickness estimates to experimental measurements

2.4.3 Mechanical Behavior of Al/Cu Hybrid Foam with Nano-coating

The works by Boonyongmaneerat et al. [40], Bouwhuis et al. [6], Jung et al. [7] and Wang et al. [8] demonstrate the effectiveness in manipulating the properties of open-cell Al foams by using electrodeposited nano-crystalline metal coatings. However, it can be observed from their reported work that the hybrid foams had a behavior that differs considerably from that of conventional (uncoated) metal foams. The typical compressive response of a metal foam (e.g., Al open-cell foam) can be described by three stages [13-18]: an elastic stage, followed by a collapse stage (or stress plateau stage) where a relatively constant stress level can be maintained

up to a large strain level, and then the densification stage where the stress level rises rapidly due to the contact between cell walls (closed cell foam) or ligaments (open-cell foam), as shown in Figure 2-3. However, a large stress drop after the initial peak, especially for specimens with thicker coatings, was observed in the behavior of the Al/Ni-W and Al/Ni hybrid foams reported by Boonyongmaneerat et al. [40], Bouwhuis et al. [6] and Jung et al. [7] and the Al/Cu hybrid foams reported by Wang et al. [8], as shown in Figure 2-11 and Figure 2-12. No detailed discussion on this behavior was made in the noted studies except for the observation noted by Bouwhuis et al. [6] of cracks and wrinkling of the Ni sleeve (coating) after the peak stress was reached. Thus, it is clear that the large stress drop greatly decreases the energy absorption capacity and efficiency of hybrid foams and that the failure mechanism needs to be investigated in detail in order to get a better understanding of their performance and for possible improvement of their manufacturing process.

The Ni-W, Ni or Cu coatings in the studies previously mentioned were applied using direct current or pulsed electrodeposition and had a nanocrystalline structure. According to the Hall-Petch relationship [62, 63] (see Equation 2-10), where C is a constant and d is the mean grain size), the strength of a material increases with smaller grain size. However, the higher strength of electrodeposited nanocrystalline material is usually accompanied by a significantly reduced ductility capacity [65-68]. The increased brittleness may cause local coating failure in the hybrid foam material and lead to concentrated deformations in weakened critical sections at low strain levels. As most of the energy absorbed by metal foams is in the form of large plastic deformations, the consequences of a brittle coating in hybrid foams may overtake the enhancement gained from the additional strength and inhibit the improvement of energy absorption capacity.

$$\sigma_y = \sigma_0 + \frac{C}{\sqrt{d}} \qquad \text{Equation 2-10}$$

While the macroscopic performance of hybrid foams with nano-coating has been evaluated experimentally. An understanding of the detailed failure mechanisms and influence parameters such as the coating properties is still lacking; and thus the unique behavior of such material cannot be clearly explained. In addition, methods to numerically study and simulate the behavior of metal hybrid foams are not well established.

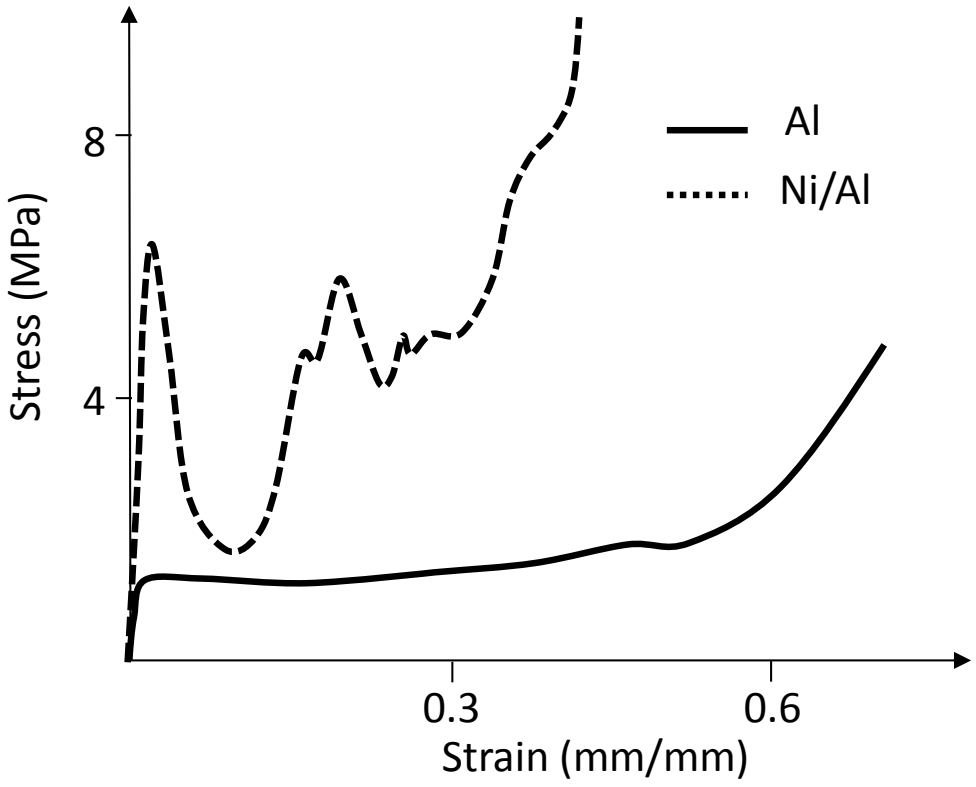

Figure 2-11 Typical stress-strain curves of uncoated foam samples and with nickel coating (Adapted from Bouwhuis et al. [6])

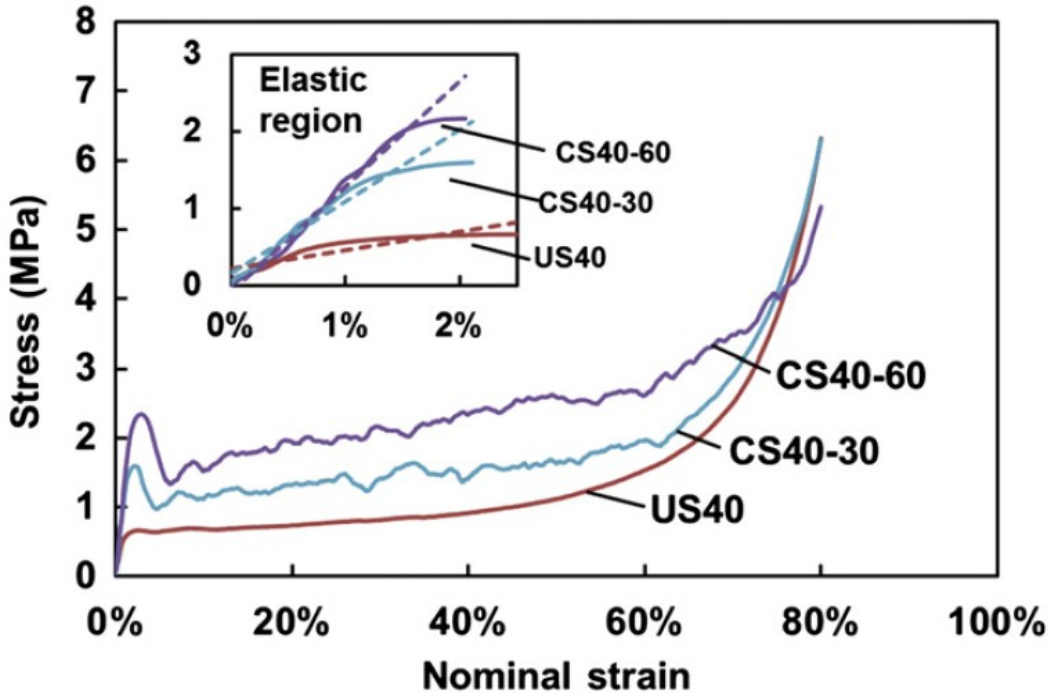

Figure 2-12 Compressive stress-strain response of 40 ppi plain Al foam and copper coated Al/Cu hybrid foams [8]

2.5 Annealing of Deformed Metals

As discussed in Section 2.3, electroplated films in the as-deposited state usually have rather low ductility due to the fine grain size and large concentration of structural defects. These features are responsible for the mechanical properties of electrodeposited metals, such as high strength and hardness, and low ductility. The microstructure of electrodeposited metal is similar to that of metal material after large plastic deformation [37].

A large amount of energy can be stored in an electrodeposited, or highly deformed polycrystalline material (e.g., metals), due to the structural defects such as dislocations, twins, grain boundaries. This leads to a material that is thermodynamically unstable. The unstable defects are retained in the material as the atomistic mechanisms needed to remove the defects are

usually very slow at normal temperature. However, when the material is subjected to high temperature, or heat treatment such as annealing, the large amount of stored energy may provide the driving force for recovery and recrystallization [37]. By this way, the defects can be removed or rearranged to a lower energy state due to thermally activated processes such as solid state diffusion [47].

Usually cold worked metals undergo three stages when subjected to annealing, namely, recovery, recrystallization and grain growth [47]. In the recovery stage, annihilation and rearrangement of the dislocations occurs and the microstructure of the metal can be partially restored. The changes in microstructure during recovery are usually within the deformed grains and do not affect the grain boundaries. The dislocations are not completely removed during recovery but rather entering a metastable state. New grains without any dislocation are formed in the next stage, called recrystallization, which grow and consume the old grains. This leads to a new grain structure with low dislocation density. With further annealing, the smaller grains are eliminated while the larger grains grow (grain grow stage). A lower energy configuration is then achieved with the reduction of grain boundaries.

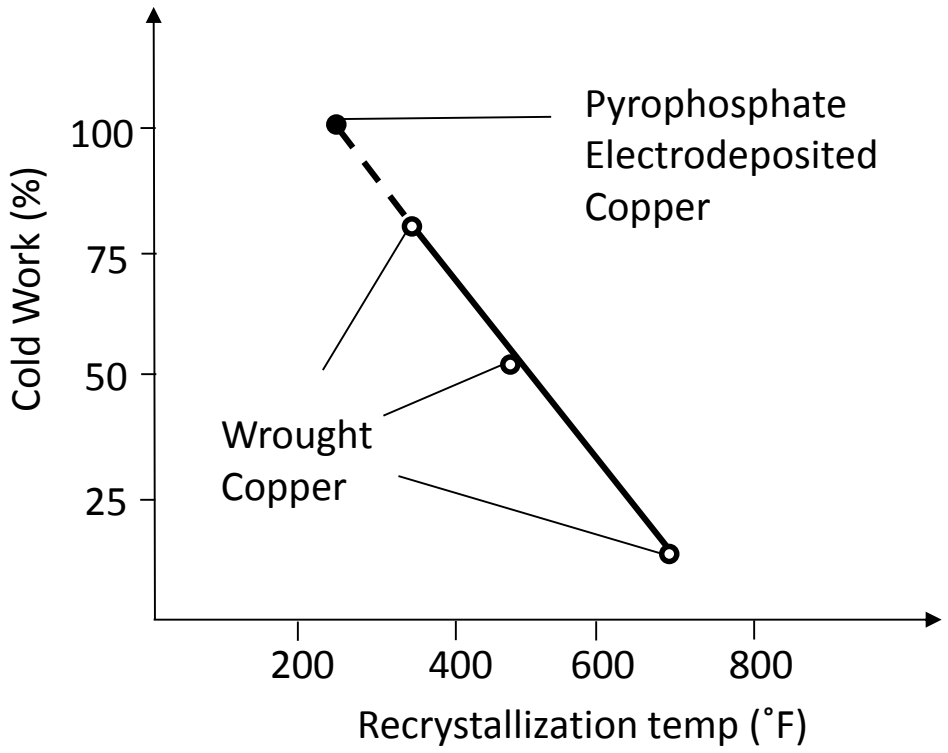

Figure 2-13 Recrystallization temperature for various copper materials (Adapted from Sherlin and Bjelland [69])

Figure 2-13 shows a plot of recrystallization temperature for electrodeposited pyrophosphate copper and wrought copper with different levels of cold work [69]. It indicates that the electrodeposited copper has behavior similar to that of 100% cold worked material. In addition, it can be seen from the figure that the higher the percentage of cold work, the quicker the recrystallization behavior is upon heating.

The mechanical properties of metals heavily depend on the dislocation densities and grain sizes. The dislocation density of an electrodeposited metal, or a heavily deformed metal, can go up to 10^{16} m^{-2}, which is much higher compared with a dislocation density of about 10^{11} m^{-2} for a metal in an annealed state. As discussed in Section 2.3, this leads to a much higher yield strength and lower ductility for electrodeposited or heavily deformed metals. On the other hand,

dislocation loss and rearrangement can occur once the electrodeposited or deformed metals are subjected to annealing, which results in a decrease in strength and increase in ductility, as shown for example in Figure 2-14 for electrodeposited copper.

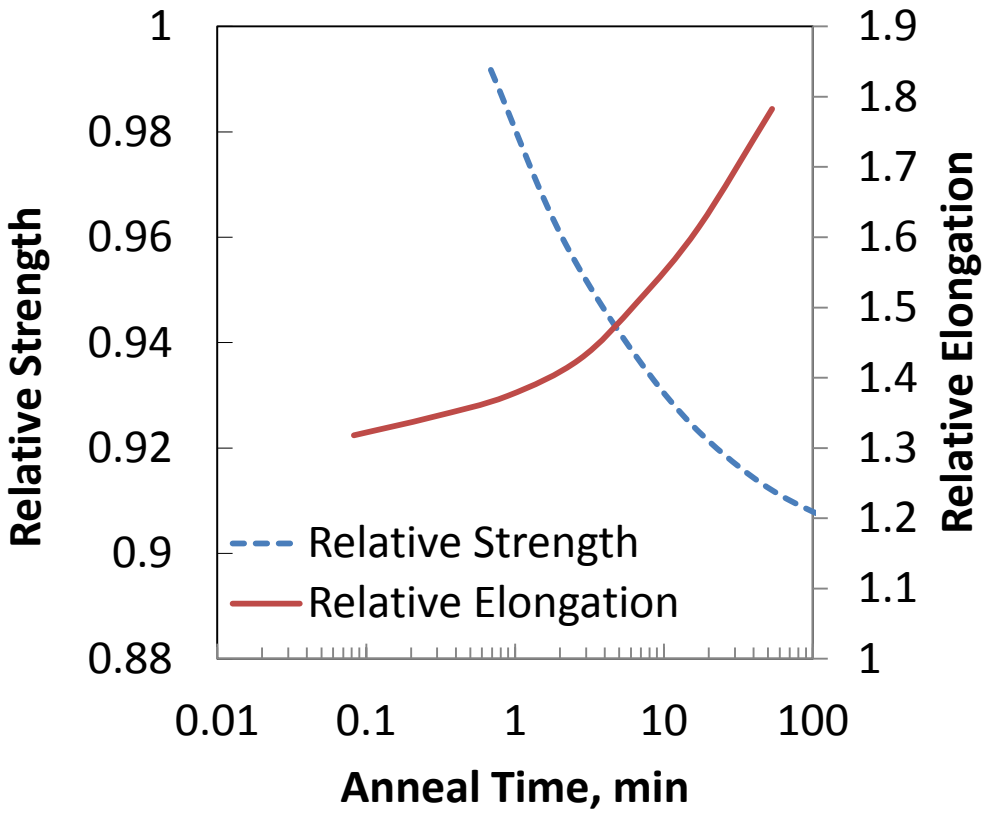

Figure 2-14 Relative ultimate strength loss and relative total elongation gain at 23 ˚C for electrodeposited copper foil (Adapted from Merchant [45])

2.6 Modeling and Simulation of Open-cell Foams

The macroscopic behavior of open-cell foams can be studied by investigating the behavior and mechanism of foam cell at the micro-scale. As shown in Section 2.2, Gibson and Ashby [13] derived semi-empirical solution for open-cell foams by studying a simple cubic cell model. The effect of the cell geometry was accounted for by introducing constants, which were

calibrated based on experimental data, into the analytical solutions. Meanwhile, numerical approaches are often used to study of open-cell foam materials as it allows a more sophisticated way to analyze both micro- and macro-scale behavior.

In many studies on the simulation of open-cell foam materials, numerical models are established with a foam microstructure idealized with Kelvin's cell structure, while the ligaments are usually modeled using beam-type elements. Such method has been shown to be successful in simulating the behavior of open-cell materials in their ability of reproducing most of its mechanical properties.

Laroussi et al.[70] investigated the plateau stress of an elastic open-cell foam material under compression based on a periodic lattice structure consists of tetrakaidecahedral cells. Gong et al. [14, 15] also established numerical models based on a Kelvin cell assuming linear elastic material behavior to study the response of a polyester urethane foam. The ligaments were modeled as shear-deformable extensional beams with non-uniform cross section along ligament length, based on a cell morphology study. Equation 2-11 shows the relationship between the ligament cross-sectional area along their length and the distance from the mid-span of the ligament [15], in which A is the cross sectional area at location of interest, A_0 is the cross-sectional area at mid-span of ligament, ξ is the ratio of the distance from the mid-span to the location of interest and the ligament length. The constants were determined by fitting the experimental data and it was found that $a = 86$ and $b = 1$ for the polyester urethane foam tested by Gong et al [15]. The model established by Gong et al. was able to adequately predict the modulus of the elastic foam studied and was used to investigate the crushing of elastic foam due to ligament buckling.

Jang and Kyriakides [18, 71] conducted thorough microscopic measurements on the geometry of aluminum (Al) open-cell foam ligaments and established beam-element-based finite element models using unit or multiple characteristic cells to predict the macroscopic compressive behavior of aluminum open-cell foams. Equation 2-11 was also used to define the cross-sectional area of the aluminum foam ligament along its length. The constants used in the equation were a = 36 and b = 1 for the aluminum foam studied by Jang and Kyriakides [18, 71]. Through this work Jang and Kyriakides showed that that proper definition of the ligament geometry is essential in the numerical simulation of metallic foams [18, 71].

Another factor that needs to be considered in the geometry of open-cell foam models is the randomness of the cell structure. It has been shown that the introduction of small perturbations to the basic Kelvin cell microstructure has advantages over the use of a perfect geometry, by breaking up the symmetry of the banded collapse localization of the perfect case and leading to a more random distributed buckling and collapse [71]. Furthermore, Gaitanaros et al. [72] established foam models using realistic random soap froth generated using the Surface Evolver software [51, 73] and found crushing patterns that were more similar to observations in corresponding experiments. As a result, it is necessary to consider certain randomness in the modeling of open-cell foams.

$$A(\xi) = A_0 f(\xi) = A_0\left(a\xi^4 + b\xi^2 + 1\right), \text{ where } \xi = x/l \qquad \text{Equation 2-11}$$

In addition to a proper representation of the foam cell structure, there are several other important factors in the modeling and simulation of open-cell foams when large deformation are considered, such as the contact between ligaments and material nonlinearity. Cell collapse occurs during the plateau regime in the compressive behavior of open-cell foams. When a cell collapses

completely, contact between ligaments occurs, which stiffens the local region and causes sequential collapse of neighboring cells. For numerical models based on Kelvin cell structures, spring elements can be introduced between collinear nodes in the loading direction to simulate ligament contacts [14, 15, 17, 71]. It needs to be noted that such method is usually only applicable to simulate uniaxial compressive behavior. On the other hand, beam to beam contact has been adopted to simulate the ligament contact in foam with random foam structures [72]. In this case, the cross-section size needs to be considered so that contact occurs on the outer surface of the ligament. Material nonlinearity needs to be included in the modeling of open-cell metal foams when large deformation is considered. Previous researchers have demonstrated that the compressive response of plain metal alloy foams is governed by localization at the ligament/cell level and thus simple material constitutive models (elastic-perfect plastic) have been shown to be sufficient to appropriately simulate the behavior. [13, 71].

Compared to the conventional open-cell metal foams, hybrid open-cell metal foams have more than one material and more complicated failure mechanisms. Thus, existing numerical models for are inadequate to capture the behavior of hybrid foams. First, existing models assume a homogeneous material, while a coating material with constitutive characteristics different from the base material need to be considered for simulating hybrid foams. Another factor needs to be addressed in numerical simulations of a composite material system is the differences in stiffness, strength and post-yield behavior (hardening and/or softening) of the constituents. This implies the use of constitutive models that are more realistic. Zhou et al. (Zhou et al., 2005) investigated the tensile behavior of an individual strut (ligament) extracted from an Al open-cell foam using micro-tests and found it to behave differently than the corresponding bulk alloy. In addition, as discussed in Section 2.3.3, the coating materials in hybrid foams are usually produced using

electrodeposition, leading to a nanocrystalline structure with higher yield stress but lower ductility compared to its bulk counterpart [46, 66, 74]. The noted material features can have great influence on the performance of hybrid foams and need to be considered. Thus, the use of elastic-perfect plastic material behavior obtained from bulk material testing, which has been typically used in most reported studies on open-cell metal foams, is inappropriate for the simulation of hybrid foams.

2.7 Concepts of Stress-wave Propagation in Solids

The behavior of objects when subjected to rapid changing loads can be quite different from its behavior under static or quasi-static conditions. A static equilibrium is maintained in quasi-static deformation in which the summation of forces acting on any element in the body is close to zero. However, when the deformation occurs at a very high rate, the associated stress and strain is not instantaneously transmitted from the deformed region to other regions of the body. Rather, they travel through the body at specific velocities and thus form waves [75].

The wave propagation in solids can be understood by imaging atoms connected by interatomic forces as spheres connected by springs, as shown in Figure 2-15. When force is applied, the resulted momentum is transferred from sphere to sphere (atom to atom) at a rate which provides the velocity of wave propagation.

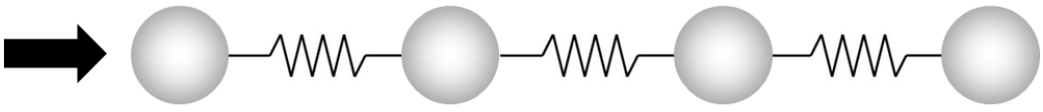

Figure 2-15 Transmission of disturbance from atom to atom

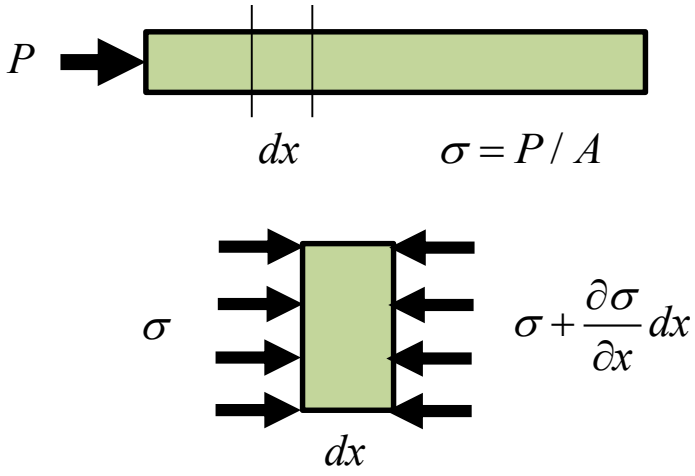

Figure 2-16 Wave propagation in a bar

The simplest case is wave propagation in a uniform, homogeneous bar, as shown in the schematic in Figure 2-16. By considering a segment in the bar and using Newton's second law, one can get the following equation [75]:

$$\frac{\partial \sigma}{\partial x} = \rho \frac{\partial^2 u}{\partial t^2} \qquad \text{Equation 2-12}$$

If assuming the deformation is elastic and Hookes's law holds:

$$E = \frac{\sigma}{\varepsilon} \qquad \text{Equation 2-13}$$

$$\varepsilon = \frac{\partial u}{\partial x} \qquad \text{Equation 2-14}$$

The following equation is then obtained:

$$\frac{\partial^2 u}{\partial t^2} = \frac{E}{\rho} \frac{\partial^2 u}{\partial x^2} \qquad \text{Equation 2-15}$$

And the velocity of the wave is:

$$C_0 = \sqrt{\frac{E}{\rho}} \qquad \text{Equation 2-16}$$

It can be seen that the speed of elastic wave in solids is related to the modulus and density of the material. It can be shown that the general solution to Equation 2-15 is in the form of Equation 2-17 [75], in which *F* and *G* are functions that describe the shape of pulses propagating in the positive and negative directions along the *x* axis, at a velocity of C_0. The shapes of these waves are unchanged with time.

$$u(x,t) = F(x - C_0 t) + G(x + C_0 t) \qquad \text{Equation 2-17}$$

Another important concept is the sonic impedance of the material, which is defined as the product of the medium density and its elastic wave velocity (note $\rho C = \sqrt{E\rho}$). When an elastic wave encounters a medium with different sonic impedance, it will be reflected and refracted, as shown in Figure 2-17. It needs to be noted that the figure only shows the reflected and refracted longitudinal waves while actually there will be reflected and refracted transverse waves (shear waves) [75]. The refraction and reflection angles are related to each other as stated in Equation 2-18 [75].

$$\frac{\sin\theta_1}{C_1} = \frac{\sin\theta_2}{C_1} = \frac{\sin\theta_3}{C_2} \qquad \text{Equation 2-18}$$

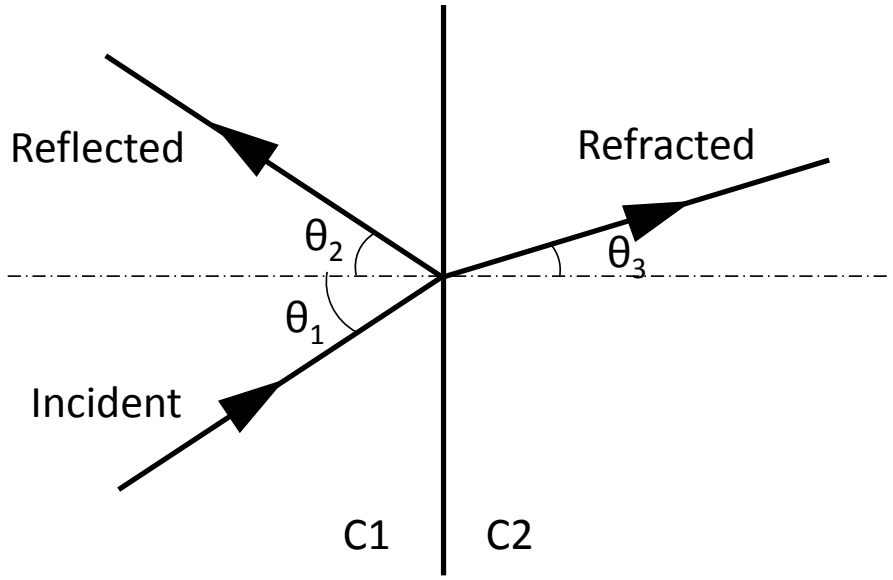

Figure 2-17 Reflection and refraction of longitudinal elastic wave encounters different medium

It is much simpler when the incident wave is normal to the interface, in which case a longitudinal wave only reflects and refracts longitudinal waves [75]. Considering a longitudinal wave travels from medium A to medium B, while the medium A has a larger sonic impedance (see Figure 2-18), one can calculate the amplitudes of the transmitted and reflected waves based on the densities and wave velocities of the two media, as given by Equation 2-19 and Equation 2-20 [75].

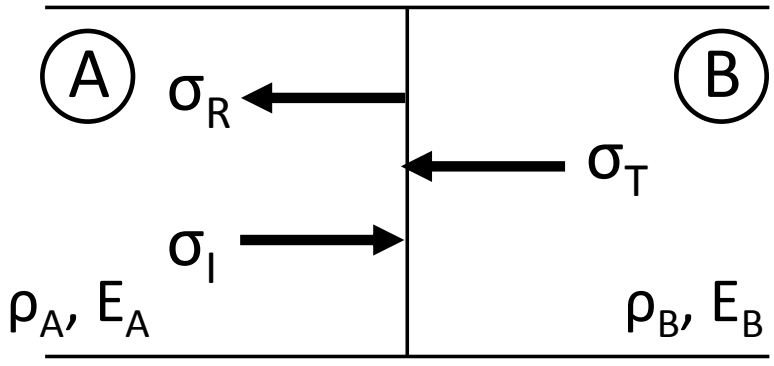

Figure 2-18 Longitudinal wave encountering boundary between medium A and medium B

$$\frac{\sigma_T}{\sigma_I} = \frac{2\rho_B C_B}{\rho_B C_B + \rho_A C_A} \qquad \text{Equation 2-19}$$

$$\frac{\sigma_R}{\sigma_I} = \frac{\rho_B C_B - \rho_A C_A}{\rho_B C_B + \rho_A C_A} \qquad \text{Equation 2-20}$$

Equation 2-19 and Equation 2-20 show that the amplitude of the transmitted and reflected pulses are determined by the impedances of the materials. If $\rho_B C_B > \rho_A C_A$, the reflected pulse has the same sign as the incident pulse. On the other hand, if $\rho_B C_B < \rho_A C_A$, the reflected pulse would have an opposite sign to that of the incident pulse.

In a ductile material, plastic deformation occurs when the stress in a material exceeds the elastic limit. When the amplitude of a pulse transmitted to a material has an amplitude exceeding the elastic limit of the material, the pulse will be decomposed in to two components, an elastic wave and a plastic wave. The velocity of the plastic wave is given by Equation 2-21, in which $d\sigma / d\varepsilon$ is the slope of the plastic region of the stress-strain curve.

$$V_p = \left(\frac{d\sigma / d\varepsilon}{\rho} \right)^{1/2} \qquad \text{Equation 2-21}$$

It can be noted that within elastic limit, $d\sigma / d\varepsilon$ is the modulus *E* for a material, which is usually higher in the elastic regime than the plastic one. As a result, the plastic wave travels at a lower speed than an elastic wave.

2.8 Functionally Graded foam materials

When a structural component is subjected to certain loading and boundary conditions, the demand in material performance may vary with location within the component. In a functionally graded material the microstructure and composition has a gradual variation over the structure,

which results in an overall optimized performance of the components while meeting the requirement of a specific function and application [19, 20].

As discussed in Section 1.2.3, many cellular materials found in nature such as bone, wood and bamboo are functionally graded. Inspired by these naturally engineered products, many studies have been conducted over the past two decades in the development of so called functionally graded cellular/foam materials. The fabrication of graded cellular materials can be basically grouped into three categories. First, cellular materials with graded properties can be obtained by creating a density gradient directly in metallic porous materials through chemical or electrochemical processing. Neubrand [24] fabricated functionally graded porous materials based on the evolution of porosity gradients in porous electrodes that undergo dissolution or deposition due to electrochemical gradation. Alternatively, Matsumoto et al. [25] used chemical dissolution to create a density gradient in Al open-cell foams. However, the strength and stiffness of the fabricated materials were found to decrease more rapidly with respect to density than that of typical metallic foams.

Metallic cellular materials with density gradient can also be fabricated through replication process based on graded precursors or performs. Pollien et al. [26] produced sandwich beams with graded foam core using replication processing with a preform of compacted salt layers of different density. It was found that the graded foam beams had little advantage in stiffness-limited design but may be beneficial in load-limited design. Brothers and Dunand [2, 4] fabricated density-graded Al foams using replication based on non-uniformly compressed polymer foam precursors and observed a smoothly rising plateau (plastic) stress. Hangai et al. [5] produced functionally graded closed-cell Al foam by bonding precursors that have various amounts of blowing agent using friction stir processing and the obtained material

had two different deformation stages and two plateau regions. Hassani et al. [76] fabricated graded foams using a powder-space holder technique and found that the cell-size graded foams has better energy absorbing performance compared to the non-graded foams.

In another approach to obtain graded designs, layers of cellular materials with different densities can be combined to create step-wise property gradients. Gupta [28] fabricated graded syntactic foams filled with hollow particle (microballoons) with a wall thicknesses gradient and found it possible to control the compressive modulus, strength and total energy absorption. Zeng et al. [29] studied the impact behavior of functionally graded cellular materials made of graded polymeric hollow sphere agglomerates and found that by placing the hardest layer at the impact end and the weakest layer at the remote end leads to maximized energy absorption and minimized transmitted forces. In addition, studies on functionally graded foams fabricated by bonding foam layers with different densities have also been reported [30, 77, 78].

Since foams structures are usually used as energy absorbers and impact resistant layers, many studies have been conducted to investigate the performance of functionally graded foam structures under dynamic loading conditions. Cui et al. [1, 33] investigated the behavior of functionally graded foam materials under impact using finite element analyses and found that functionally graded foams can reduce the duration of the high acceleration during an impact and have superior energy absorption performance over equivalent uniform foams under low energy impacts. They also found that convex gradients perform better than concave gradients and that a better performance can be achieved by increasing the density range. Zeng et al. [29, 79] found that placing the hardest layer as the first impacted layer and the weakest layer on the remote side had some benefit to maximize energy absorption with a minimum force level transmitted to the protected structures. However, placing the weakest layer at the impacted end is preferable to

avoid the breakage of the face sheet for sandwich panels subjected to localized impact. Ajdari et al. [34] studied the in-plane crushing of regular, irregular and functionally graded honeycombs using numerical methods and found that a density gradient could significantly change the deformation mode and energy absorption of cellular structures under both low and high crushing velocities. Wang et al. [30] and Gardner et al. [31, 32] conducted shock tube experiments to study the dynamic response of sandwich panels with graded styrene foam cores. They found that the overall blast performance and structural integrity can be improved by increasing the number of monotonically graded foam core layers and by applying polyurea between the foam core and the back face sheet. Zhou et al. [78] studied low velocity impact response on sandwich structures with foam core that has graded densities using experimental and numerical method and found a better performance of graded core structures over the monolithic cores.

The experimental studies conducted on functionally graded cellular/foam materials so far have been limited to one-dimensional property gradient (usually the loading direction). And to the author's knowledge, there is no reported experimental effort for the fabrication and investigation of two-dimensional functionally graded foams in public literature. This can be partly attributed to the difficulty in creating gradients with higher dimensions. However, the higher dimensional spatial variations in the properties of cellular/foams in analogy to cortical bone [22] offer greater opportunity to optimize mechanical performance when foam materials are used as structural elements. Wang et al. [35] considered graded cellular structure in conceptual design of an acetabular component which changes from solid metal at the liner section to high porosity at the implant-bone interface to encourage bone growth upon implantation. Daxner et al. [36] conducted a numerical study and found that the distribution of foam density can be optimized with respect to structural strength and stiffness for a given loading condition. However,

none of the complex designs can be realized with manufacturing processes for traditional cellular materials. Thus, development of fabrication methods and the investigation of cellular/foam structures with two-dimensional property gradient are of great interest.

CHAPTER 3 MODELING AND SIMULATION OF QUASI-STATIC COMPRESSIVE BEHAVIOR OF AL/CU HYBRID FOAMS

3.1 Overview

In this chapter, finite element method approaches considering both coating and base material damage are used to investigate the failure mechanisms and mechanical performance of nanocrystalline hybrid open cell foams at the micro- and macro-scales. First, models of single foam ligaments combined with sectional analyses were used to obtain further understanding of micro-scale failure mechanisms. Experimentally validated multi-cell models are then presented to study the macroscopic compressive behavior.

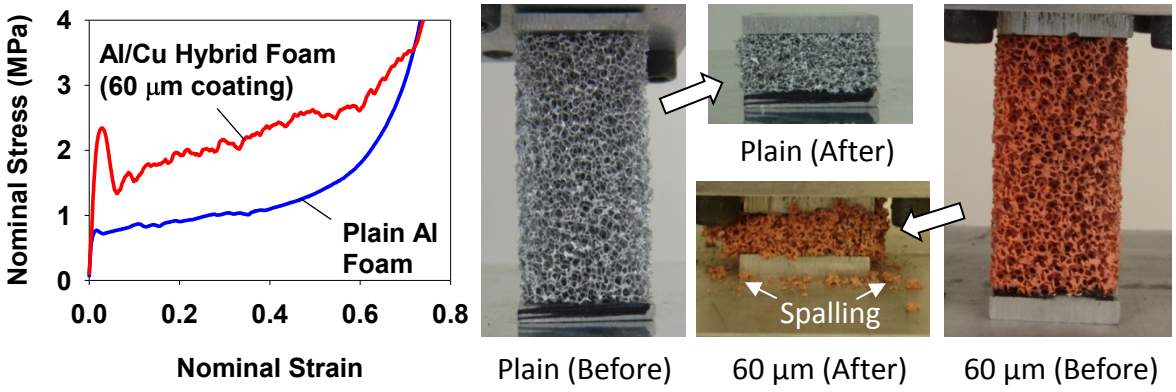

Figure 3-1 Stress-strain curve and pictures of 40 PPI plain Al foam and Al/Cu hybrid foam with 60 μm coating under compressive loading [8].

Due to the multi-material characteristics and the more complicated failure mechanisms in hybrid foams, existing numerical models for traditional open cell metal foams are inadequate to capture the behavior of hybrid foams. First, existing models assume a homogeneous material, while a coating material with constitutive characteristics different from the base material need to

be considered for simulating hybrid foams. Another factor needs to be addressed in numerical simulations of a composite material system is the differences in stiffness, strength and post-yield behavior (hardening and/or softening) of the constituents. This implies the use of constitutive models that are more realistic. Zhou et al. (Zhou et al., 2005) investigated the tensile behavior of an individual strut (ligament) extracted from an Al open-cell foam using micro-tests and found it to behave differently than the corresponding bulk alloy. In addition, the coating materials in hybrid foams are usually produced using electrodeposition, leading to a nanocrystalline structure with higher yield stress but lower ductility compared to its bulk counterpart [46, 66, 74]. The noted material features can have great influence on the performance of hybrid foams and need to be considered. Thus, the use of elastic-perfect plastic material behavior obtained from bulk material testing, which has been typically used in most reported studies on open-cell metal foams, is inappropriate for the simulation of hybrid foams.

3.2 Material Model

As mentioned in Section 3.1, material properties based on macro-scale tests are not appropriate in the simulation of Al/Cu hybrid foams, especially for the nanocrystalline coating. In this study, the material models defined for the Al core and Cu coating were based on the results from micro-scale tensile experiments on single Al foam ligaments conducted by Zhou et al. [80] and tensile experiments on thin electrodeposited Cu films by Zhang et al. [66]. Both of these studies have shown that the behavior of Al and Cu at the micro-scale is quite different from their bulk response. Figure 3-2 shows the material behavior from experiments [66, 80] and the material models used in this study. The true stress σ in the hardening region ($\sigma > \sigma_y$) was defined using Equation 3-1, where σ_0 and n are the hardening parameters.

$$\sigma = \sigma_0 \varepsilon^n \qquad \text{Equation 3-1}$$

A ductile damage model [81] was used for both Al and Cu in the numerical study such that damage would initiate once the defined fracture strain was reached and elements would degrade and fail. A summary of the key parameters used in the material model definitions is given in Table 3-1, where E is the Young's modulus, υ is the Poisson's ratio, σ_y is the yield strength, ε_{ft} is the fracture strain in tension and δ_{ft} is the effective plastic displacement at failure.

Table 3-1 Material model parameters for aluminum (Al) and copper (Cu).

Material	E (GPa)	v	σ_y (MPa)	σ_0 (MPa)	n	ε_{ft} (mm/mm)	δ_{ft} (mm)
Aluminum	70	0.33	193	511	0.17	0.5	0.005
Copper	102	0.33	150	329	0.12	0.08	0.0008

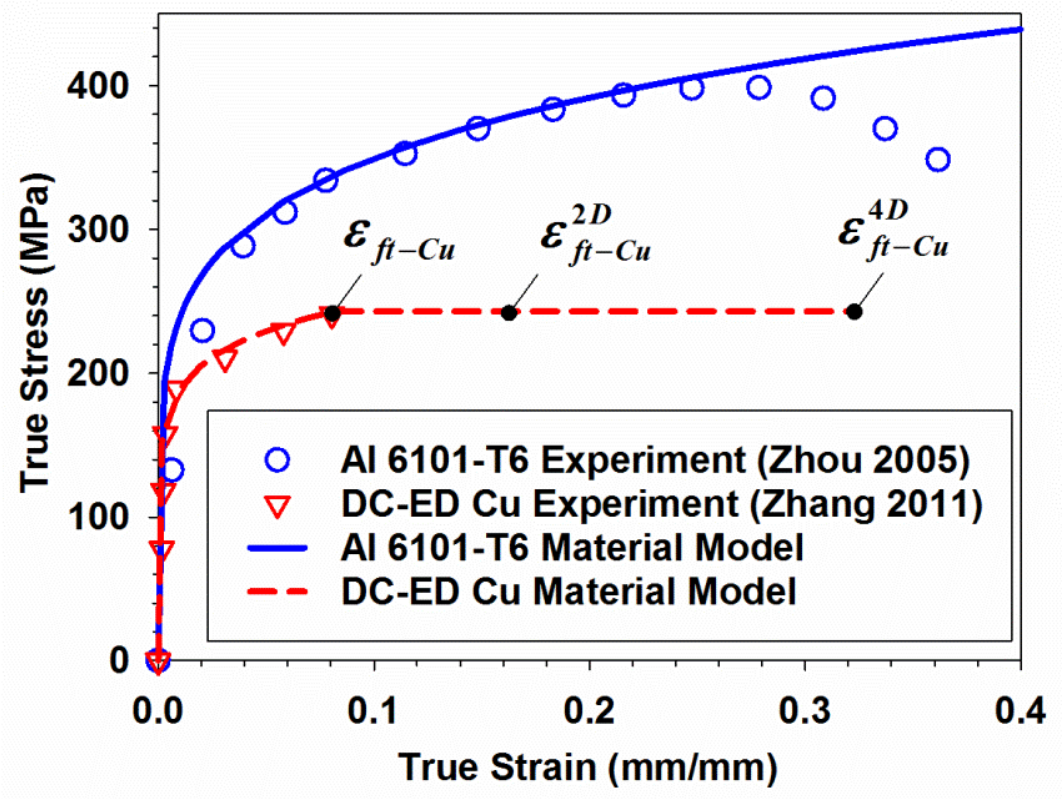

Figure 3-2 Behavior of aluminum (Al) 6101-T6 and electrodeposited copper (Cu) from literature [66, 80] and corresponding material models used in the finite element simulations

3.3 Section flexural response

The collapse of cellular foams in compression is dominated by inelastic flexural behavior. Thus, the first step taken to understand the behavior of Al/Cu hybrid foam was to evaluate their sectional flexural response. Sectional, or moment-curvature, analyses were performed on ligament cross-sections of a 40 PPI Al/Cu hybrid foam. The analyses were performed using a fiber-based approach for unidirectional bending and with uniaxial constitutive material definitions as presented in Section 3.2. The characteristic moment curvature response a hybrid foam ligament section is shown in Figure 3-3(a) while the effect of coating thickness is shown in

Figure 3-3(b). Examining Figure 3-3(a) it can be seen that the section flexural response of a hybrid foam ligament features a pronounced peak before a large capacity drop, followed by a plateau region and later further gradual degradation at larger deformations. This behavior can be explained using the bending strain and stress schematics shown in Figure 3-4. Point "a" corresponds to a state when the extreme tensile fiber in the Cu coating reaches failure. At this point, the maximum moment capacity of the section has been reached and further deformation causes progressive fracture of the coating. Point "b" refers to the state when cracking has propagated through the coating and the core is exposed, at which point the moment capacity of the section has been reduced due to the loss of coating. It can be seen in Figure 3-3(b) that such capacity loss is more significant in ligaments with thicker coating as a larger percentage of the load is carried by the coating before failure. During section deformations from point "b" to "c" there is a combination of plastification and hardening of the core and coating materials as well as further fracture of the coating material on the tensile region. Combination of these two effects leads to a relatively constant moment capacity. The onset of core fracture (point "d") takes place at large section curvature and is accompanied by rapid capacity loss. It can also be seen in Fig. 8(b) that point "c" occurs at smaller curvatures as the coating thicknesses increases. This is because fracture of core starts earlier in hybrid foams with thicker or stronger coating since both of these conditions lead to a larger compressive region in the ligament's section. The sectional analyses indicate that failure of the coating material in hybrid foam ligaments can lead to a significant loss in load carrying capacity and early ligament fracture, both of which are more severe with thicker coating.

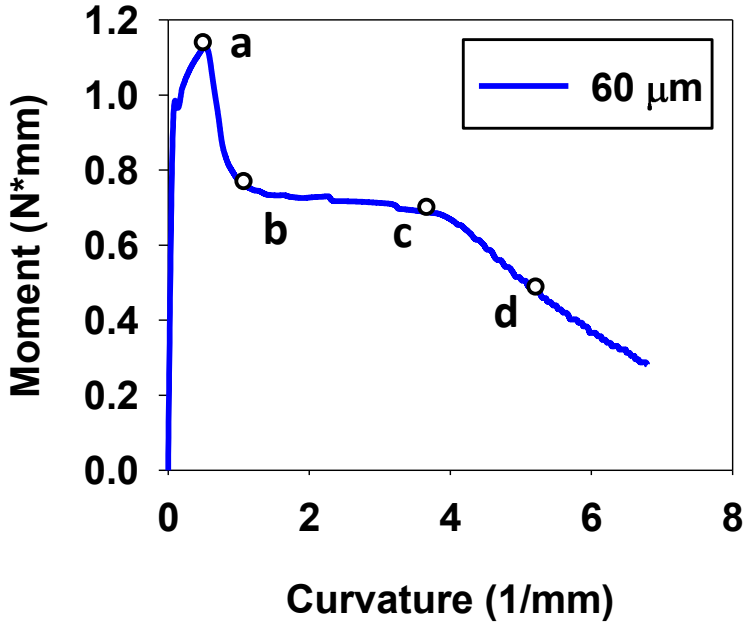

(a)

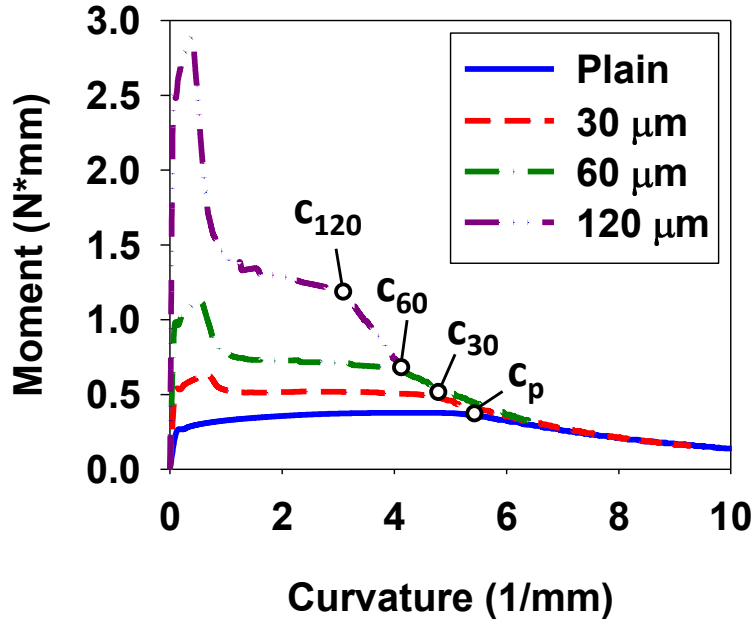

(b)

Figure 3-3 Results from sectional analyses on the mid-span sections of 40 PPI ligaments. (a) Characteristic moment-curvature response of an Al/Cu hybrid foam. (b) Moment-curvature response of mid-sections of Al/Cu hybrid foam ligaments with different coating thickness.

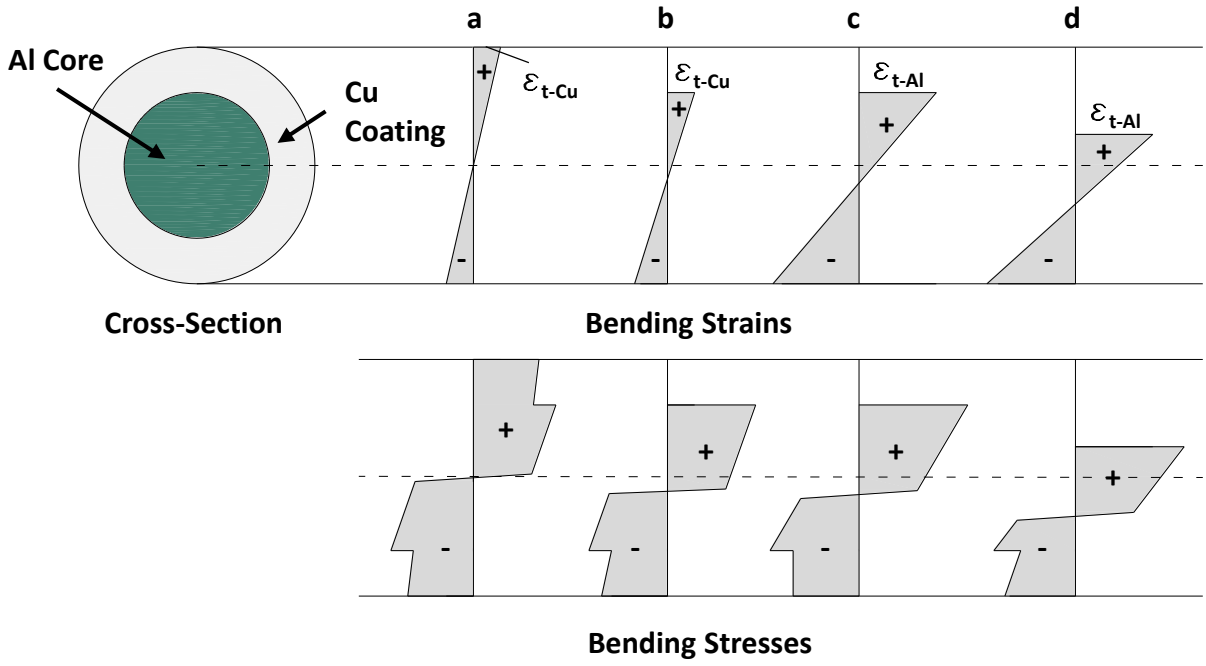

Figure 3-4 Schematic of the bending strain and stress profiles in the cross-section of a ligament in a Al/Cu hybrid foam

3.4 Single Ligament Modeling

Studying the behavior of individual ligaments can offer great information on the macroscopic performance of open-cell foams [13]. A numerical study was thus conducted on single ligament models from an Al 6101-T6 foam[81][81][81][81] to achieve a better understanding of the microscopic behavior and failure mechanisms of Al/Cu hybrid foams. The numerical analyses in this study were carried out using the commercial finite element program ABAQUS/Explicit [81] with considerations for geometric and material nonlinearities. At the micro-level the ligaments of loaded open-cell foams are subjected to complicated loading and boundary conditions and usually undergo large inelastic deformations. However, only two types of boundary conditions that represent two typical deformation modes were considered in this

study. Both the Al core and the Cu coating were discretized using solid elements (C3D8R: eight-node linear bricks with reduced integration and hourglass control). A circular shape cross-section was assumed and it was defined to be non-uniform along the length (L) of the ligament based on the model proposed by Jang and Kyriakides [71]. In the noted model the cross-sectional area A at different locations depends on the distance from the mid-span (x) and the cross-sectional area at the mid-span (A_0) of the ligament (see Figure 3-5(a) and Equation 3-2). The diameter (d_0) of the cross-section at mid-span of a base 40 PPI Al foam ligament was 0.192 mm based on the measurements by Wang [8] and the average ligament length for a 40 PPI Al-6101-T6 foam (1.04 mm) measured by Jang and Kyriakides [18] was used as the length (L) of the ligament.

$$A(\xi) = A_0 f(\xi) = A_0\left(36\xi^4 + \xi^2 + 1\right) \qquad \text{Equation 3-2}$$

, where $\xi = x / L$.

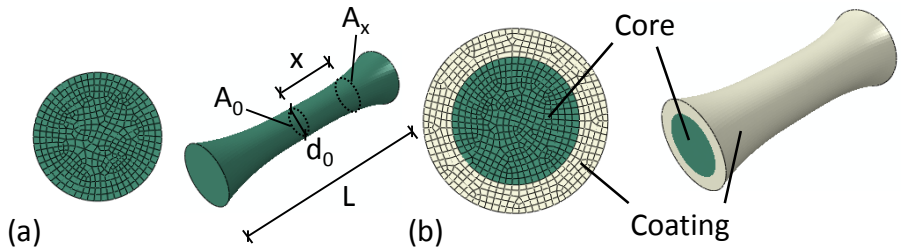

Figure 3-5 Single ligament models for 40 PPI open-cell foam. (a) Uncoated ligament model; (b) Coated ligament model

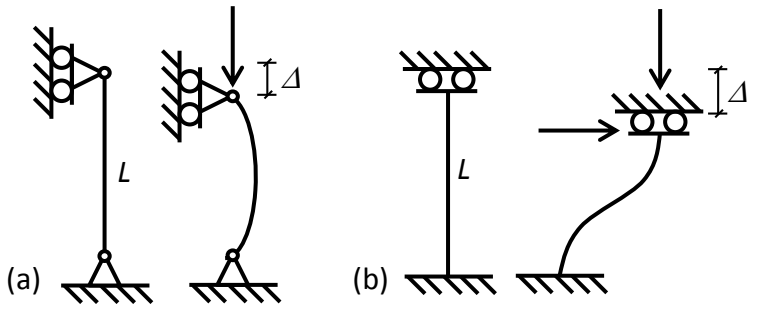

Figure 3-6 Two boundary conditions used for single ligament models. (a) Free rotation boundary condition; (b) Fixed-rotation boundary condition

The Cu coating in the model was defined by adding a sleeve with corresponding thickness around the Al core part along the ligament length (Figure 3-5(b)). A perfect bond was prescribed between the coating and core model parts. Three thicknesses were considered, namely, 30 μm, 60 μm and 120 μm. The cross-sectional surface on each end was coupled with a controlling node on which the boundary conditions were applied. Two different types of boundary conditions (see Figure 3-6) were defined for the single ligament models, namely a free-rotation boundary condition and a fixed-rotation boundary condition. The free-rotation boundary condition was used to represent ligaments with flexible ends where the deformation would be dominated by inelastic buckling and bending. For this model the ends of the ligament were allowed to rotate while only one end could move along the ligament's longitudinal axis. The loading was defined by applying a displacement on the free translational end in the axial direction. To invoke inelastic buckling behavior, an initial imperfection was seeded to the ligament geometry based on the first buckling mode shape, which was obtained from a separate eigenvalue buckling analysis. The model with fixed-rotation boundary conditions was used to

investigate the behavior of ligaments dominated by shear demands. In this case, the rotational degrees of freedom of both ends were constrained. Lateral and axial translational displacements of equal magnitude were applied on one end of the ligament while the other end was fixed.

As previously noted, ligaments in a real loaded foam specimen have more complicated boundary conditions and loading demands than what was considered in these single-ligament simulations. However, the models in this study were used to gain a better understanding of the effect of coating ductility on the failure mechanisms and performance of Al/Cu hybrid foams rather than to accurately simulate actual micro-scale behavior. Thus, the simplified models presented here are considered adequate and necessary for the purpose of this study since the major mechanism involved in the macro-level deformation of metal foams is the inelastic buckling response of ligaments [13].

3.4.1 Inelastic Buckling of Single Ligaments

Figure 3-7 and Figure 3-8 show representative results of the micro-scale evaluation of single ligament response. Specifically, the figures show the deformed shapes of the ligaments during their inelastic response and profiles of the maximum principal strain along one the surface of the Al core. The information shown in both figures corresponds to the stage at which the vertical displacement at the center of the top surface of the ligament model reaches half of it its original length L (i.e., $= 0.5L$). Elements with excessive deformation were removed from the deformed shape views. It can be observed that the inelastic deformations were mainly concentrated at the center region in the free-rotation ligament models and at two critical regions in the fixed-rotation models. The noted critical regions are those with higher curvature ( ) demands, which are qualitatively shown by considering the moment (M) gradient and the section stiffness (EI) along the ligament (Note: $= M/EI$). However, the response of coated and

uncoated ligaments was very different. Coating rupture is predicted for all hybrid models at the locations of high curvature. In addition, rupture of the Al core can be observed in the coated ligaments and is more severe in ligament with thicker coatings. This can be seen by observing the curvature profiles and the threshold line that defines the fracture strain limit for the Al core. Thus, Fig. 10 shows how at the noted deformation level the ligament with a 120 μm Cu coating has almost ruptured completely while no apparent rupture can be seen in the uncoated ligament. This can be explained by the shift of neutral axis that occurs after coating rupture as shown in Figure 3-4 and discussed in Section 3.3. The single ligament model results also show that damage tends to concentrate in the ruptured section as the coating thickness increases. That is, the regions of high curvature are smaller in models with thicker coatings. This follows from the larger capacity drop experienced by sections with thicker coatings as shown in Figure 3-3(b). The same behavior features can be seen in the fixed-rotation ligament modeling results shown in Figure 3-8. From these results it can be seen that while a thicker coating reduces the strain in the compression side of the core at critical sections, while concentrated peak strains can be seen on the tensile side. Such strain concentrations suggest possible ligament fracture at these locations. The observations and findings from the single ligament models imply that Al/Cu hybrid foams with thicker coatings will display a more brittle response during their inelastic collapse.

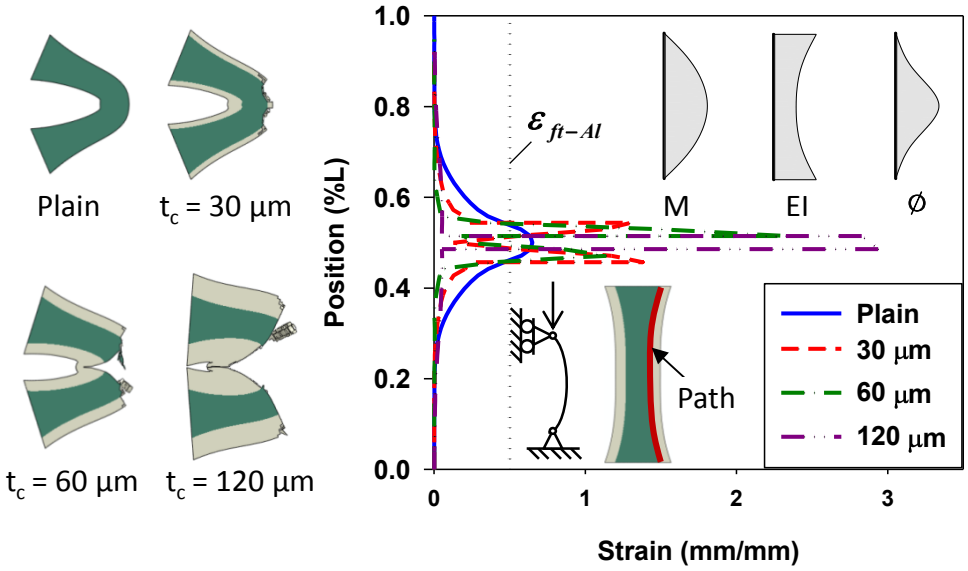

Figure 3-7 Maximum principal strain profiles on the core surface of the free-rotation single ligament model at $\Delta = 0.5\ L$

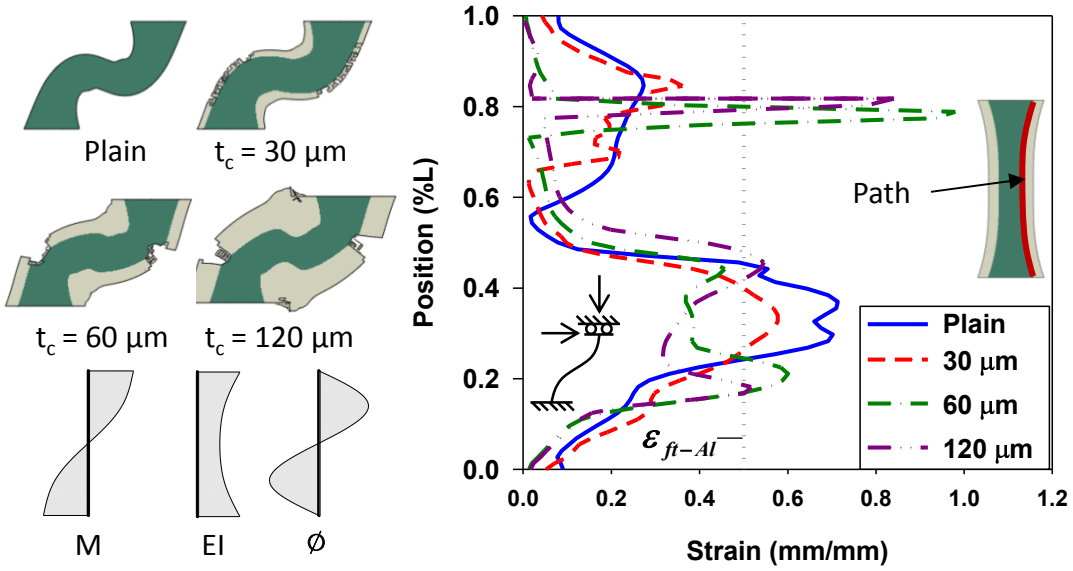

Figure 3-8 Maximum principal strain profiles on the core surface of the fixed-rotation single ligament model at $\Delta = 0.5\ L$

3.4.2 *Effect of Coating Ductility*

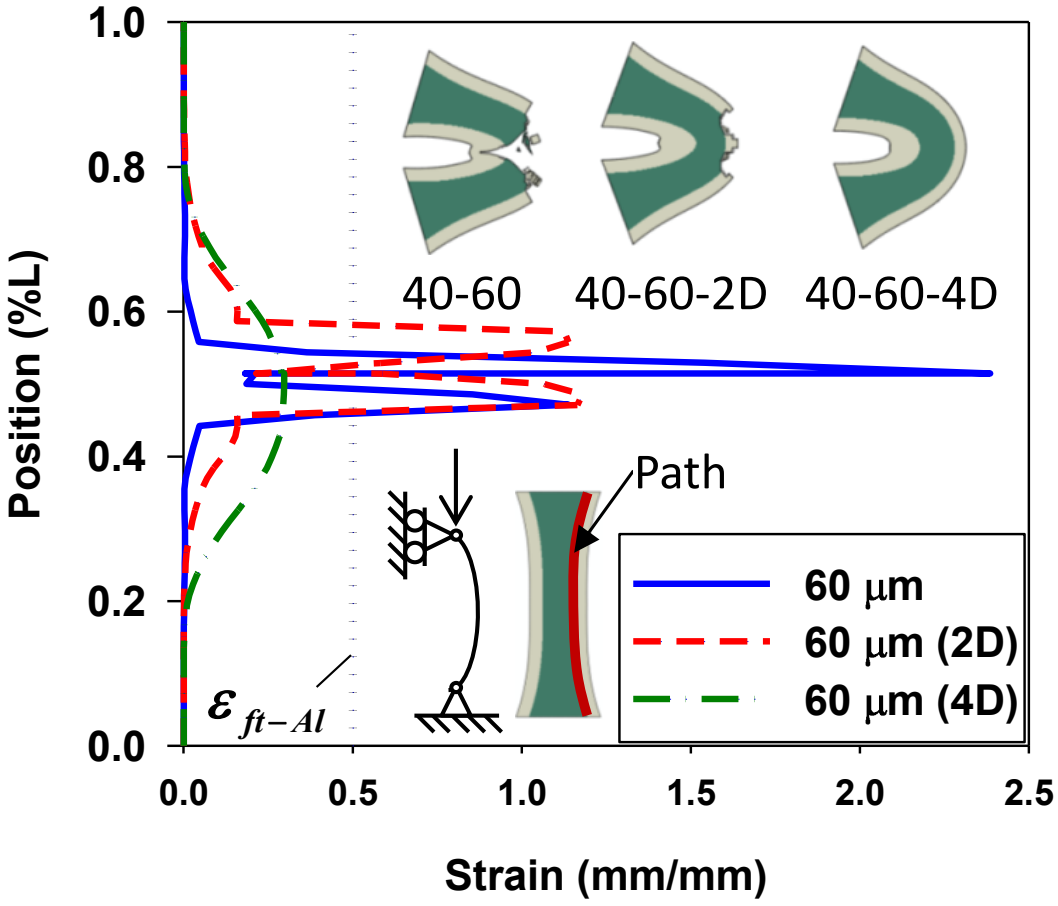

Figure 3-9 Maximum principal strain profiles of 40 PPI single ligament models coated with 60 μm Cu with different ductility capacity at $\Delta = 0.5\ L$

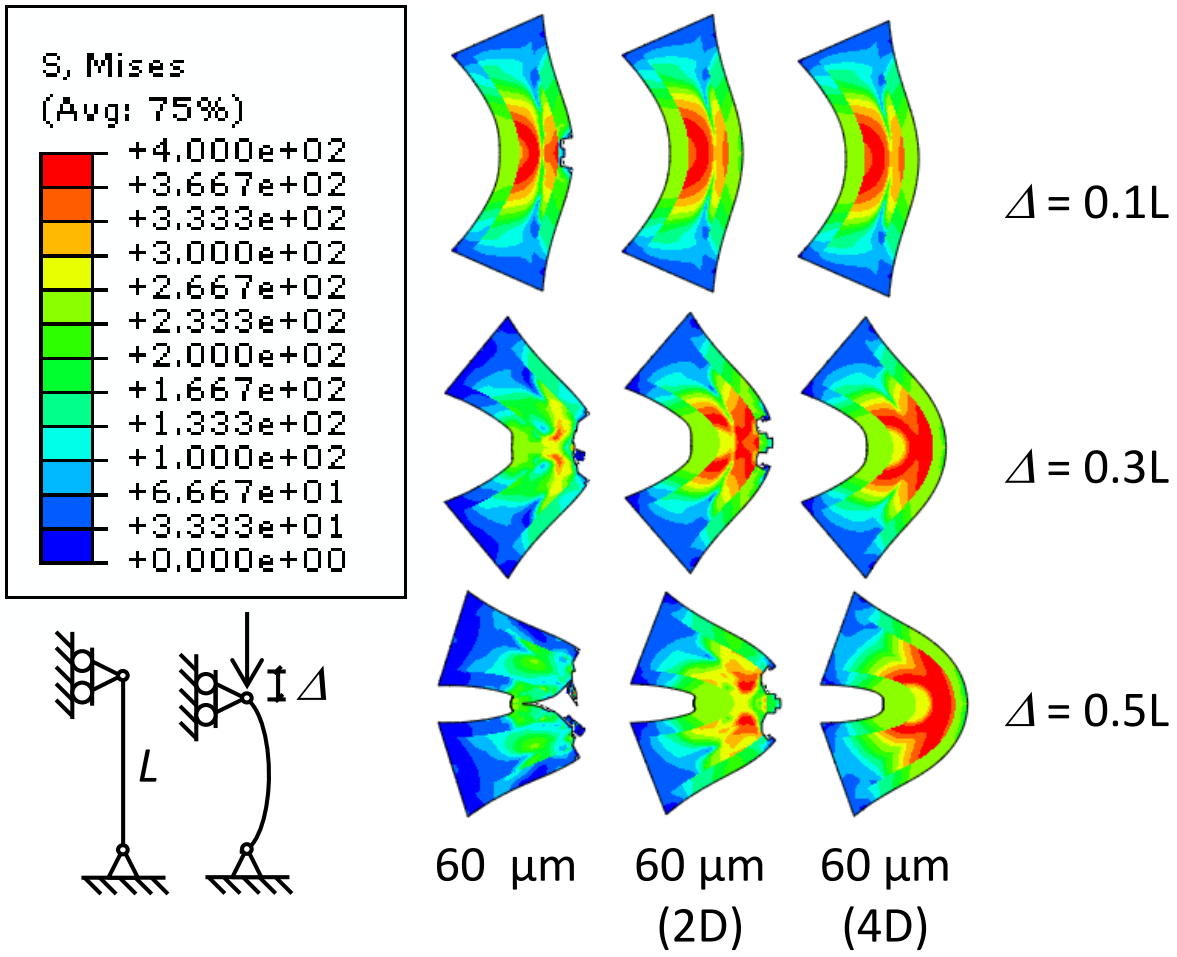

Figure 3-10 Von-Misses stress contours of 40 PPI ligament models coated with 60 µm Cu with different ductility capacities at different deformation states

The previous discussions and results have shown that rupture of the coating and ligament core can occur in Al/Cu hybrid foams at large deformations and thus lead to brittle macro-scale behavior for foams with thicker coatings. As noted earlier, this is due to the low ductility of the nanocrystalline coating material. As a result, it is of interest to investigate the effect of coating ductility on the performance of Al/Cu hybrid foams to provide guidance on possible improvements in the processing methods. Figure 3-9 shows deformed shapes and maximum principal strain profiles on the Al core for single ligament models of 40 PPI Al foam with 60 µm

nanocrystalline Cu coating and free-rotation boundary conditions. Three cases with different assumed ductility capacities for the coating material were considered. Cases with two times ($\varepsilon_{ft-Cu} = 0.16$) and four times ($\varepsilon_{ft-Cu} = 0.32$) the original ductility capacities are identified with "2D" and "4D", respectively. It can be seen that rupture of both coating and core is predicted for the model with original coating ductility. However, with increased coating ductility capacity the localized failure is reduced and no ligament fracture is predicted when the ductility capacity of the coating is increased four times. The maximum principal strain profiles show that the strain concentrations are significantly reduced and that the region experiencing large deformations becomes larger with increased coating ductility.

Figure 3-10 shows Von-Mises stress contours along a longitudinal section of the single ligament models with different coating ductility levels. It can be seen that at small axial deformations ($\Delta < 0.1L$), the stress distributions are similar in all cases. However, the decrease and redistribution of stresses is obvious as the coating and core rupture and the ligament loses load carrying capacity. It can also be seen that increased coating ductility delays fracture of the ligament, thus allowing it to resist additional load even at large deformations. Figure 3-12 shows plots of axial force and total internal strain energy versus the axial shortening displacements for ligament models with different coating ductility. The total strain energy reported by ABAQUS, which is the sum of the recoverable strain energy, the energy dissipated by plastic deformations, and the energy dissipated by damage, can be considered an indication of the energy absorption capacity. It can be seen that in all cases the axial forces peak at small deformation levels and drops rapidly during the inelastic buckling response of the ligament. From Figure 3-11 it can be seen that the peak load carrying capacity of the coated ligaments is considerably higher compared to the uncoated ligament. However, the coated ligament model with original coating

ductility loses its entire load carrying capacity at large deformations ($\Delta > 0.45L$). Conversely, increased coating ductility notably improves the ligament's residual load carrying capacity. Figure 3-12 and Table 3-2 show that the energy absorption capacity of the ligament model with original coating ductility reaches a plateau at about 0.45 strain while coatings with increased ductility can significantly improve the ligament's energy absorption capacity.

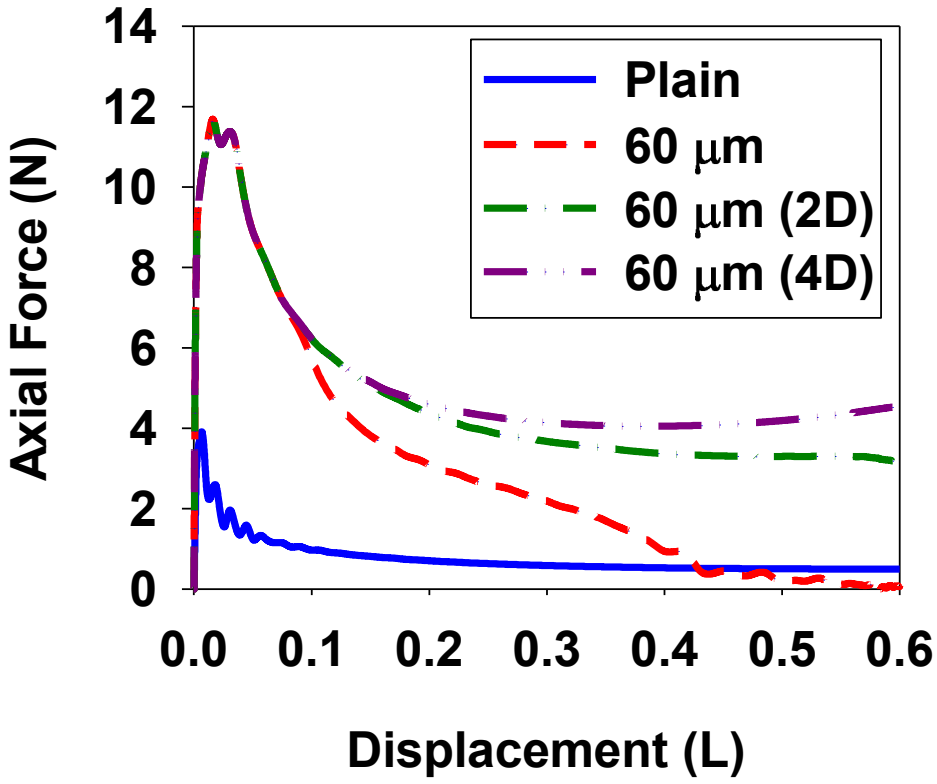

Figure 3-11 Load-displacement response of single 40 PPI ligaments with different ductility Cu coatings under compression

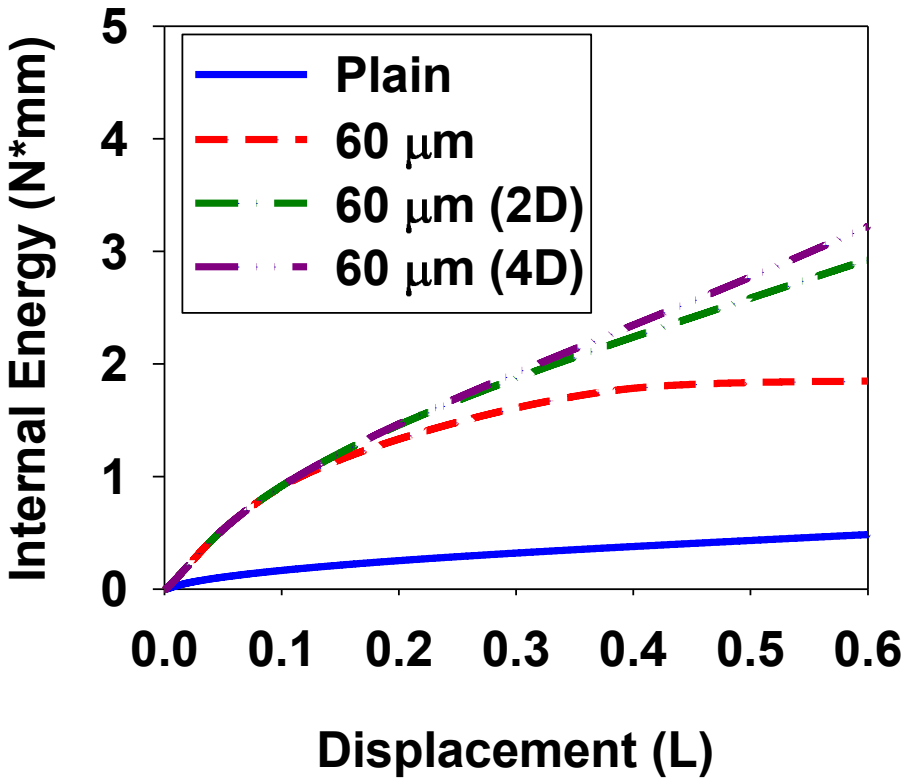

Figure 3-12 Internal Energy-displacement response of single 40 PPI ligaments with different ductility Cu coatings under compression

Table 3-2 Energy absorption of single ligament models from 40 PPI foam with 60 μm Cu coating ($\Delta = 0.6L$).

Coating Thickness	Energy Absorption (N·mm)	Energy absorption enhancement
60 μm	1.85	-
60 μm (2D)	2.93	58%
60 μm (4D)	3.22	74%

In reality the deformation mechanism of a single ligament involves axial, bi-directional bending, shear and torsion effects, which lead to more complicated loading and boundary conditions than those used in this study. However, the presented single ligament simulations have shown that coatings with low ductility will cause concentrated failure at critical sections of the foam ligaments and reduce the ligament's energy dissipation capacity. Such effect is also expected to occur under the more complex conditions in an actual loaded foam ligament.

3.5 Multi-cell Modeling

Numerical models with multiple characteristic cells were established to investigate macroscopic behavior. Jang and Kyriakides [71] have shown that a single characteristic cell model based on the Kelvin cell geometry with periodic boundary conditions can be used to adequately predict the compressive behavior of Al foam, but that obtaining a more realistic crushing response (the initiation and expansion of collapsing cell bands) requires using models with multiple characteristic cells. It needs to be noted that the numerical models used by Jang and Kyriakides [71] assumed an elastic-perfect plastic material response and did not consider

material damage or failure, which is a valid assumption in the simulation of homogeneous Al foams. However, the definition of material failure is essential for the simulation of Al/Cu hybrid foams since their failure mechanism has been observed to involve rupture of the coating, even ligaments, and to have an increasingly brittle response with thicker coatings [8]. As will be shown in Section 3.5.5, a unit-cell model with periodic boundary conditions is not suitable for the simulation of hybrid foams if the low ductility capacity of the coating is considered. As a result, numerical models with foam geometry of finite dimensions (multiple cells) were used for the investigation.

3.5.1 Foam Geometry

The models used in this study were established based on the Kelvin cell model (or tetrakaidecahedron) by packing characteristic cells as done by Jang and Kyriakides [71]. Kelvin cells have 6 squares and 8 hexagons for a total of 14 faces per cell and are highly optimized partitions of space to minimize surface energy. Such structure have been widely used to study cellular materials [14, 15, 71, 82-85] as it is deemed to naturally appear in foams due to the growth and interaction of gas bubbles during the foaming process [73]. The multi-cell models consisted of 64 characteristic cells with four cells in each dimension. Figure 3-13 shows front and isotropic views of a multi-cell model. It has been shown that the introduction of small perturbations to the basic Kelvin cell microstructure has advantages over the use of a perfect geometry, by breaking up the symmetry of the banded collapse localization of the perfect case, and leading to a more random distributed buckling and collapse [71]. The model's nodal coordinates were thus perturbed according to Equation 3-3 [71], where x is the perturbed position vector, x_0 is the initial position vector, p is a normally distributed random number between -0.5 and 0.5, φ is the amplitude of the disturbance and L is the average length of the ligament. Since

the effect of randomness is not the main interest of this study, a relatively small value was assumed for the disturbance in this study ($\varphi = 0.1$).

$$x = x0 + p\varphi L\,,\ 0 \le \varphi \le 0.5 \qquad \text{Equation 3-3}$$

Anisotropy in the foam cellular network was introduced to the Kelvin microstructure by using the same approach as Gong and Kyriakides [14]. The anisotropy λ of the foam geometry is defined by Equation 3-4, where h_1 and h_2 are the heights in rise and lateral direction of the generated structure, respectively; and was assumed to be equal to 1.2 in this study based on the measurement on similar foams in literature[71].

$$h_1 / h_2 = \lambda \qquad \text{Equation 3-4}$$

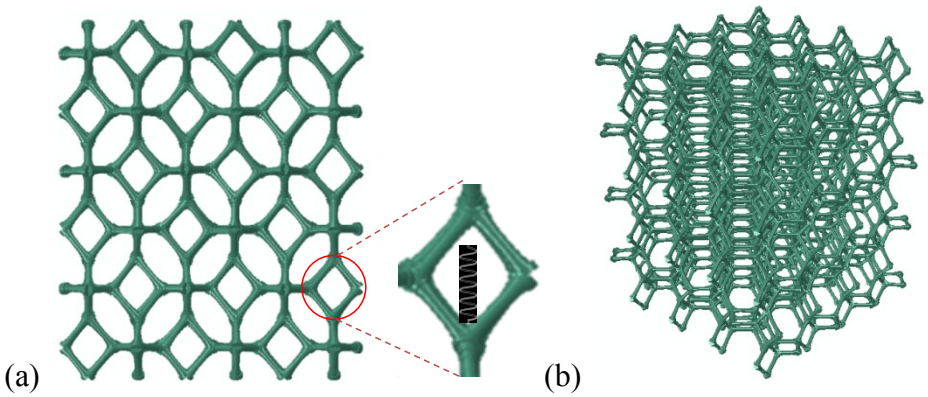

Figure 3-13 Multi-cell model with rendered cross-section (4×4×4 cells). (a) Front view; (b) Isotropic

3.5.2 Ligament Geometry

The ligaments in the multi-cell models were discretized using eight beam elements (B32: three-node quadratic shear deformable beam elements). As for the single ligament models, non-

uniform sections were defined for the ligament in the multi-cell model based on Equation 3-2. A circular section was used for the Al core. The diameter of the core section at mid-span was defined by calibrating the measured plateau stress from plain foam experiments with the results from numerical models. The calibrated mid-span diameter for the Al core was 0.18 mm, which is in the range of measured diameters of 0.192 ± 0.014 mm by Wang [8]. The coatings were modeled by duplicating the original foam structure with a pipe section with wall thickness equal to that of the corresponding coating. A "tie" constraint was used to connect the base foam part and the coating part, which lead to the assumption of a perfect bond between the coating and the base material. Representative plain and coated ligaments from the multi-cell models are shown in Figure 3-14 in rendered views to show the different section assignments.

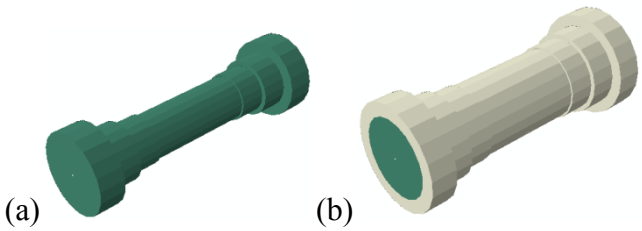

Figure 3-14 Single ligament in multi-cell models with rendered section: (a) uncoated ligament; (b) coated ligament

3.5.3 Boundary Conditions

Jang and Kyriakides [71] used periodic boundary conditions for their unit-cell model and relaxed the periodic boundary conditions (with free surfaces in one or both lateral directions) for

the multiple cell models. Periodic boundary conditions are applied by prescribing relations between the displacements of corresponding nodes on opposite surfaces of the representative volume element (RVE). Such boundary conditions work well for traditional metal foams composed of ductile ligaments. However, as shown in later sections, the deformation of Al/Cu hybrid foams (especially those with thicker coatings) under compression generally involves the fracture of ligaments. If fracture occurs in the ligaments connected to the nodes with prescribed boundary conditions, the constraint definitions for periodic boundary conditions as well as the applied displacement will not be appropriate. Thus, a continuous loading surface is preferred for the simulation of Al/Cu hybrid foams. Two rigid surfaces (normal to the loading direction) were defined at the top and bottom surfaces of the foam model. The bottom surface was fixed while a displacement boundary condition was defined on the top surface. Coulomb friction with a coefficient of 0.5 was used in the contact definition between the rigid surfaces and the foam model.

3.5.4 Contact Simulation

The densification feature in the compressive response of open cell foams follows from the contact that develops between ligaments as they collapse. Cell collapse starts locally and then propagates to other regions after densification of the initially collapse region is reached. This pattern continues and propagates throughout the foam domain and densification at a macro-scale is observed when most of the cells have collapsed [13]. In this study, the contact between ligaments was simulated based on the approach proposed by Jang and Kyriakides [71]. Non-linear spring elements were defined between collinear nodes in the cell vertices in the loading direction (see Figure 3-13(a)). The stiffness of the nonlinear springs defined in this study follow the recommendation of the work by Jang and Kyriakides [71] and are shown in Table 3-3, where

y is the gap between adjacent nodes in the rise (i.e., loading) direction as defined by Equation 3-5, where d_n is the core diameter of the ligament cross section evaluated using Eq. 1 at $x = 0.5L$ plus two times the coating thicknesses, if any.

$$\psi = \sqrt{2}\lambda L - d_n \qquad \text{Equation 3-5}$$

Table 3-3 Non-linear stiffness of spring elements for ligament contact simulation.

K (N/mm)	Displacement δ (mm)
0	$\delta < 0.2\psi$
5	$0.2\psi < \delta < 0.7\psi$
110	$0.7\psi < \delta$

It can be seen from Table 3-3 and Equation 3-5 that the stiffness of the nonlinear springs depends on the ligament size, which increases with coating thickness. However, the deformation of Al/Cu hybrid foams under compression usually involves fracture and separation of the coating and sometimes complete ligament fracture. This leads to a complicated contact phenomenon at large deformation (densification region). Thus the densification strain of Al/Cu hybrid foams (with non-ductile coatings) is not solely related to the original ligament size. Consequently, the focus of this study was to understand the failure mechanisms and the prediction of peak and plateau stresses in Al/Cu hybrid foams, and not intended to characterize the densification region.

3.5.5 *Size Effect in Multi-cell Models*

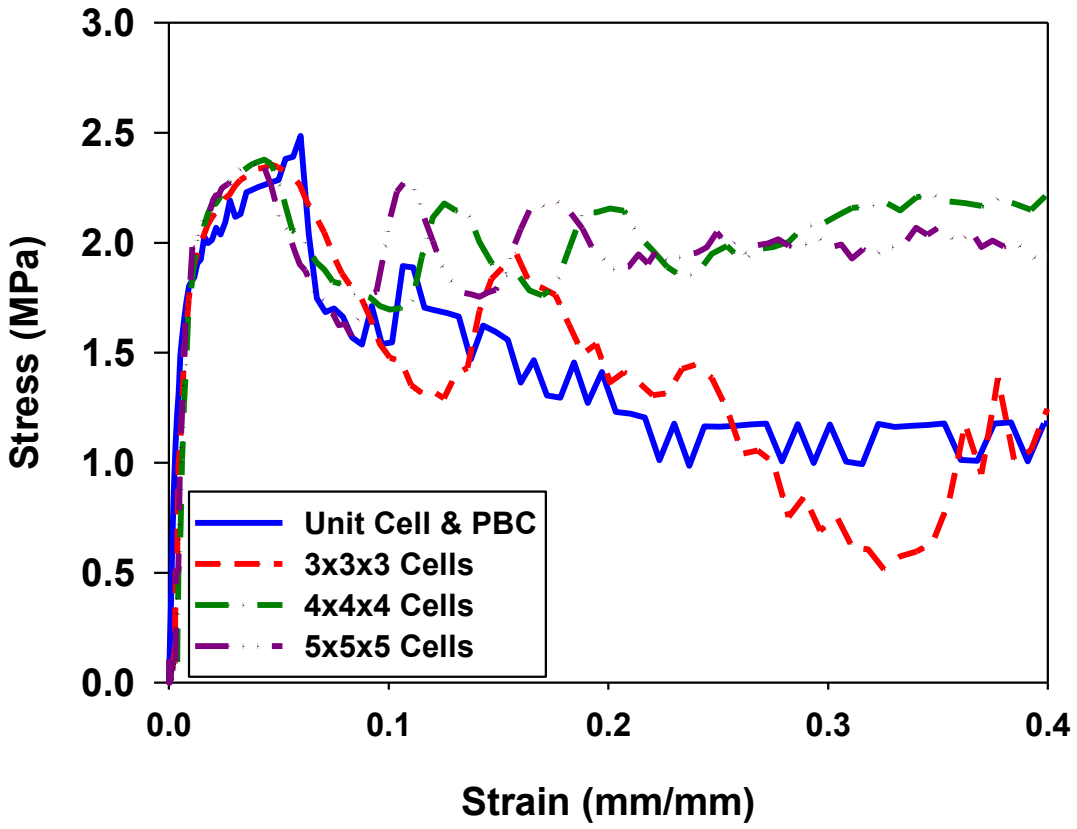

Figure 3-15 Quasi-static compressive stress-strain response from beam-element based finite element models with different sizes and boundary conditions

Multi-cell models were established to investigate the macroscopic compressive behavior of Al/Cu hybrid foams. Different size models were evaluated to determine a proper size. Figure 3-15 shows the result of three different model sizes for 40 PPI Al/Cu hybrid foams with 60 μm Cu coating. Also shown in the figure is the response obtained by using a single cell with periodic boundary conditions. It can be seen that even though all models predict almost the same initial

stiffness and similar peak stress, the post-peak behavior varies significantly. The unit cell model with periodic boundary condition shows a negative slope in the stress plateau region. This is because the model assumes uniform collapse of all the foam material that it represents. Such assumption is valid if the foam behavior is ductile and has no localized softening region (e.g., Al foam). Localized damage of the coating material in Al/Cu hybrid foams causes softening in concentrated regions and leads to fluctuations on the stress plateau in its macroscopic behavior, which can only be captured using models with multiple cells. Such stress fluctuation on the stress plateau is shown to be captured by the multi-cell models. However, the 18-cell model (3x3x3) had an irregular behavior due to the instability of the spring elements at large deformation. On the other hand, predictions from 64-cell (4x4x4) and 125-cell models (5x5x5) were very close. The 4x4x4 multi-cell models were thus chosen for this study.

3.5.6 *Quasi-static Compressive Response*

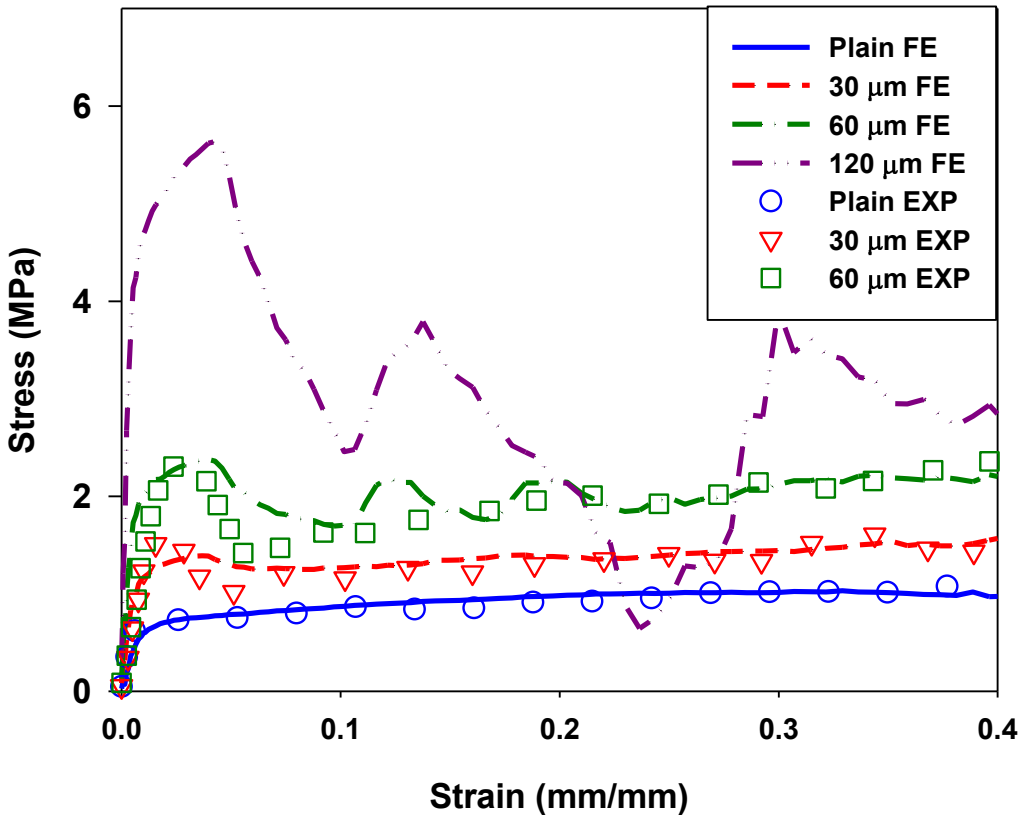

Figure 3-16 Simulated and experimental quasi-static compressive stress-strain response for 40 PPI plain Al and Al/Cu hybrid foams

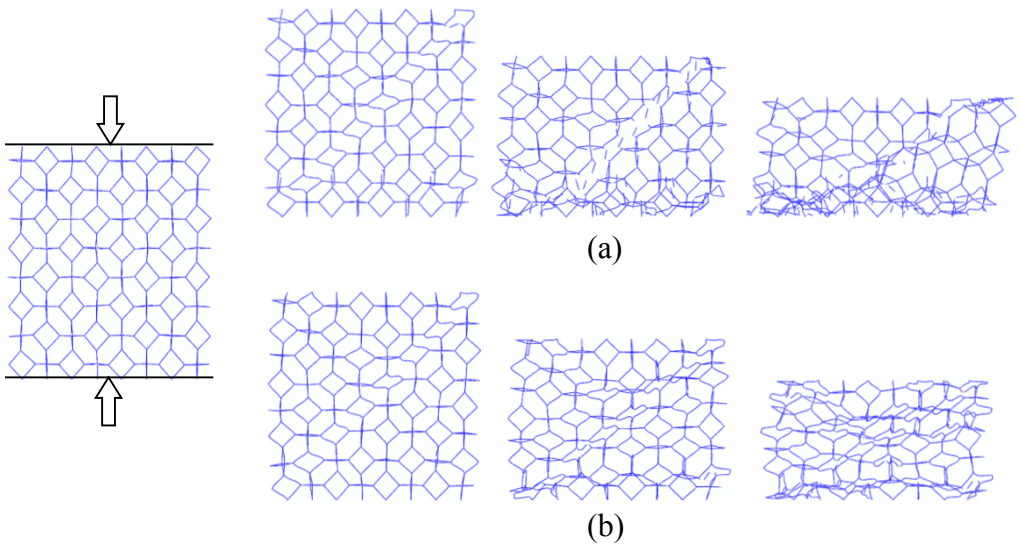

Figure 3-17 Simulated collapse progression of coated (120 μm) foam under uniaxial quasistatic compression; (a) Low ductility coating; (b) High-ductility coating.

Figure 3-16 presents results for the quasi-static response of hybrid foams obtained from the 4x4x4 multi-cell model. Responses for plain Al foam as well as hybrid foams with 30, 60, and 120 m Cu coating are shown. Experimental results (average of 3 samples) are shown for the plain foam and Al/Cu hybrid foams with 30 and 60 m coating thicknesses. The numerical results compare well with the experimental data, being able to capture the peak stress, the follow-up stress drop (which increases with coating thickness), and the fluctuating response, with a slight hardening global trend, in the plateau region. Of all these features, the ability to capture the large stress drop after the initial peak stress in the hybrid foams (and its increase with coating thickness) is the most notable characteristic of the simulation results. Values for the elastic modulus E_{foam}, maximum stress σ_{max} (i.e., initial peak stress), post-peak minimum stress σ_{min} and plateau stress $\sigma_{plateau}$ (defined as the average stress within 15% to 40% strain range) are

shown in Table 3-4. The models led to a good prediction of the elastic modulus for plain Al foam but overestimated the elastic modulus of Al/Cu hybrid foams, especially with thick coatings. This may be due to differences between the actual stiffness of the electrodeposited copper and the values used in the numerical models, which were adopted from the literature [66]. However, the deviations in predicted vs. experimental elastic modulus do not affect the main findings of this study. The post-peak stress drop in the behavior of Al/Cu hybrid foams is caused by the localized collapse of cells in an inclined shear band (Figure 3-16(a)). The fluctuation observed after the peak is primarily caused by the successive collapse and densification of cells at different regions during loading. As presented in Section 3.3, section loss from the failure of thicker coatings has a bigger impact on the overall load carrying capacity of foam ligaments. As a result, the macro-scale initial stress drop, as well as the magnitude of the fluctuations in the plateau region, is larger in Al/Cu hybrid foams with thicker coatings; which is captured by the simulation results. It should be noted that the simulation for a hybrid foam with 120 μm coating showed a very brittle response (see Figure 3-16), as shown by the significant initial stress drop and the large fluctuations in the stress plateau region. The solution also suffered from convergence problems at large deformation. This indicates that low ductility nanocrystalline depositions can be detrimental to the stable compressive response and energy absorption capacity of foams with thick coatings.

Table 3-4 Comparison of stress values between results from experiment and FE simulations.

	Plain			30 μm			60 μm			120 μm		
	Exp	LD	HD	Exp	LD	HD	Exp	LD	HD	Exp	LD	HD
E_{foam} (MPa)	80	76	-	122	162	174	135	322	322	-	819	819
σ_{max} (MPa)	0.77	0.79	-	1.6	1.39	1.53	2.34	2.38	2.55	-	5.64	5.93
σ_{min} (MPa)	0.72	0.72	-	0.97	1.25	1.53	1.34	1.70	2.35	-	2.46	4.35
$\sigma_{plateau}$ (MPa)	0.98	1.00	-	1.40	1.44	1.64	2.05	2.05	2.62	-	2.44	5.80

Note: Exp = Experimental data; LD = Numerical simulations with low ductility coating; HD = Numerical simulations with high ductility coating.

3.5.7 Effect of Coating Ductility

This section presents simulation results to highlight the effect of increased ductility of the coating material on the macro-scale compressive behavior of Al/Cu hybrid foams. Multi-cell model simulations employing coating material definitions with large ductility were conducted. The tensile fracture strain of Cu coating was assumed to be the same as the Al core ($\varepsilon_{ft-Cu} = \varepsilon_{ft-Al} = 0.5$).

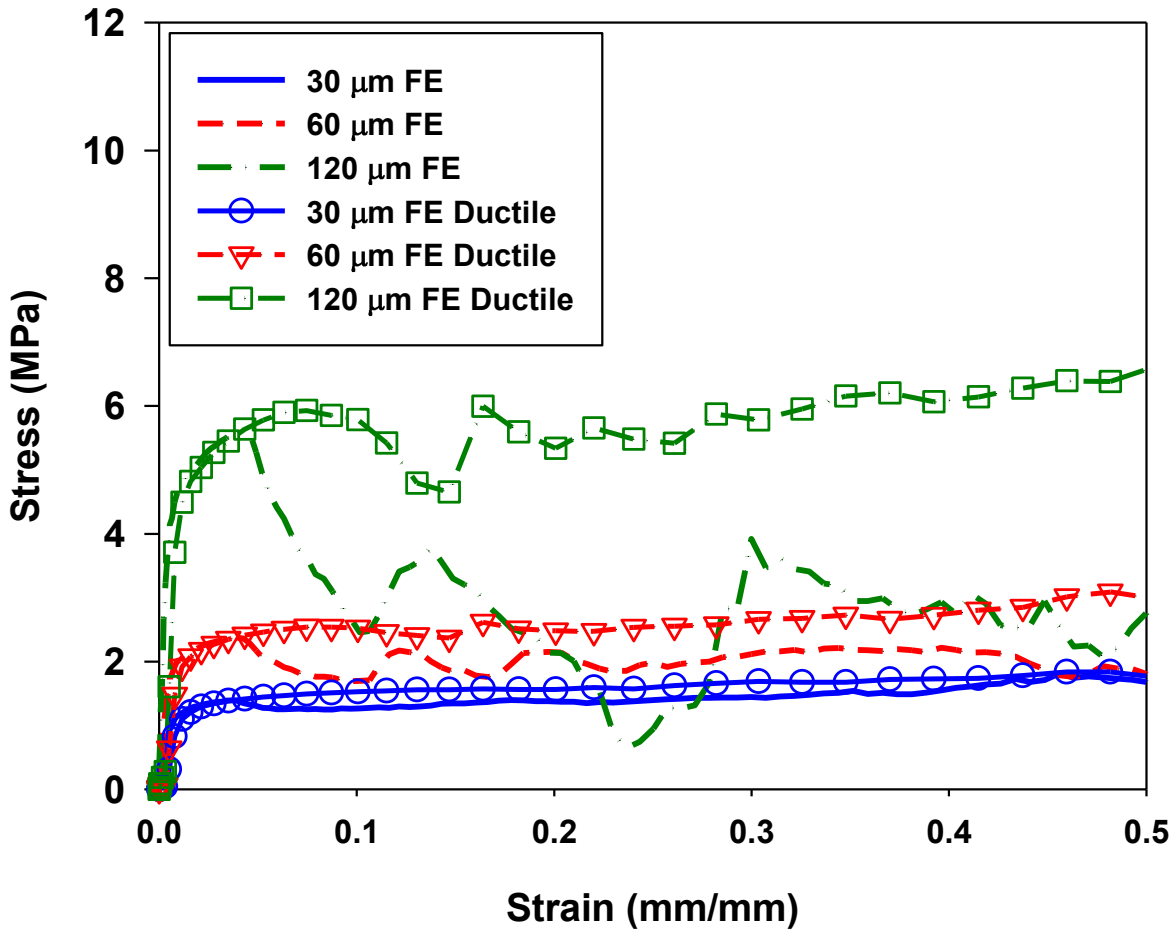

Figure 3-18 Simulated quasi-static compressive stress-strain response of Al/Cu hybrid foams with low and high coating ductility

Figure 3-17 shows the simulated collapsing response of a Al/Cu hybrid foam (120 μm Cu thickness) with low and high ductile coatings. In both cases failure is caused by the formation of a shear band of cells that starts collapsing under the compressive load. This state corresponds to the peak stress response and occurs at low global deformations. The collapse sequence of for the low-ductility coating model (Figure 3-17(a)) shows that as global deformations increase damage concentrates in the collapse region and fracture of the ligaments occurs. Conversely, the deformation sequence for the high-ductility coating model (Figure 3-17(b)) shows that other

regions in the foam start collapsing after the first collapsing band forms, which leads to a more uniform densification of the foam domain. Thus, a hybrid foam with high-ductility coating will have a failure mode similar to that exhibited by homogeneous metal foams. Otherwise, hybrid foams with low-ductility coatings will exhibit a more brittle failure and non-uniform damage regions; especially highly reinforced foams through thicker or stronger coatings.

Figure 3-18 compares the simulated stress-strain compressive response of Al/Cu hybrid foams with low and high coating ductility. Values for the maximum stress σ_{max}, post-peak minimum stress σ_{min} and plateau stress $\sigma_{plateau}$ are given in Table 3-4. It can be seen that coating ductility does not affect the peak stress level. However, the subsequent stress drop that is so prominent in hybrid foams with low-ductility coatings is mostly eliminated by the use of a high-ductility coating, and the stress fluctuation in the plateau region is reduced significantly. This is because the high-ductility coating permits the ligaments to remain integral and thus capable of sustaining load at large deformations, even if they have reached their plastic limit at critical sections along their length. The energy absorbed by the Al/Cu hybrid foam models up to 50% strain were calculated by determining the area under a stress-strain curve and listed in Table 3-5. The results show the significant enhancement in energy absorption capacity that can be obtained with improved coating ductility, especially for foams with thicker coatings.

Table 3-5 Energy absorption of multi-cell models of 40 PPI Al/Cu foams up to 50% strain

Coating Thickness	Low coating ductility (N·mm)	High coating ductility (N·mm)	Enhancement
30 μm	0.71	0.79	11%
60 μm	1.05	1.26	20%
120 μm	1.43	2.76	93%

3.6 Discussion

The quasi-static behavior of Al/Cu hybrid foams under compression has been investigated using nonlinear finite element simulations and it has been shown that their overall performance can be significantly enhanced if the ductility of the coating material is improved. The ductility of metals can be improved by annealing due to the recrystallization and grain growth that occurs at high temperature [46, 58]. The effect of coating ductility on the performance of Al/Cu hybrid foams will be presented in CHAPTER 4. It needs to be noted that the discussion on the effect of coating ductility also reflects the consequences of lacking reliable material properties at the scale of the base metal foam ligaments and the electrodeposited coatings. It is clear that if the bulk material properties for Cu and Al, which usually have a high ductility level, were used in the simulations predicted capacities and the deformation mechanisms of the hybrid foams would have been incorrect.

The presented simulations and discussions were based on Al/Cu hybrid foams; however, the methods and findings are considered to apply similarly to the compressive behavior Al/Ni hybrid foams manufactured using similar processes due to the reported low ductility of

electrodeposited nickel [86]. Actually, since electrodeposited nickel usually has much higher strength compared to electrodeposited Cu, the effect of embrittlement and reduction in energy absorption efficiency due to the low-ductility coating will be more significant for Al/Ni hybrid foams. Figure 3-19 shows the compressive stress-strain curves of Al/Ni hybrid foams with various coating thicknesses reported by Bouwhuis et al. [6] and simulated responses using numerical methods presented in this study. It can be seen that both the initial stress peak and the post-peak stress drop are more significant for Al/Ni hybrid foams compared to Al/Cu hybrid foams with similar coating thicknesses.

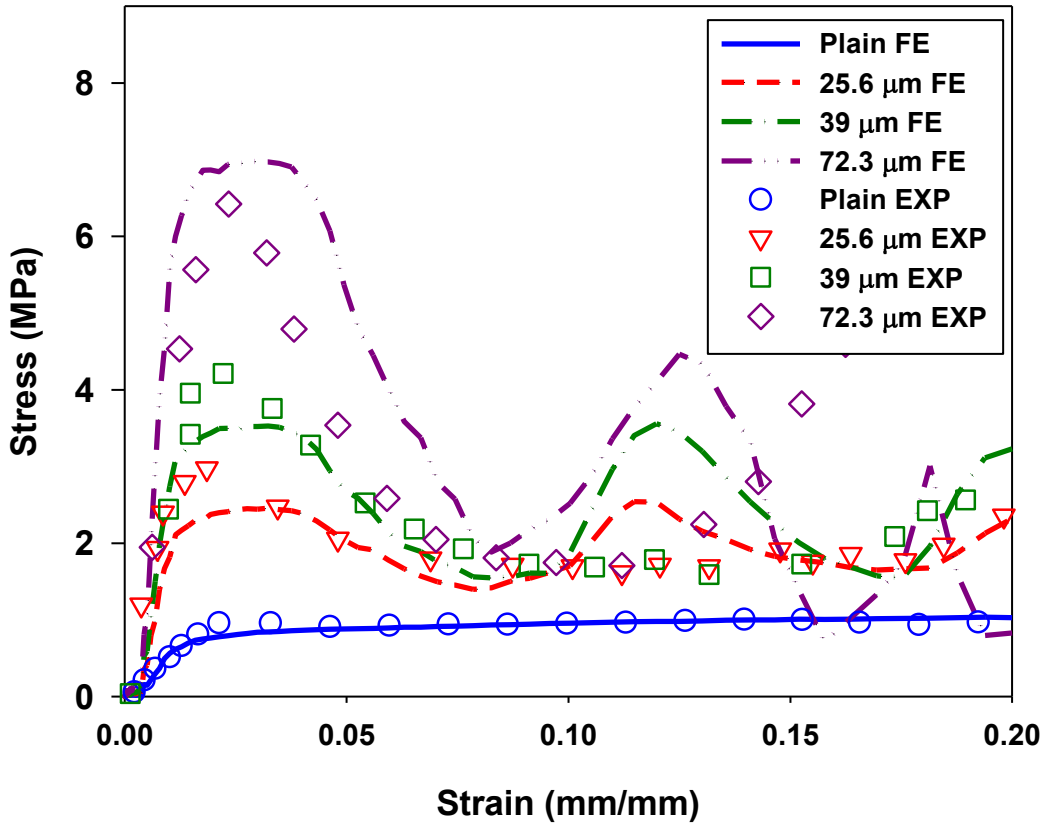

Figure 3-19 Simulated and experimental quasi-static compressive stress-strain response for 20 PPI plain Al and Al/Ni hybrid foams

3.7 Conclusions

The quasi-static compressive behavior of Al/Cu hybrid open-cell foams manufactured by the electrodeposition of nanocrystalline Cu onto open cell Al foams was studied through nonlinear finite element simulations at different scales. Detailed failure mechanisms at the micro-scale level were studied conducting fiber-based sectional analyses and simulations on single ligament models discretized using continuum-type finite elements. The stress-strain compressive response at the macro-scale was studied through multi-cell models, based on repeating Kelvin cells in three dimensions, established using composite beam elements. The following conclusions are drawn from this study:

1) The numerical simulations have shown that rupture of the electrodeposited Cu coating is a prevailing failure mechanism and fracture of the ligaments can occur in Al/Cu hybrid foams loaded in compression. Such behavior is due to the low ductility of the electrodeposited nanocrystalline coating and needs to be considered in the simulation of hybrid foams.

2) Sectional analyses and micro-scale simulations of single ligaments have shown that coating rupture occurs at locations under large flexural curvature demands, with an increasing detrimental effect proportional to the coating thickness; an effect that can lead to fracture of the cell ligaments. As a result, ligaments in Al/Cu hybrid open cell foams with thicker coating have a brittle response as they collapse under compressive loads.

3) Macro-scale simulations using multi-cell models were shown to adequately capture the unique quasi-static behavior of Al/Cu hybrid foams as validated by experimental data. The models were able to capture the enhancement of strength and stiffness with coating thickness as well as the increased stress drop upon the initiation of cell collapse, and the large response fluctuation in the stress plateau region. These features were shown to increase in

proportion to the Cu coating thickness and the stress drops and fluctuations are due to the reduced ductility capacity of the electrodeposited Cu. Thus, while increased coating thickness improve strength and stiffness, the lack of coating ductility limits and jeopardizes the overall energy absorption capacity of the system, especially for foams with thick coatings. While such behavior had been previously observed in experimental results no explanation or ways to numerically simulate it had been reported before this study.

4) The micro- and macro-level simulations have shown that the performance of Al/Cu hybrid foams under compression can be enhanced by improving the ductility of the coating material. Coatings with higher ductility can reduce fracture of the ligaments at the micro level and avoid the localization of collapsed regions at macroscopic level. Such improvement can lead to a sustained load carrying capacity under compression and improved energy absorption characteristics, an enhancement that would be more significant for Al/Cu hybrid foams with thicker coatings.

CHAPTER 4 EFFECT OF COATING DUCTILITY ENHANCEMENT

4.1 Overview

It has been demonstrated that hybrid foams can have an enhanced and controllable modulus, strength and energy absorption capacity. The numerical investigation in CHAPTER 3 has shown that the low ductility of the nanocrystalline structured coating materials in hybrid foams can cause rupture and separation of the coating material and significantly reduce their energy absorption capacity. In this chapter, Al/Cu hybrid foams manufactured through electrodeposition were subjected to an annealing process with the aim of increasing the ductility of the coating and thus achieve improved performance and the effect of annealing temperature and time on their macro- and micro-level behavior under compression and tension were investigated using experimental methods.

Figure 3-1 shows the compressive stress-strain response and test pictures of Al and Al/Cu hybrid (with 60 μm Cu coating) open cell foams. Both samples had a cell size of 40 pores per inch (PPI) and a relative density of 6 %. It can be observed that Al/Cu hybrid foam shows a large stress drop after the initial peak (onset of cell plastification) and a plateau region with considerably more fluctuations compared to the plain Al foam. The post-peak stress drop observed in the Al/Cu hybrid foam was accompanied by ligament breakage and material spalling, which is characteristic of Al/Cu hybrid foams and seen to increase with coating thickness [8]. Similar behavior has been reported for Al/Ni hybrid foams [6, 7, 40]. Bouwhuis et al. [6] observed cracking and wrinkling of the nickel coating in Al/Ni hybrid foams and thought it that could be caused by the low ductility of the coating.

The electrodeposited coatings in hybrid foams have a nanocrystalline structure [7, 8] that usually leads to higher yielding strength but significantly less ductility compared to the bulk material counterparts [46, 62, 63, 66, 74, 87]. Numerical simulations in CHAPTER 3 indicate that the resulting local coating failures lead to concentrated deformations at weakened critical sections at low strain levels and thus inhibit the energy absorption performance of hybrid foam materials [88]. It is thus hypothesized that the energy absorption performance of metallic hybrid foams can be effectively enhanced by improving the ductility of the electrodeposited coating.

4.2 Annealing Procedure

Annealing is a well-established heat treatment process for metals to release internal stresses and enhance ductility through recrystallization and grain growth, which also usually results in a lower modulus and yield strength [46, 58, 89]. All annealing processes were performed in a Centorr M60 vacuum annealing furnace. The specimen chamber was evacuated by a Varian VHS-4 diffusion pump. Annealing was conducted at temperatures of 180 °C and 400 °C at a base vacuum pressure of 3×10^{-5} torr. The annealing temperature was measured using an Omega Type-K thermocouple inside the furnace, which was positioned close to the samples. The noted temperatures were about one third or one half, respectively, of the melting temperature for copper (absolute temperature scale), between which the atomic mobility is sufficient to affect mechanical properties [58].

The annealing process was carried out by first evacuating the specimen chamber. The heating process was not initiated until the desired pressure within the chamber was achieved. The temperature was controlled to achieve a ramp-up rate of about 20 °C/min. Upon reaching the target annealing time the heating element of the furnace was turned off and the specimen was allowed to cool down through heat dissipation of the system. The annealed specimen was taken

out of the furnace after the chamber temperature was below 100 °C. The time at which heating element was turned off and specimen was removed were recorded and the cool down rate was estimated to be about 6 °C/min based on the records. Thus, the actual exposure time was longer than the nominal annealing time, especially when annealing was carried out at 400 °C.

Table 4-1 shows the test matrix for the reported study on the effect of annealing on the performance of Al/Cu hybrid foams. The samples were identified based on the testing method, copper coating thickness, nominal annealing temperature and annealing time considered, and the naming convention is shown in Figure 4-1. The nominal annealing time is defined as the time during which the sample temperature was kept at the target value. Also listed in Table 4-1 is the nominal relative density of the hybrid foam samples (*RD'*), defined as the ratio of the volume of the solid (volume of Al and Copper, $V_{Al} + V_{Cu}$) to the volume of the sample (V_s), was calculated based on the relative density of the base aluminum foam (*RD*) and the weight gain from the copper coating (m_{Cu}) after the electrodeposition process using Equation 4-1.

$$RD' = \frac{V_{Al} + V_{Cu}}{V_s} = RD + \frac{m_{Cu}}{\rho_{Cu} V_s} \qquad \text{Equation 4-1}$$

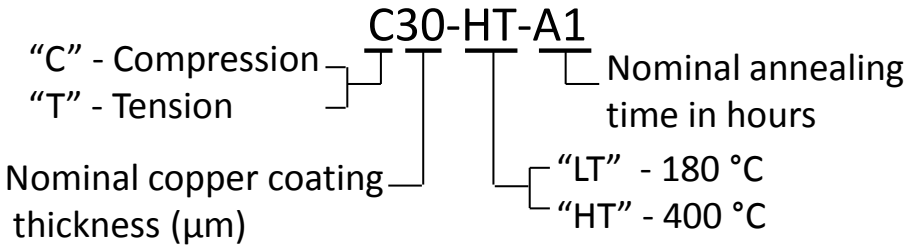

Figure 4-1 Naming convention of test samples

Table 4-1 Test Matrix

Sample ID	Nominal Coating Thickness (μm)	Annealing Temperature (°C)	Annealing Time (h)	Weight needed (g)	Nominal Relative Density (%)
C30/T30	30	-	-	6.1	8.1
C60/T60	60	-	-	13.8	10.7
C90	90	-	-	22.5	13.7
C30-LT-A1	30	180	1	6.1	8.1
C60-LT-A1	60	180	1	13.8	10.7
C30-HT-A1 T30-HT-A1	30	400	1	6.1	8.1
C60-HT-A0*	60	400	0.0833	13.8	10.7
C60-HT-A1 T60-HT-A1	60	400	1	13.8	10.7
C60-HT-A2	60	400	2	13.8	10.7
C90-HT-A1	90	400	1	22.5	13.7

*Note: Samples were annealed at the target temperature for 5 minutes.

4.3 Mechanical Testing and Characterization

Quasi-static compression and tension tests were conducted on the plain Al and hybrid Al/Cu foams samples (size: 25.4 mm x 25.4 mm x 50.8 mm) using a universal loading frame as shown in Figure 4-2. The samples were loaded along their long dimension. For compression testing aluminum plates (3 mm thick) were bonded using epoxy to the ends of the foam samples before testing to provide the sample with uniform loading surfaces. The tension tests were conducted by mounting the foam samples ends using epoxy to two loading fixtures that were then connected to the loading frame. In order to include more cells in the section area perpendicular to the loading direction, no section reduction was applied to the prism specimen. The rate of loading was 2.54 mm/s for the compression tests and 0.12 mm/s for the tension tests.

The annealed and unannealed Al/Cu hybrid foam samples were evaluated with a JEOL JSM 6610 LV field emission scanning electron microscope (SEM). The effect of annealing on the micro-scale deformation mechanism of Al/Cu hybrid foams were investigated using secondary electrons (SE) with a 15 kV acceleration voltage. In addition, backscattered electrons (BSE) with an acceleration voltage of 10 kV were used to evaluate the formation of intermetallic compound at the Al/Cu interface.

Table 4-2 Information for Al and Al/Cu foam samples

Cu Coating Thickness (μm)	Cu Coating Weight (g)	Relative Density (%)
0	0	6
30	6.1	8.1
60	13.8	10.7

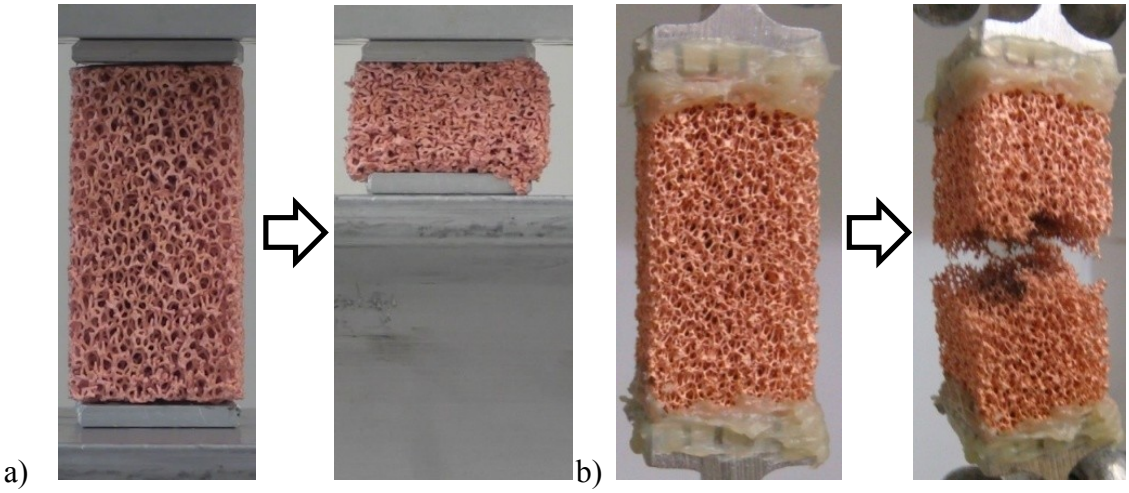

Figure 4-2 Images of hybrid Al/Cu foams samples with uniform coating in a) Uniaxial compressive test; and b) Uniaxial tensile test

X-ray diffraction (XRD) was used to evaluate the effect of annealing on the crystallite size of the copper coating in the Al/Cu hybrid foams. XRD patterns were obtained on a Bruker D8 DaVinci diffractometer equipped with Cu X-ray radiation operating at 40 kV and 40 mA. Peak intensities were obtained by counting the Lynxeye detector every 0.01^{o} at sweep rates of 0.5^{o} 2θ/min. The crystallite size of the deposited Cu was determined using the Williamson-Hall method [90] as detailed in the results section.

4.4 Results

4.4.1 Crystallite Size

Figure 4-3 shows the first two peaks of the XRD diagram obtained for two Al/Cu hybrid foam specimens, one of which was annealed after electrodeposition while the other one was not. The peak positions of the observed pattern are summarized in Table 4-3 together with the peak positions for copper reported in the literature [91]. It can be seen that the peak positions in the pattern of the Al/Cu foams agree well with those for copper since the aluminum was covered by the copper coating.

The crystallite size of nano-copper coating was determined using the averaged estimation of the first three peaks and the Williamson-Hall method [90]. In this method the true peak broadening is assumed to be composed of crystallite size broadening and strain broadening, given by Equation 4-2 where d is the mean crystallite size, K is shape factor, λ is the X-ray wavelength (0.15406 nm), β is the line broadening at half the maximum intensity (FWHM), and θ is the Bragg angle and ε is the microstrain. The microstrain was determined to be 0.4 percent for Al/Cu hybrid foam and 0.06 percent for annealed Al/Cu hybrid foam. It can be seen in Table

4-3 that the annealed specimen had a significantly increased crystallite size, which indicates the occurrence of grain growth from annealing.

$$\beta \cos\theta = \frac{K\lambda}{d} + \varepsilon \sin\theta \qquad \text{Equation 4-2}$$

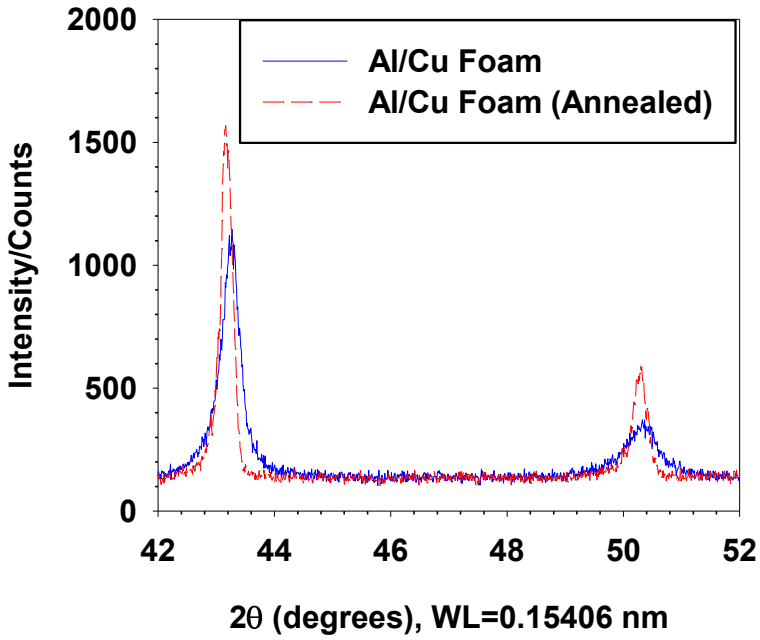

Figure 4-3 First two peaks of XRD patterns of copper (Cu) coated aluminum (Al) foam specimens with and without annealing

Table 4-3 Summary of results from XRD measurements on Al/Cu hybrid foam specimens.

Material	1st Peak Position	2nd Peak Position	3rd Peak Position	Estimated Average Crystallite Size (nm)
Al/Cu Hybrid Foam	43.23°	50.32°	73.99°	38
Al/Cu Hybrid Foam (Annealed)	43.15°	50.26°	73.97°	56
Copper [91]	43.30°	50.43°	74.13°	-

4.4.2 Compressive Response

Figure 4-4 shows the compressive response for plain Al foam and Al/Cu hybrid foams with and without an annealing process (400 °C for 1 h). It can be seen in Figure 4-4a that the annealed plain Al foam had a reduced plateau stress and thus lower energy absorption capacity. This is because the original plain Al foam has been heat treated to increase its strength and the annealing process causes relaxation due to reorganization of the crystal structure.

The compressive response for the unannealed Al/Cu hybrid foams shown in Figure 4-4b to Figure 4-4d feature an initial peak stress at the onset of plastification (defined as the onset of plastic collapse of the foam cells) followed by a drop in stress and then a stress plateaus with considerably more fluctuations than for the annealed samples. It can be seen that the noted stress drop and the fluctuations become more pronounced as the coating thickness increases.

The response features just noted are caused by the concentrated local damage and brittle behavior of the unannealed samples as shown in Figure 4-5a. It can be seen in Figure 4-5a that an inclined collapsing band forms at a small strain level and that the subsequent deformation is caused by crushing of foam material within that region. On the other hand, no significant stress drop and a smoother stress plateau, with a magnitude similar to or higher than the stress level at onset of plastification, were observed in the stress-strain response of the annealed Al/Cu hybrid foam samples.

It is of interest to point out that the plastification stress of the annealed samples is close to or higher than the corresponding stress level in the unannealed samples, even though the yielding and plateau stress decreased in the plain Al foam samples after annealing. The enhanced response of the annealed Al/Cu hybrid foam samples compared to the unannealed samples was more significant in samples with thicker coatings. This can be expected as the influence of the

low ductility coating on foam performance is more severe as the ratio of coating thickness to the original strut cross-section dimensions increases [92].

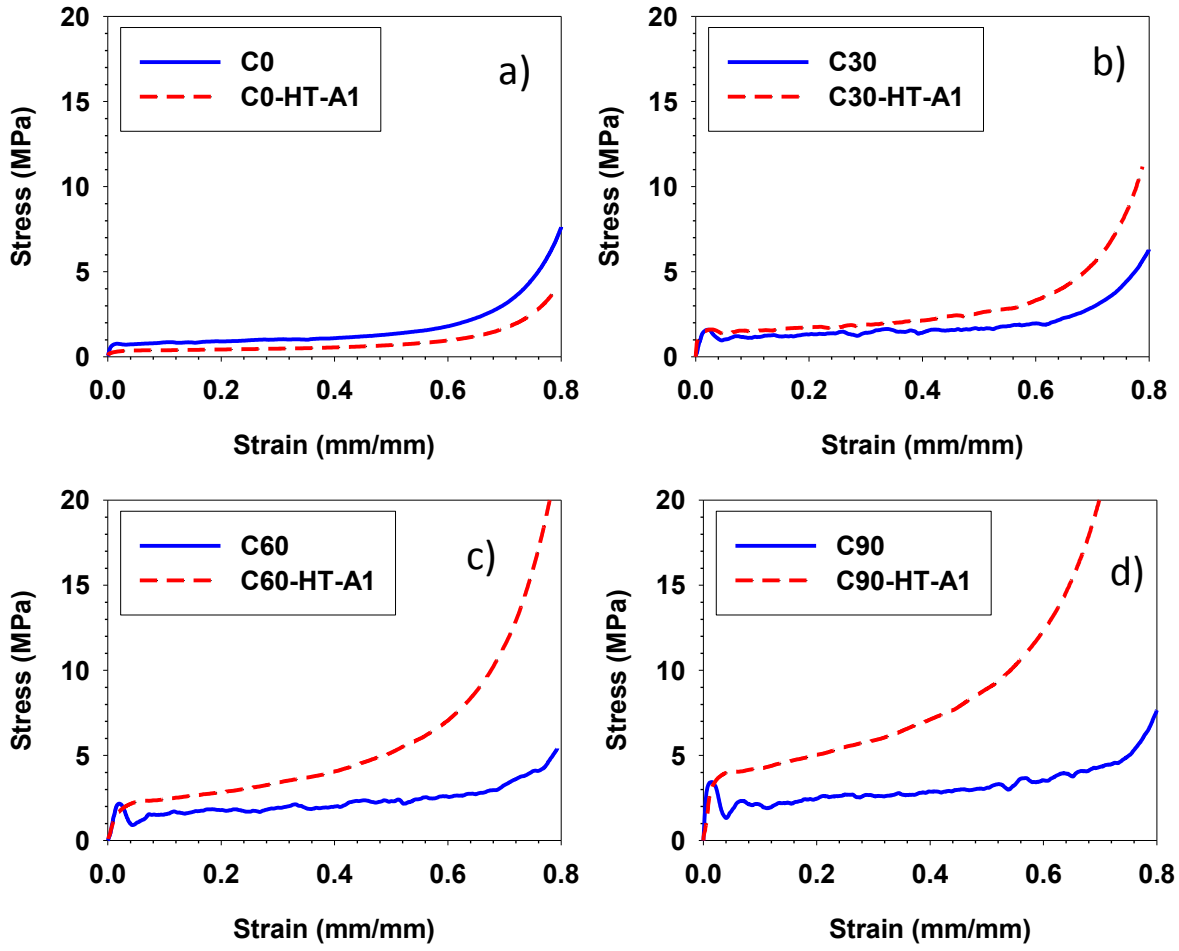

Figure 4-4 Compressive stress-strain responses of Al/Cu hybrid foams with different coating thicknesses

The improved ductile macroscopic behavior of the annealed samples can be attributed to the fact that there is no localized damage and the samples stay intact throughout the deformation, as shown in Figure 4-5b. It can also be seen from Figure 4-4 that the densification region starts

earlier in the annealed samples. However, it needs to be noted that the densification strain (the strain at which densification region starts, which can be defined as the strain level at the intersection of the best fitting lines (using a least square fit) of the collapse region and the densification region, respectively) is overestimated in the unannealed samples due to the severe separation and breakage of material during the deformation (see Figure 4-5a).

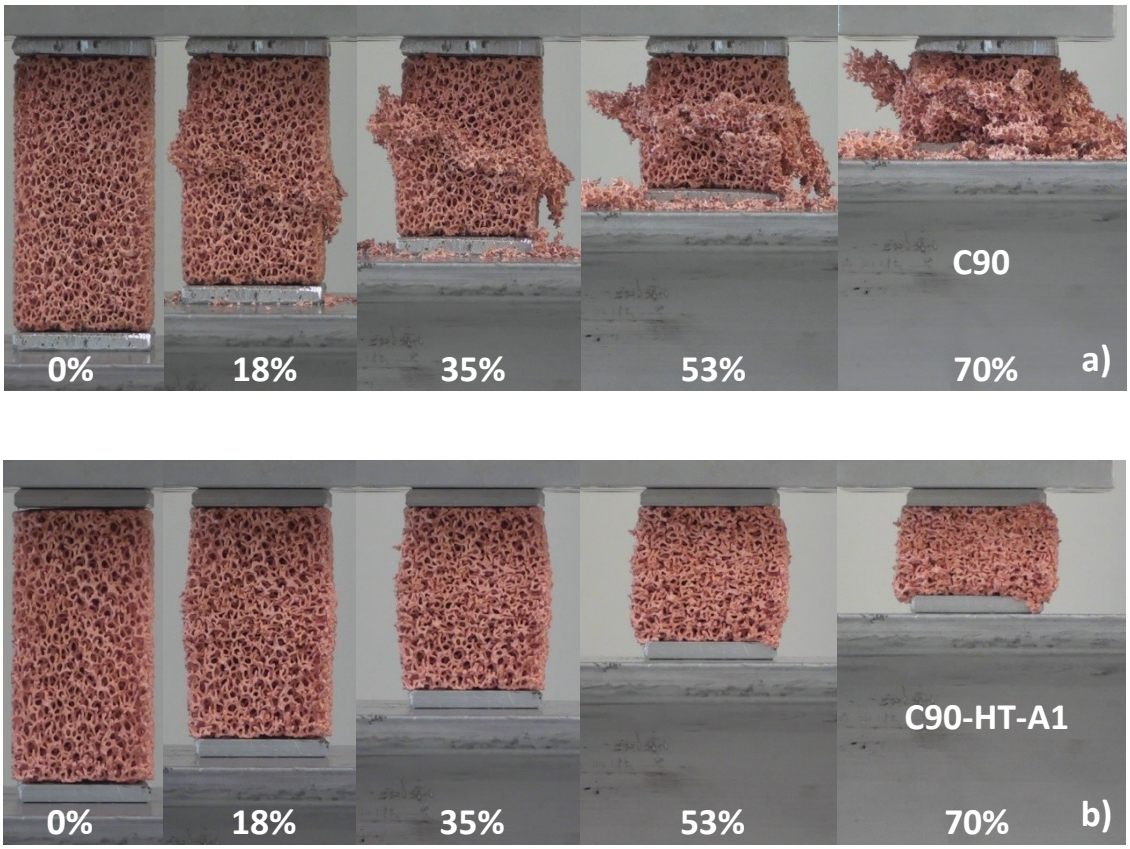

Figure 4-5 Sequential images from the compression testing of Al/Cu hybrid foam samples of (a) C90 and (b) C90-HT-A1

To provide further understanding of the effect of annealing on Al/Cu hybrid foams an investigation on the micro-scale failure mechanisms was conducted. Two Al/Cu hybrid foams samples (with and without annealing) with a nominal coating thickness of 50 μm were

compressed to about 6% strain and SEM (scanning electron microscope) images were taken at a region of collapsed cells (see Figure 4-6).

The noted strain level was chosen since it is shortly after the stress drop after the onset of plastification was observed in the compressive behavior of the unannealed sample. Rupture of the copper coating (see arrows in Figure 4-6a) was observed in the unannealed sample. A similar observation was reported by Bouwhuis et al. [6] for Al/Ni hybrid foams. The coating rupture can be attributed to the low ductility of the electrodeposited metal which usually has a nanocrystalline structure [66, 74, 92].

The resulting loss in load carrying capacity of the ligaments as a result of coating failure is considered to be the main cause for the observed stress drop and the fluctuating plateau trace in the compressive behavior of unannalead hybrid foams. Conversely, Figure 4-6b shows some largely deformed ligaments in the annealed sample at the same deformation level, where no obvious damage or rupture of the coating can be seen. This enhanced response of the ligaments led to the more ductile macroscopic behavior observed in the prism samples. The effect of annealing is more significant in Al/Cu hybrid foam samples with thicker coating as the rupture of coating has larger influence on the load carrying capacity of the ligaments in those samples.

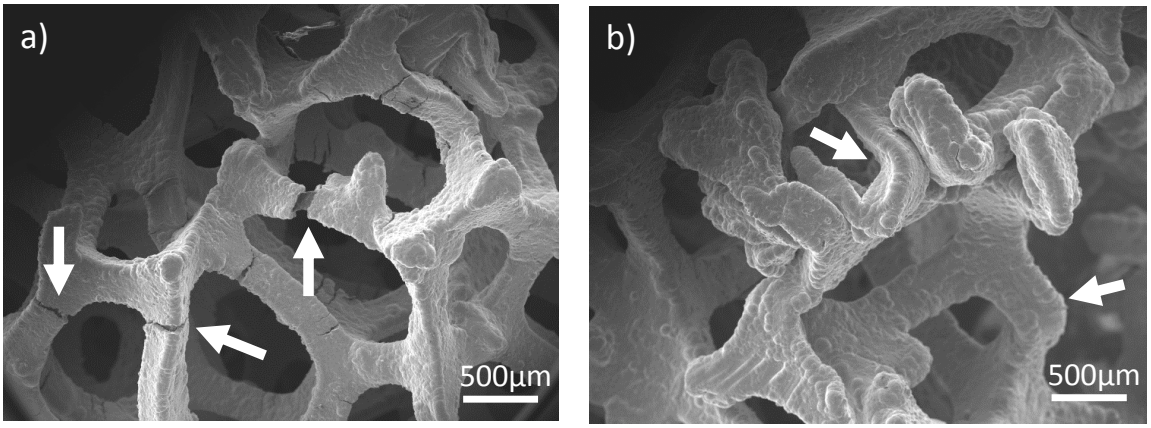

Figure 4-6 SEM images of ligament deformation in 40 PPI Al/Cu hybrid foam samples (50 μm copper coating) compressed after the onset of plastification to about 6 % strain: (a) without annealing; (b) with 1 hour annealing at 400 °C

4.4.2.1 Effect of Annealing Temperature

Figure 4-7 shows the compressive behavior of Al/Cu hybrid foams annealed at different temperatures. Two temperature levels were considered, namely, 180 °C and 400 °C. All samples in this discussion were annealed for one hour. It can be seen that the samples with 30 μm coating had basically the same performance after been annealed at different temperatures (see Fig. 9a). However, at a large strain level, fracture was observed in the sample with 60 μm coating annealed at 180 °C (C60-LT-A1) as shown in Figure 4-8, which led to a delayed densification region in the stress-strain response shown in Fig. 9b.

The observed fracture in sample C60-LT-A1 was not as severe as that observed in unannealed samples and it is considered to be caused by insufficient annealing. The observed behavior of Al/Cu hybrid foams annealed at different temperature indicates that the enhancement on the mechanical performance from annealing can be achieved at lower temperature (180 °C). However, in order to achieve a ductile behavior at large strain level, additional time may be

needed when annealing is conducted at lower temperature, especially for Al/Cu hybrid foams with thicker coating.

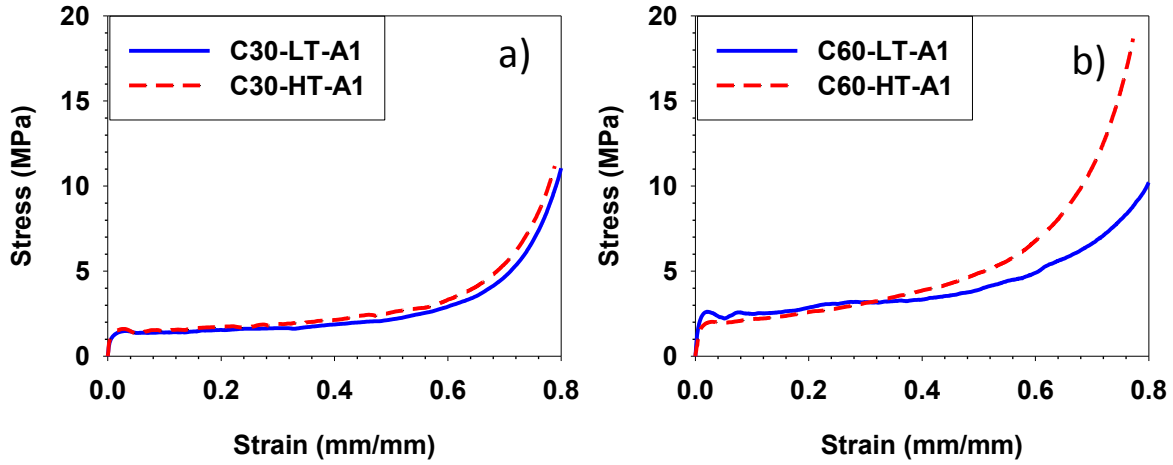

Figure 4-7 Compressive response of Al/Cu hybrid foams annealed at different temperature

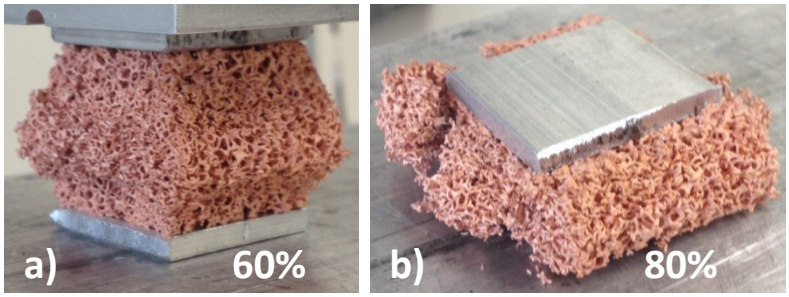

Figure 4-8 Images from the compressive testing of sample C60-LT-A1 at 60 % and 80 % strain

4.4.2.2 Effect of Annealing Time on Compressive Behavior

Figure 4-9 shows a comparison of the compressive behavior of Al/Cu hybrid foam samples (60 µm nominal coating thickness) annealed for 5 minutes (A0), 1 hour (A1) and 2 hours (A2), respectively at 400 °C. It can be observed that the responses of the C60-HT-A0 and C60-HT-A1 samples were almost identical. The two samples showed a very ductile behavior

(see Fig. 11b) and no fluctuations were observed on the stress-strain traces. Thus, a short annealing period at 400 °C was sufficient for Al/Cu hybrid foams with 60 μm nominal copper coating thickness. However, brittle ligament failures were observed during the deformation of the sample annealed for 2 hours (C60-HT-A2). This is seen in the post-test debris in Figure 4-9c as well as the stress-strain trace for this sample in Figure 4-9a, which shows increased fluctuations in the plastification region and a larger onset for the densification region due to the loss (i.e., breakage) of material.

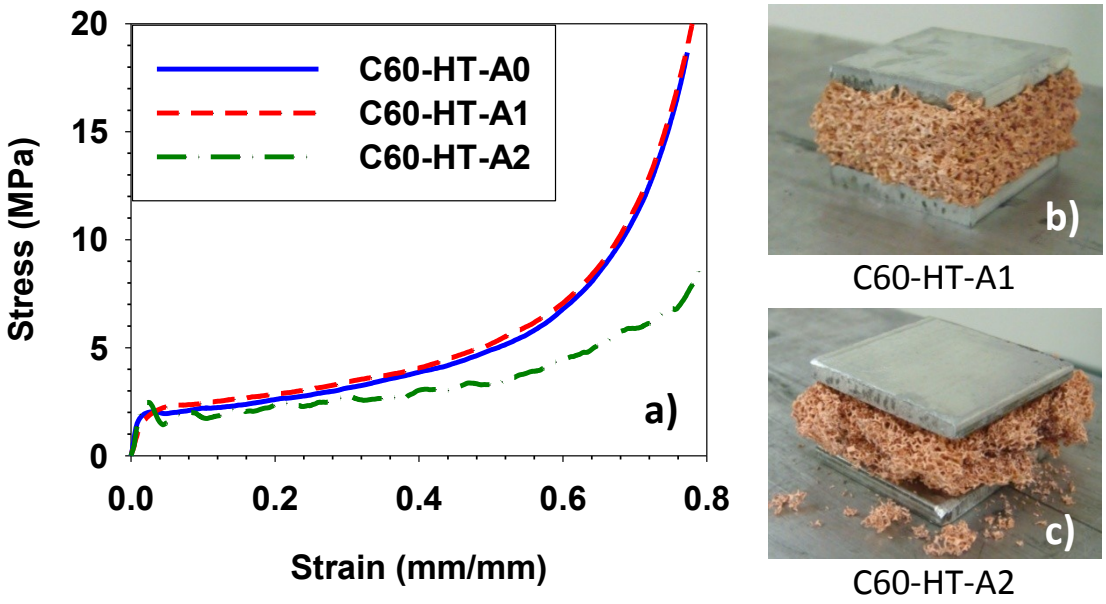

Figure 4-9 Compressive behavior of Al/Cu hybrid foams with different annealing time

The observed behavior of sample C60-HT-A2 is similar to that of an unannealed Al/Cu hybrid foam. However, the low coating ductility is not considered to be the cause in this case, as it has been shown that the ductility of copper coating can be sufficiently enhanced with annealing for an even shorter period. Rather, it is known that intermetallic compounds (IMC) such as Al_2Cu, Al_4Cu_9, AlCu, Al_3Cu_4, and $AlCu_3$ can form at the Al/Cu interface during cold roll

welding, hot pressing, flash welding, friction stir welding, and annealing processes [93-100]. The intermetallic compounds are usually brittle phases and the bond strength can reduce sharply and promote crack propagation as this region increases in size [95, 98]. As the IMC thickness increases with annealing time [94, 96, 97, 100], it is considered as a possible reason for the observed brittle behavior of hybrid foam samples with longer annealing time, and thus an investigation into this effect was carried out.

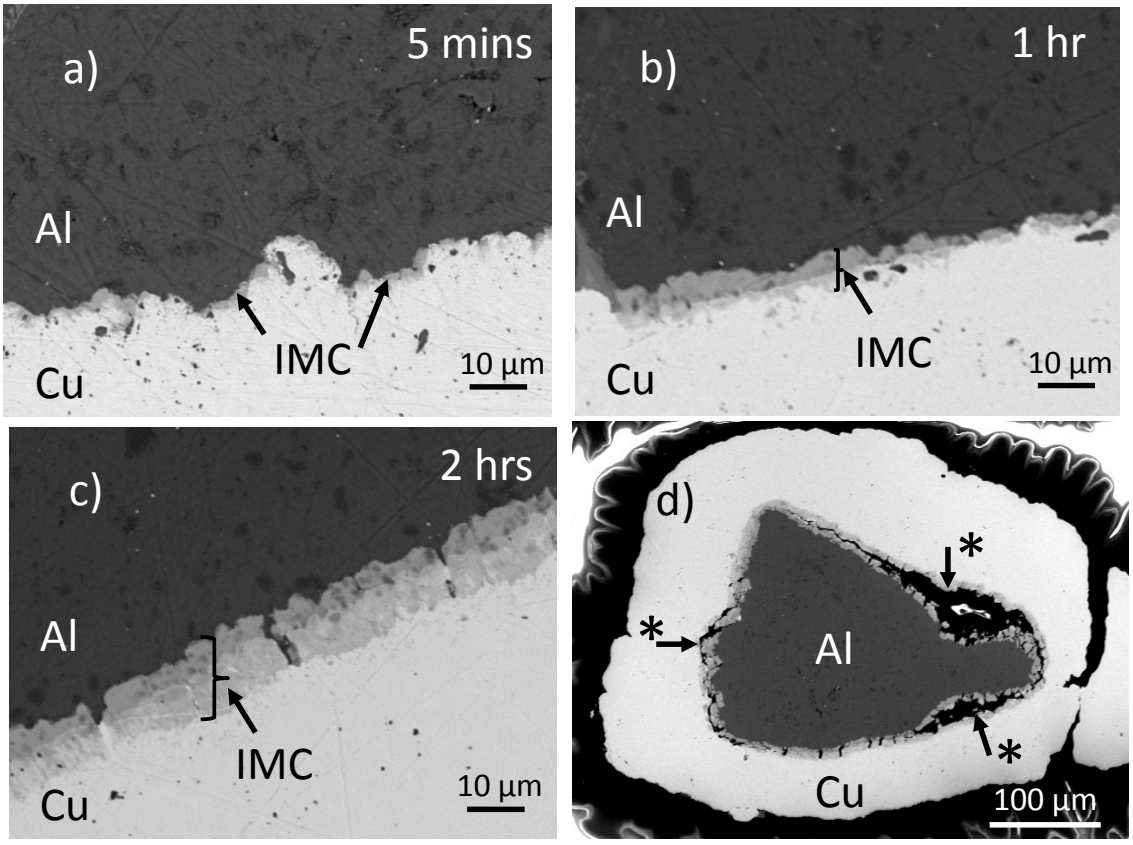

Figure 4-10 SEM images of Al-Cu interface in Al/Cu hybrid foams after annealing time of (a) 5 minutes; (b) 1 hour; and (c-d) 2 hours

Table 4-4 Width of intermetallic compound with different annealing time

Annealing Time	Thickness (μm)
5 minutes	1.6
1 hour	4.9
2 hours	10.5

Fig. 12 shows SEM images (using backscattered electrons) of the Al/Cu interface of hybrid foam samples after different annealing times. The IMC region can be observed at the Al/Cu interface in all annealed samples, which can be seen as an intermediate grey color region separating aluminum and copper. The estimated IMC width in the different samples is shown in Table 4-4. The reported values are the averages of at least five measurements taken for each sample. It can be seen that the size of the IMC increases with annealing time and that the width of the IMC in samples after 2 hours of annealing reached 10.5 μm.

Due to the different material thermal properties of Al and Cu (the thermal expansion coefficient is 23×10^{-6}/°C for aluminum and 17×10^{-6}/°C for copper), stress may be accumulate at the Al/Cu interface caused by the mismatch of deformation during the annealing and cooling stages. Fracture of the IMC may thus occur once such buildup stress exceeds the strength of the IMC, which, as previously mentioned, reduces in proportion to the thickness of the region.

Figure 4-10d shows fracture of the IMC, which led to separation between the Al core and the Cu coating, indicated by arrows with an asterisk ("*") in sample C60-HT-A2. Failure of the IMC caused by reduction in bond strength is considered to be the main cause for the brittle response observed in the C60-HT-A2 sample. Thus, a proper amount of annealing time needs to

be chosen to provide sufficiently improved ductility of the electrodeposited coating while limiting the size of the IMC created.

4.4.3 Tensile Response

Foams are usually used in compression due to their unique energy absorption capacity,. However, foams may be subjected to tension in certain cases, e.g., in a sandwich panel or when used as structural components. Thus it is considered important to study the behavior of Al/Cu hybrid foams and the effect of annealing under tensile loading conditions.

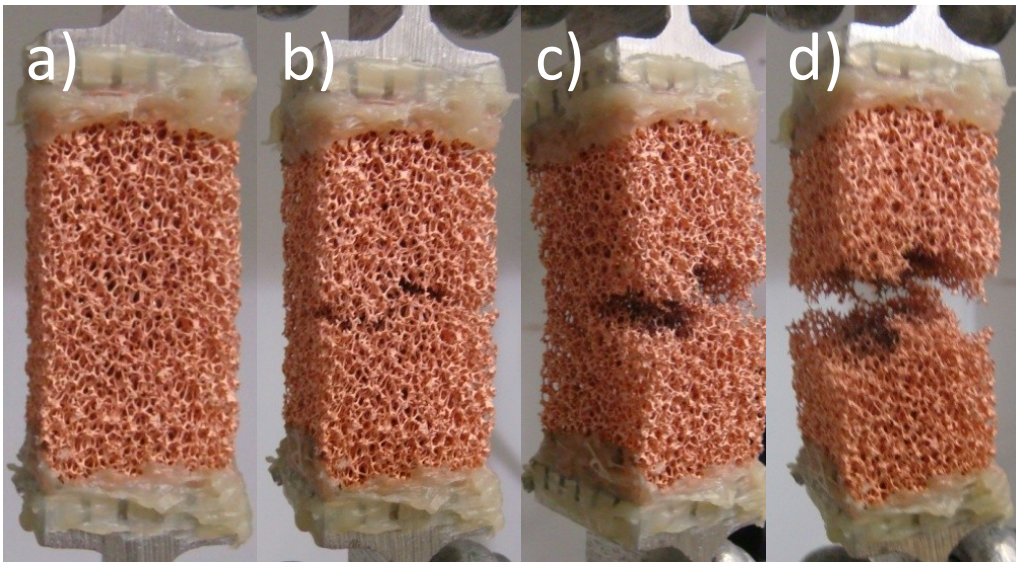

Figure 4-11 Images from the tensile testing of foam sample C30-HT-A1

Images from the tensile testing of sample C30-HT-A1 is shown in Figure 4-11. It can be seen that failure was localized at the center of the sample and not at the bonding surfaces with the loading fixtures. Figure 4-12 shows the tensile stress-strain curves for plain Al foam and Al/Cu hybrid foam samples with and without annealing (400 °C for 1 h) treatment. In the figure,

plots (a) and (c) show complete traces for 30 μm and 60 μm Cu coatings, respectively, while plots (b) and (d) show corresponding closer views of the initial region of the stress-strain response. The yielding point was determined by finding the intersection of the first and second linear portion of the stress strain curves.

It can be seen from Figure 4-12c that the plain Al foam yields at about 1 % strain followed by some hardening until fracture happens at about 5 % strain. The post-yielding hardening is attributed to the hardening of the material and the re-alignment of foam ligaments to the tension loading axis [13]. A stiffer behavior was observed for the Al/Cu hybrid foams at low strain levels since the foam ligaments are reinforced by the copper coating. The hybrid foam specimens also show a lower strain for the onset of yielding compared to the plain unannealed Al foam. This is due to the relatively low yielding strength of annealed of copper (the yield strength of unnanealed Al is 193 MPa while that of annealed Cu is 33.3 MPa [101]).

Yielding of the copper coating leads to a stiffness change that is similar to that of the plain Al foam during the post-yielding stage. A much earlier fracture (at about 2 % strain) happens in the unannealed hybrid foam samples and the load carrying capacity drops more rapidly compared to the plain Al foam. This is a direct consequence of the low ductility of the copper coating, with a larger brittle effect observed for unannealed hybrid foam samples with thicker coatings.

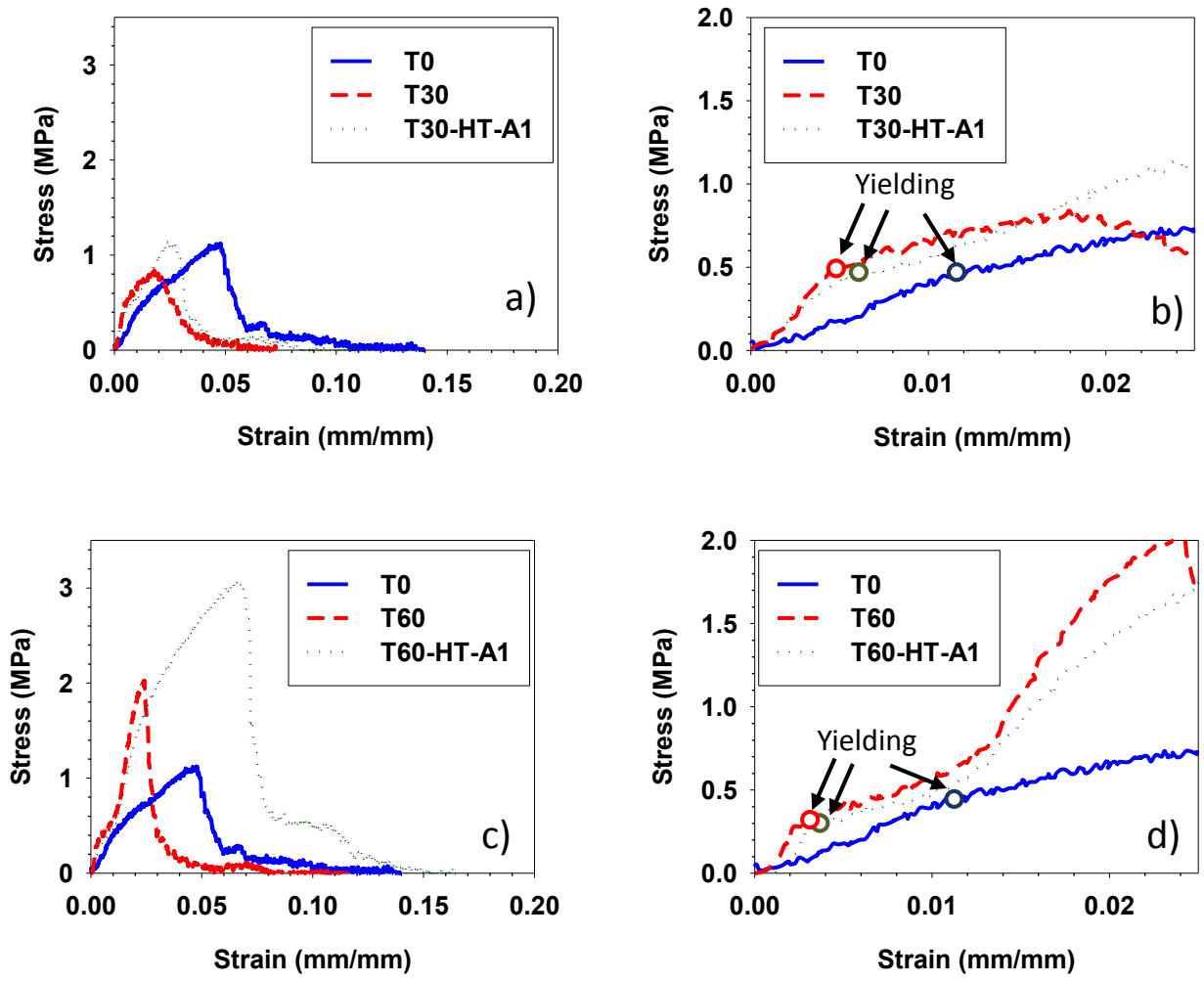

Figure 4-12 Tensile stress-strain response of Al/Cu hybrid foams

On the other hand, the annealed hybrid foam samples showed a similar behavior at lower strain level to the unannealed samples but the post-yielding response branch continues to larger strain level, especially in hybrid foams with 60 μm coating. It needs to be noted that the sample with 30 μm coating was expected to fracture at a higher strain level (close to that with 60 μm coating) if a proper amount of annealing was provided but the performance of the samples tested may have been degraded due to the formation of excessive IMC at the Al/Cu interface.

It can be seen that the tensile behavior of Al/Cu hybrid foams is distinct from their compressive behavior. More specifically, the low fracture strain of the hybrid foams significantly limited the performance in tension and such behavior may be detrimental in certain applications. Conversely, the annealed hybrid foams showed a promising performance with enhancement in both strength and ductility. It is believed that similar tensile behavior as that observed in Al/Cu hybrid foams and their enhancement with annealing will be characteristic in other hybrid foam systems (e.g., Al/Ni hybrid foams [6, 7, 40]).

4.5 Discussion

Figure 4-13 shows the comparison of the energy absorption capacity under compression of different foams with respect to coating thicknesses. The data points for plain Al foams with different coating thicknesses represent unannealed Al foams with the same relative density (RD) as the Al/Cu hybrid foams with corresponding coating thicknesses.

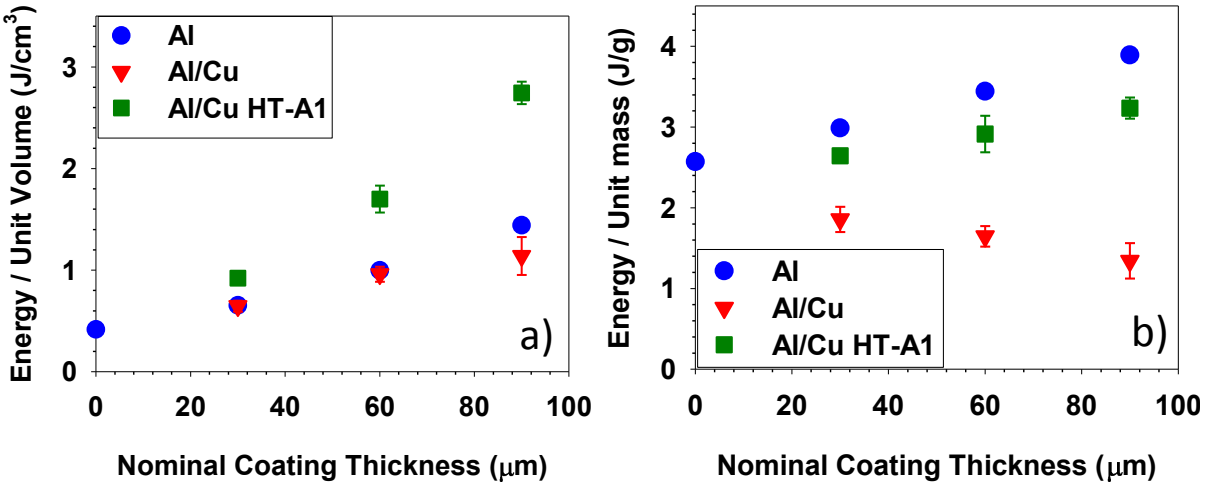

Figure 4-13 Comparison of energy absorption capacities for different foam samples: (a) per unit volume; (b) per unit mass. The error bars represent the standard deviations

For Al/Cu hybrid foams, the energy absorption capacity per unit volume was calculated as the area under the compressive stress strain curve up to a strain level of 50% (ε_{max}= 50%) using Equation 4-3. The energy absorption capacity per unit volume of plain Al foams was calculated using Equation 4-4 assuming a perfectly plastic stress plateau after yielding [40], where the yield stress (or plateau stress) σ_y, yield strain ε_y and modulus of elasticity E were calculated using Equation 4-5Equation 4-7 [13], respectively. The product of $C\sigma_s$ in Equation 4-5 was determined to be 56.9 (MPa) based on the plateau stress of the uncoated Al foam (6% nominal relative density) tested in this study.

$$U_h = \int_0^{\varepsilon max} \sigma d\varepsilon \qquad \text{Equation 4-3}$$

$$U_p = \sigma_y \left(\varepsilon_{max} - 0.5\varepsilon_y \right) \qquad \text{Equation 4-4}$$

$$\sigma_y = C\sigma_s \left(RD \right)^{3/2} \qquad \text{Equation 4-5}$$

$$\varepsilon_y = \sigma_y / E \qquad \text{Equation 4-6}$$

$$E = E_s \left(RD \right)^2 \qquad \text{Equation 4-7}$$

It can be seen from Figure 4-13a that the energy absorption capacity per unit volume for Al/Cu hybrid foams increases with the Cu coating thickness (i.e., relative density) since more materials are used. This is expected and has also been shown in other studies on hybrid foams [7, 8, 40].

Compared to plain Al foams with the same relative density, the unannealed Al/Cu hybrid foams showed similar energy absorption capacity per unit volume at coating thicknesses less than 90 μm but showed a lower capacity for higher coating thicknesses. The limited performance for the unnanealed hybrid foams with thicker coatings was due to the brittle behavior caused by

the low ductility of copper coating. In contrast, the annealed hybrid foams showed significantly higher energy absorption capacity per unit volume compared to the unannealed Al/Cu hybrid foams and the plain Al foams for different coating thicknesses.

A different trend was observed when the energy absorption capacity per unit mass for the different foams was compared, as shown in Figure 4-13b. As the density of copper is more than three times that of aluminum, Al/Cu hybrid foams (with and without annealing) generally showed a lower energy absorption capacity per unit mass compared to plain Al foams with equal relative density. In fact, in such comparison the performance of unannealed Al/Cu hybrid foams decreases with coating thickness. This indicates a poor performance of unannealed Al/Cu hybrid foams for weigh/mass critical applications. Similar behavior for Al foams with Ni-W coatings has been reported [40]. However, the energy absorption capacity per unit mass of annealed Al/Cu hybrid foams shows an increasing trend with coating thickness, which is similar to the behavior of plain Al foams. Such behavior indicates a more efficient performance of the annealed Al/Cu hybrid foams with thicker coatings.

The difference in energy absorption performance of Al/Cu hybrid foams before and after a proper annealing process indicates a significant enhancement due to annealing. It is believed that a similar improvement can be obtained through annealing in other hybrid foams manufactured using electrodeposition (e.g., Al/Ni hybrid foams).

4.6 Conclusions

1) The energy absorption performance of Al/Cu hybrid foams under compression can be effectively improved by proper annealing, which enhances the ductility of the electrodeposited copper coating. Such effect is more significant in hybrid foams with thicker coatings.

2) Annealing of hybrid foams can be conducted at one third to one half of the melting temperature of the coating material. However, additional time is needed when annealing at a lower temperature.

3) To efficiently enhance the energy absorption performance of Al/Cu hybrid foams, the annealing time should be sufficient to cause a ductility increase in the coating material but limited to avoid the formation of excessive intermetallic compounds (IMC) at the Al/Cu interface, which may cause fracture within the IMC and consequently reduced performance.

4) A low ductility coating in Al/Cu hybrid foams causes early fracture of in tension, which limits the macroscopic strength and ductility of the foam. However, proper annealing can significantly improve both strength and ductility of Al/Cu hybrid foams in tension.

CHAPTER 5 ANALYTICAL SOLUTION FOR HYBRID FOAM

The enhanced performance of Al/Cu hybrid foam with nano-copper coating through electrodeposition has been demonstrated. In addition, it has been shown both numerically and experimentally that the performance of Al/Cu hybrid foams can be further improved with a proper amount of annealing after the electrodeposition process. By varying the coating thickness, the properties of Al/Cu hybrid foams can be modified. The behavior of Al/Cu hybrid foam with different levels of coating thicknesses can be predicted using the beam-element based finite element models developed in CHAPTER 3. However, a simple but reliable analytical model is usually more appropriate and convenient for the purpose of engineering design. As a result, analytical solution for the prediction of compressive behavior of Al/Cu hybrid foams was derived and is presented in this section.

Among many theoretical studies on the behavior of cellular materials [13, 52, 102, 103], the work by Gibson and Ashby [13] is widely recognized due to its simplicity as well as accuracy. The semi-empirical solution derived by Gibson and Ashby [13] can be used to predict properties of open-cell foam materials by simply using the relative density of the foam and the properties of base material. The theoretical solution for open-cell foam material derived by Gibson and Ashby is based on a cubic unit cell model with square cross section (see Figure 2-5). When combined with several experimentally calibrated constants, solution with a good accuracy can be obtained using such unit cell model. However, such unit cell is not a good representation of the actual foam structure. In the current work, the analytical solution was based on the characteristic cell geometry used by Jang and Kyriakides [71], which was based on a Kelvin cell model.

A Kelvin cell has 24 ligaments and 18 nodes (see Figure 5-1). It is assumed that ligaments in the vertical plane have a length L and an angle of θ with respect to the horizontal plane. According to the study by Jang and Kyriakides [18], an anisotropy λ can be observed in open-cell foam structures, which can be defined using Equation 5-1. As a result, the space occupied by the unit cell has a width and depth of $4L\cos\theta$ and a height of $4L\sin\theta$.

$$\lambda = \tan\theta \qquad \text{Equation 5-1}$$

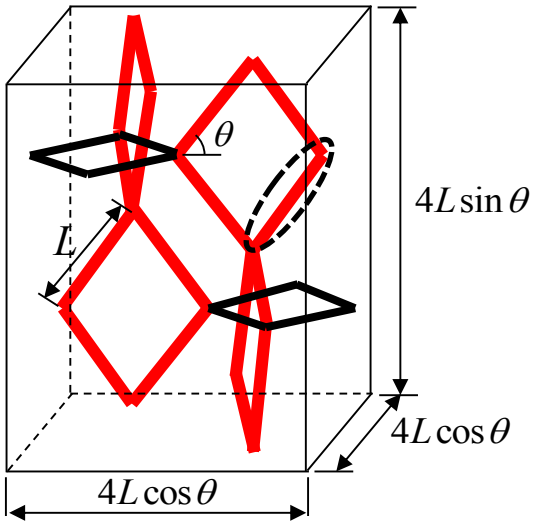

Figure 5-1 Geometry of Unit Cell [71]

The size of the characteristic unit cell used is much smaller compared to the size of the component made with foam material. Thus it is assumed that the unit cell is within an infinite domain and thus any boundary effect is neglected. When the unit cell is subjected to uniaxial stress (e.g., stress in vertical direction in Figure 5-2), it is assumed the unit cell can expand freely in the direction perpendicular to the loading direction (e.g., horizontal direction in Figure 5-2). As a result, the 8 ligaments within horizontal plane will not be loaded when the unit cell is loaded in vertical direction.

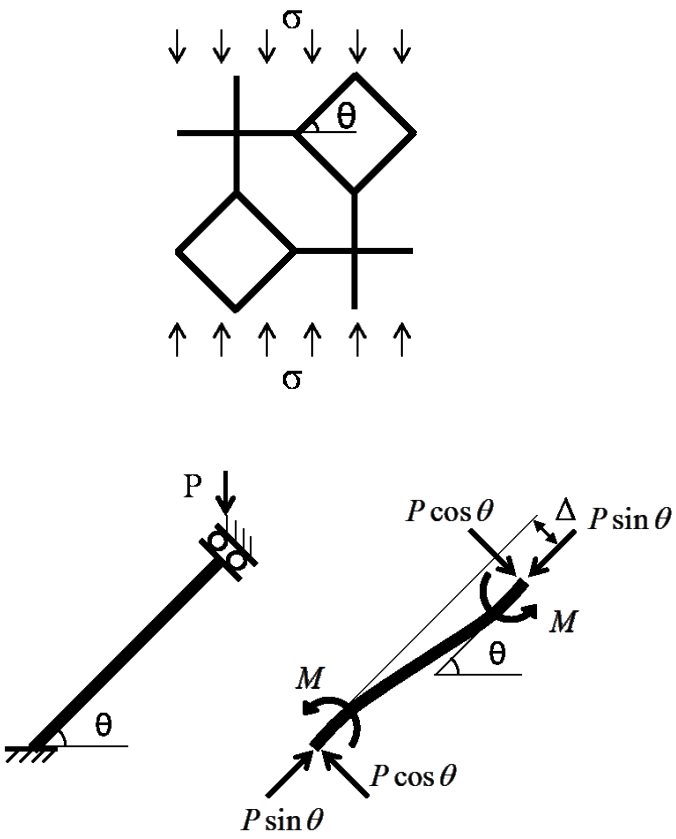

Figure 5-2 Simplification of unit cell model

The loaded 16 ligaments have identical geometry and are subjected to the same loading condition due to symmetry (see Figure 5-2). In other words, the problem of a unit cell subjected to uniaxial stress loading condition can be simplified to the problem of one loaded ligament with boundary conditions and loading as shown in Figure 5-2, in which the moment at the ends of ligament can be calculated by:

$$M = \left(P\cos\theta L\right)/2 \qquad \text{Equation 5-2}$$

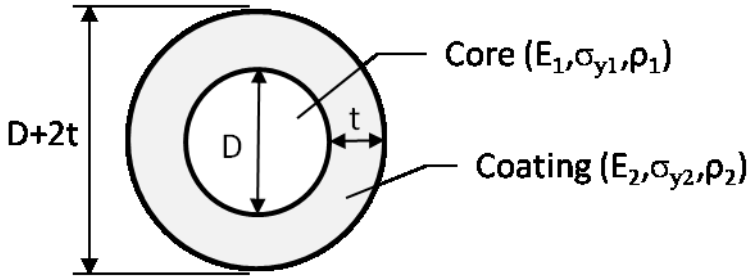

Figure 5-3 Cross section of composite ligament in hybrid foam

It has been demonstrated that relative density is the most important parameter that affecting the properties of open-cell foam materials [13]. The relative density of single-material open-cell foams can be calculated as the ratio of the density of the foam material with respect to the base material density. However, there are more than one base material in a hybrid foam and thus it is difficult to calculate the relative density in terms of density. Instead, the relative density is considered to be the ratio of the volume of solids with respect to the volume/space occupied by foam material. As a result, the relative density of plain foam RD can be calculated using Equation 5-3 while the relative density for a hybrid foam can be calculated using Equation 5-4.

$$RD = \frac{V_{core}}{V_{foam}} \qquad \text{Equation 5-3}$$

$$RD' = \frac{V_{core} + V_{coating}}{V_{foam}} = RD + \frac{m_{coating}}{\rho_{coating} V_{foam}} \qquad \text{Equation 5-4}$$

The relative density of hybrid foam can thus be calculated based on the relative density of base foam and the mass of the coating material, which is convenient as the mass of coating is usually easy to know in a hybrid foam. Similar to the numerical model discussed in CHAPTER 3, it is assumed that the ligament in base foam and hybrid foam has a circular cross section (see

Figure 5-3). For the purposes of simplification, it is assumed that the ligament has a uniform cross-section along the ligament length. With the cross section and the unit cell geometry, the relationship between relative density and ligament size can be calculated as follows.

For unit cell in a plain foam, the volume of solid is:

$$V_{core} = 24 \times \pi d^2 / 4 \times L = 6\pi d^2 L \qquad \text{Equation 5-5}$$

The space occupied by the unit cell is:

$$V_{foam} = (4\,\mathrm{L}\cos\theta)^2 \times 4\,\mathrm{L}\sin\theta = 64\sin\theta\cos^2\theta L^3 \qquad \text{Equation 5-6}$$

Then the relative density RD of plain form can be calculated as:

$$RD = \frac{V_{core}}{V_{foam}} = \frac{6\pi d^2 L}{64\sin\theta\cos^2\theta L^3} = k\left(\frac{d}{L}\right)^2 \qquad \text{Equation 5-7}$$

where

$$k = \left(\frac{3\pi}{32\sin\theta\cos^2\theta}\right) \qquad \text{Equation 5-8}$$

Equation 5-7 can also be written in the following form:

$$\frac{d}{L} = \sqrt{\frac{RD}{k}} \qquad \text{Equation 5-9}$$

Similar to plain foam, the relationship between relative density of hybrid foam (RD') and ligament geometry can be obtained as shown in Equation 5-10 and Equation 5-11:

$$RD' = k\left(\frac{d+2t}{L}\right)^2 \qquad \text{Equation 5-10}$$

or,

$$\frac{d+2t}{L} = \sqrt{\frac{RD'}{k}}\,. \qquad \text{Equation 5-11}$$

The assumptions in ligament cross-section and unit cell geometry discussed were used for all analytical solutions presented in this Chapter. First, the analytical solution to predict the

modulus of hybrid foam consisting two different materials are presented in Section 5.1. It has been shown that the coating ductility has great influence on the macro behavior of hybrid foams. Thus the analytical solutions for post-yield behavior for hybrid foams were derived considering two schemes. More specifically, the analytical solutions in Section 5.2 are based on hybrid foam with ductile coating material (e.g., annealed Al/Cu hybrid foam). And Section 5.3 presents the analytical solutions for the post-yield behavior of hybrid foams with brittle coating material (e.g., as-built Al/Cu hybrid foam).

5.1 Modulus of Hybrid Foam

The modulus of a foam can be calculated based on the load applied to the unit cell and the resulting deformation. The force P applied to one ligament can be calculated based on the stress σ applied to the unit cell (note that there are four loaded ligaments in a horizontal plane).

$$P = \frac{\sigma \times (4L\cos\theta)^2}{4} = 4(L\cos\theta)^2\sigma \qquad \text{Equation 5-12}$$

or,

$$\sigma = \frac{P}{4(L\cos\theta)^2}. \qquad \text{Equation 5-13}$$

Based on classic beam theory, the displacement Δ at the top of the ligament can be calculated according to Equation 5-14:

$$\Delta = \frac{P\cos\theta L^3}{12EI} \qquad \text{Equation 5-14}$$

The displacement component δ and the corresponding strain ε in the loading direction can then be calculated with Equation 5-15 and Equation 5-16. The modulus of the foam material can be calculated using σ and ε Equation 5-17.

$$\delta = \Delta\cos\theta = \frac{P\cos^2\theta L^3}{12EI} \qquad \text{Equation 5-15}$$

$$\varepsilon = \frac{\delta}{L\sin\theta} = \frac{P\cos^2\theta L^2}{12EI\sin\theta} \qquad \text{Equation 5-16}$$

$$E = \frac{\sigma}{\varepsilon} = \frac{3EI\sin\theta}{(\mathrm{L}\cos\theta)^4} \qquad \text{Equation 5-17}$$

The cross section of a ligament in a hybrid foam is a composite section. Thus, the section flexural stiffness, *EI*, can be calculated using Equation 5-18.

$$\begin{aligned} EI &= E_1 I_1 + E_2 I_2 \\ &= \frac{\pi}{64}\left\{E_1 d^4 + E_2\left[(\mathrm{d}+2\,\mathrm{t})^4 - d^4\right]\right\} \\ &= \frac{\pi}{64}\left[(E_1 - E_2)d^4 + E_2(\mathrm{d}+2\,\mathrm{t})^4\right] \end{aligned} \qquad \text{Equation 5-18}$$

Assuming that $E_2/E_1=a$, then:

$$EI = \frac{\pi}{64}E_1\left[(1-a)d^4 + a(\mathrm{d}+2\,\mathrm{t})^4\right] \qquad \text{Equation 5-19}$$

Then modulus of a hybrid foam can then be calculated with Equation 5-20 and Equation 5-21, in which the relationship between foam relative density and ligament geometry derived in Equation 5-9 and Equation 5-11 were used.

$$E = \frac{3\pi\sin\theta}{64\cos^4\theta}E_1\left[(1-a)\left(\frac{d}{L}\right)^4 + a\left(\frac{\mathrm{d}+2\,\mathrm{t}}{L}\right)^4\right] \qquad \text{Equation 5-20}$$

$$\frac{E}{E_1} = 0.147\frac{\sin\theta}{\cos^4\theta k^2}\left[(1-a)\left(RD\right)^4 + a(RD')^4\right] \qquad \text{Equation 5-21}$$

In Equation 5-21, θ and k are constants based depending on the anisotropy of the foam. Thus, the modulus of a hybrid foam can be calculated simply using the relative density of the plain foam and the hybrid foam and the properties of two base materials.

5.2 Analytical Solution for Hybrid Foams with Ductile Coating

5.2.1 Plastic Stress

The stress plateau observed in the stress-strain curve of conventional metal foams is caused by plastic collapse of the foam ligaments when loaded beyond the linear-elastic range [13]. Plastic collapse occurs when the localized bending moment demands exceeds the plastic moment capacity of the ligament section and creating plastic hinges, as shown in Figure 5-4. Based on the boundary conditions of a single ligament, it can be seen plastic hinges will form at the ends of the ligament, where the maximum moment is.

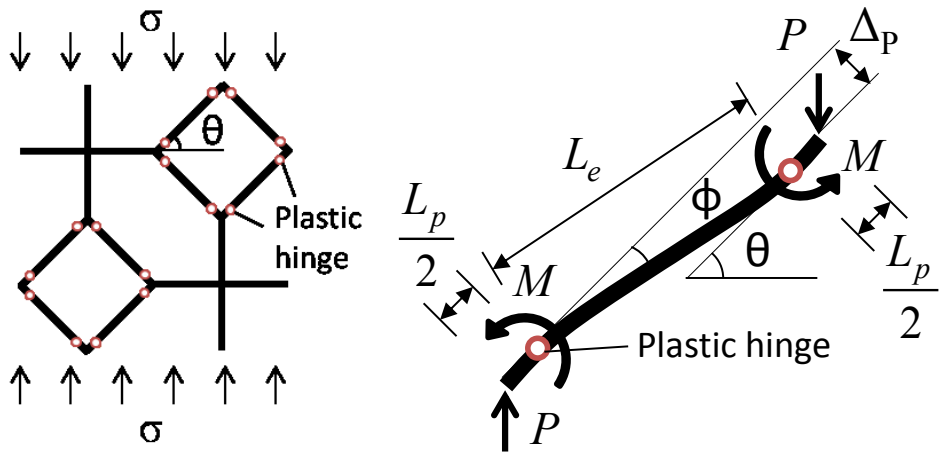

Figure 5-4 Plastic hinge location

An idealized plastic hinge has zero length and all plastic deformation occurs at the plastic hinge. However, in reality plastic deformations occurs within a region of finite length (plastic hinge length). Thus, it is assumed that the location of the plastic hinge is at a distance of $L_p/2$

from both ends, where *Lp* is plastic hinge length. The plateau stress can be obtained by equating the external work done by the force during plastic rotation ϕ of the two plastic hinges in each ligament to the internal plastic work done at the hinges:

$$2M_p\phi = P\Delta_p \cos\theta \qquad \text{Equation 5-22}$$

where,

$$P = 4\left(L\cos\theta\right)^2 \sigma \qquad \text{Equation 5-23}$$

$$\Delta_p = \phi L_e = \phi\left(L - L_p\right) \qquad \text{Equation 5-24}$$

A simple estimate of the plastic hinge length is [104]:

$$L_p = \frac{d}{2} \qquad \text{Equation 5-25}$$

Then,

$$L_e = xL \qquad \text{Equation 5-26}$$

$$\text{Where, } x = 1 - \frac{1}{2}\frac{D}{L} = 1 - \sqrt{\frac{RD}{k}} \qquad \text{Equation 5-27}$$

Then from Equation 5-22, the yield stress (plastic stress) can be derived:

$$\sigma = \sigma_{pl} = \frac{M_p}{2x(\mathrm{L}\cos\theta)^3} \qquad \text{Equation 5-28}$$

The same result can be obtained by assuming that the moment at the plastic hinge location is equal to the plastic moment M_p:

$$M_x = \left[P\cos\theta\left(xL\right)\right]/2 = 2x\left(L\cos\theta\right)^3 \sigma = M_p \qquad \text{Equation 5-29}$$

And then,

$$\sigma = \frac{M_p}{2x(\mathrm{L}\cos\theta)^3} \qquad \text{Equation 5-30}$$

Assuming an elastic-perfect plastic constitutive model for both core and coating material, the moment for full section plastification, *Mp*, can be calculated using Equation 5-31, in which $Z_p=d^3/6$ is the plastic section modulus for circular section.

$$\begin{aligned} M_p &= \sigma_y Z_p \\ &= \sigma_{y1} Z_{p1} + \sigma_{y2} Z_{p2} \\ &= \frac{1}{6}\sigma_{y1} d^3 + \frac{1}{6}\sigma_{y2}\left[(\mathrm{d}+2\,\mathrm{t})^3 - d^3\right] \\ &= \frac{1}{6}\left[(\sigma_{y1}-\sigma_{y2})d^3 + \sigma_{y2}(\mathrm{d}+2\,\mathrm{t})^3\right] \end{aligned} \qquad \text{Equation 5-31}$$

Assuming

$$\sigma_{y2} = b\sigma_{y1} \qquad \text{Equation 5-32}$$

Then:

$$M_p = \frac{1}{6}\sigma_{y1}\left[(1-b)d^3 + b(\mathrm{d}+2\,\mathrm{t})^3\right]. \qquad \text{Equation 5-33}$$

The ratio between plastic stress and yielding stress of core material is given in Equation 5-34, where the relations between relative density and ligament geometry from Equation 5-9 and Equation 5-11 were used.

$$\begin{aligned} \frac{\sigma_{pl}}{\sigma_{y1}} &= \frac{1}{12x(\cos\theta)^3}\left[(1-b)\left(\frac{d}{L}\right)^3 + b\left(\frac{\mathrm{d}+2\,\mathrm{t}}{L}\right)^3\right] \\ &= \frac{1}{12x(\cos\theta)^3 k^{3/2}}\left[(1-b)\left(RD\right)^{3/2} + b\left(RD'\right)^{3/2}\right] \end{aligned} \qquad \text{Equation 5-34}$$

Similar to the solution obtained by Gibson and Ashby [13], Equation 5-34 does not require information about the ligament geometry, Instead, it shows that the plateau stress of a hybrid foam made with two metal materials can be calculated based on the relative density of the foam before and after electrodeposition.

The post-yield behavior was modeled based on the method used by Gibson and Ashby [13] using Equation 5-35Equation 5-37. The values for constants *D* and m were determined by fitting the stress-strain curve to the equations. A value of 1.2 for *D* and 1 for *m* were found to yield a good prediction of the post-yield behavior of Al/Cu hybrid foam.

$$\varepsilon_D = 1 - 1.4RD \qquad \text{Equation 5-35}$$

$$\frac{\sigma}{\sigma_{pl}} = 1 \text{ when } \varepsilon \le \varepsilon_D\left(1 - \frac{1}{D}\right) \qquad \text{Equation 5-36}$$

$$\frac{\sigma}{\sigma_{pl}} = \frac{1}{D}\left(\frac{\varepsilon_D}{\varepsilon_D - \varepsilon}\right)^m \text{ when } \varepsilon > \varepsilon_D\left(1 - \frac{1}{D}\right) \qquad \text{Equation 5-37}$$

5.2.2 Results

The derived analytical solution was used to predict the compressive response of Al/Cu hybrid foams. Only samples subjected to an annealing process were considered, since the analytical solution was based on an elastic-perfect plastic constitutive material model for the core and coating. The input information is for the analytical solution is shown in Table 5-1. It needs to be noted that annealed copper has a very low yielding stress (about 70 MPa) and a long hardening branch in its constitutive model [105]. As a result, the ultimate stress is much higher compared to its yield stress.

Beyond the elastic regime, the deformation of metal foams involves localized large deformations (i.e., localized collapse of foam cell structures) and thus large rotations at the plastic hinge location. Therefore, it is considered that significant hardening of the copper coating will happen at the plastic hinge location and thus the ultimate stress was used. A value of 1.2 was

used for the anisotropy factor λ as suggested by Jang and Kyriakides [71] based on measurements of ligament geometry on open-cell Al foams.

Table 5-1 Input parameters for analytical solution

Material	E (GPa)	σ_y (MPa)	λ	D	m
Core (Al6101, annealed) [80]	70	90	1.2	1.2	1
Coating (Copper, annealed) [105]	110	210 (σ_u)			

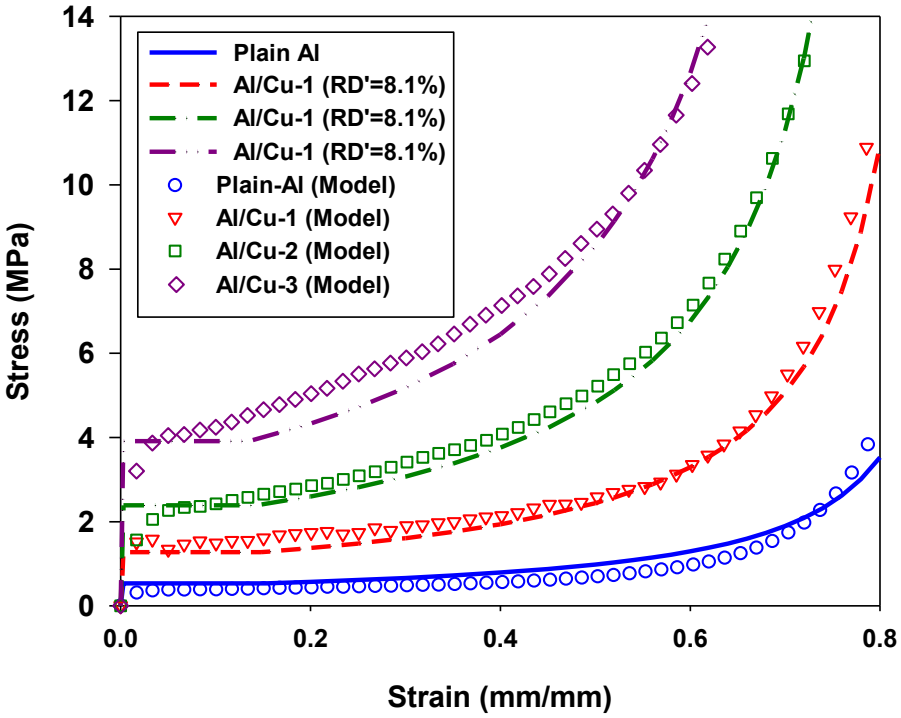

Figure 5-5 Comparison between experimental data and analytical solution

Figure 5-5 shows the comparison between the presented analytical solution and experimental data from Al/Cu hybrid foams with different levels of coating. The experimental

data was based on annealed samples (both plain Al and Al/Cu hybrid foams). It can be seen that the plateau stress and post yield behavior predicted by the analytical solution agrees well with the experimental data. However, deviation was observed between the analytical solution and the experimental data within elastic region. This difference in results can be attributed to the fact that the analytical solution was based on a simple elastic-perfect plastic material model while the copper coating in Al/Cu hybrid foams actually has early yielding and a significant hardening.

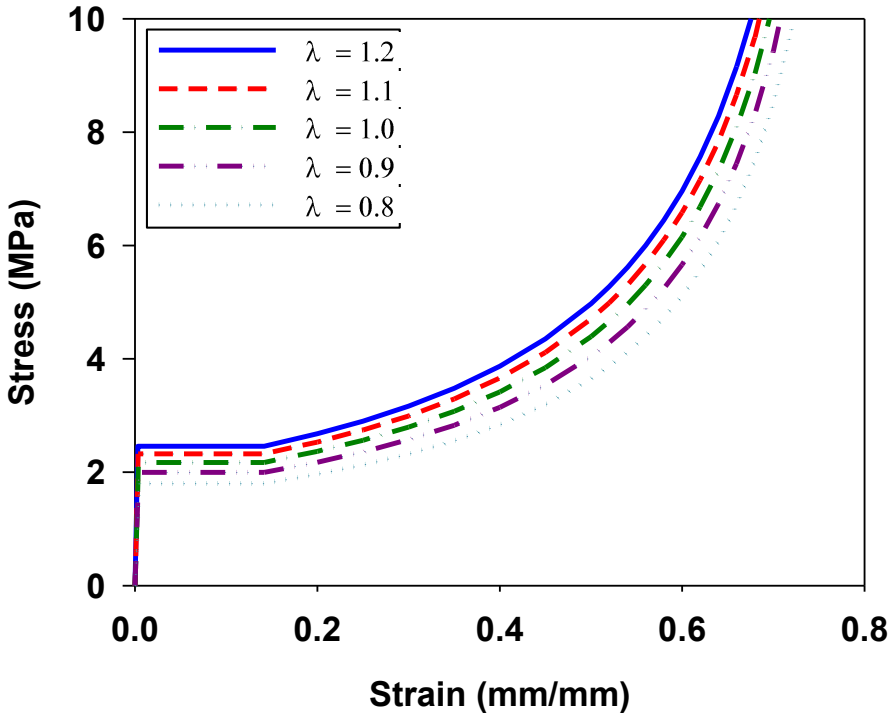

Figure 5-6 Stress strain curve of Al/Cu hybrid foam (RD=6%, RD'=10.7%) with different anisotropy

Figure 5-6 shows the stress strain curve for Al/Cu hybrid foams with a nominal coating thickness of 60 μm and different levels of anisotropy. The relative density for the base foam and the hybrid foam is 6% and 10.7%, respectively. It can be seen that hybrid foam with higher

anisotropy has a higher yielding stress and plateau stress. This agrees with the observation by Jang and Kyriakides [71] using multi-cell finite element models.

5.3 Analytical Solution for Hybrid Foams with Low Ductility Coating

The analytical solution derived in 0 provides a good prediction on the compressive behavior of Al/Cu hybrid foams with annealing process. The solution assumed that both the coating and core material have a ductile behavior and fracture of the material will not occur. However, the analytical solution is not appropriate for as-built Al/Cu hybrid foams (i.e., no annealing process introduced), which shows brittle behavior in compression due to the low ductility of the electrodeposited copper coating. The compressive behavior of as-built Al/Cu hybrid foams can be simplified as shown in Figure 5-7. Upon reaching the stress peak (σ_{fr}), fracture of the ligaments occurs and the stress drops to a lower level (σ_{low}). The low stress level continues through the plateau region until the densification allows the stress to increase at large strains. It can be seen that a good prediction of the two stress level (σ_{fr} and σ_{low}) is the key for an analytical model. In this section, an analytical solution is derived for Al/Cu hybrid foams without annealing process. The derivation is based on the single ligament model used for ductile Al/Cu hybrid foams (i.e., with annealing process introduced after electrodeposition).

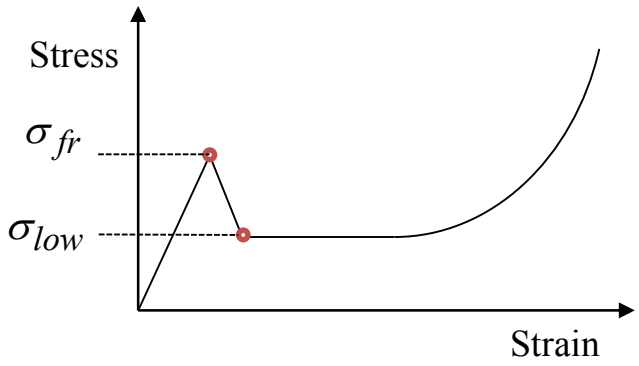

Figure 5-7 Typical behavior of Al/Cu hybrid foams

5.3.1 Stress at Fracture

The strain and stress distribution across the cross section of a ligament subjected to pure bending is shown in Figure 5-8. Based on classic beam theory the strain distribution across the cross section is linear with zero strain at the neutral axis. The normal stress across the cross section can be simply calculated using $\sigma = E\varepsilon$. It is assumed that coating fracture in AL/Cu hybrid foams happens when the stress level at the extreme fiber of the copper coating exceeds the fracture stress of electrodeposited copper, σ_{fr-Cu}.

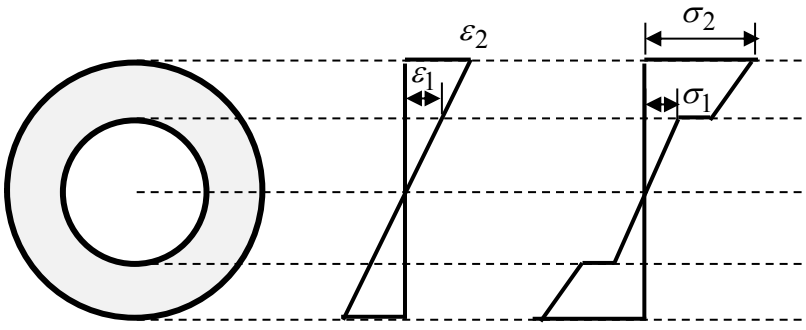

Figure 5-8 Strain and stress across ligament cross section

The moment capacity of the pre-fractured cross section, M_{fr} ,can be calculated as the sum of contributions from the core (M_1) and the coating (M_2):

$$M_{fr} = M_1 + M_2 \qquad \text{Equation 5-38}$$

It is assumed that the core and coating material remain elastic prior to fracture. Thus M_1 and M_2 in Equation 5-38 can be calculated using Equation 5-39, Equation 5-40, Equation 5-41, and Equation 5-42:

$$M_1 = \frac{\sigma_1 I_1}{d/2} = \frac{\pi \sigma_1 d^3}{32} \qquad \text{Equation 5-39}$$

$$\text{where, } I_1 = \frac{\pi d^4}{64} \qquad \text{Equation 5-40}$$

$$M_2 = \frac{\sigma_2 I_2}{(d+2t)/2} = \frac{\pi \sigma_2}{32} \frac{(d+2t)^4 - d^4}{d+2t} \qquad \text{Equation 5-41}$$

$$\text{where, } I_2 = \frac{1}{64}\left[(d+2t)^4 - d^4\right] \qquad \text{Equation 5-42}$$

Prior to ligament fracture, the stress level at the extreme fiber in the coating material equals the fracture stress of the coating material ($\sigma_2 = \sigma_{fr-Cu}$ for Al/Cu hybrid foams). And the stress level at the extreme fiber in the core can be calculated using Equation 5-43.

$$\sigma_1 = \frac{\sigma_2 E_1}{E_2} \frac{d}{d+2t} \qquad \text{Equation 5-43}$$

It is assumed that strength degradation of the as-built (i.e., brittle) Al/Cu hybrid foam initiates at the onset of coating fracture in the ligament. As a result, the initial peak stress in the compressive behavior of as-built Al/Cu hybrid foams equals the strength prior to coating fracture

(σ_{fr}), which can be calculated based on M_{fr} using a relation derived for plastic stress, as shown below in Equation 5-44.

$$\begin{aligned}
&\sigma_{fr} \\
&= \frac{M_{fr}}{2x(L\cos\theta)^3} \\
&= \frac{\pi}{64x(\cos\theta)^3}\left\{\sigma_1\left(\frac{d}{L}\right)^3 + \sigma_2\left[\left(\frac{d+2t}{L}\right)^3 - \left(\frac{d}{L}\right)^3\left(\frac{d}{d+2t}\right)\right]\right\} \\
&= \frac{\pi\sigma_{fr}}{64x(\cos\theta)^3}\left\{\frac{E_1}{E_2}\frac{d}{d+2t}\left(\frac{d}{L}\right)^3 + \left[\left(\frac{d+2t}{L}\right)^3 - \left(\frac{d}{L}\right)^3\left(\frac{d}{d+2t}\right)\right]\right\} \\
&= \frac{\pi\sigma_{fr}}{64x(\cos\theta)^3}\left\{\frac{E_1}{E_2}\sqrt{\frac{RD}{RD'}}\left(\frac{RD}{k}\right)^{3/2} + \left[\left(\frac{RD'}{k}\right)^{3/2} - \left(\frac{RD}{k}\right)^{3/2}\sqrt{\frac{RD}{RD'}}\right]\right\}
\end{aligned} \qquad \text{Equation 5-44}$$

5.3.2 Post-peak Stress

Sectional behavior is of the coated ligament is more complex once coating fracture occurs. Thus, several assumptions were made to ease the derivation of an analytical solution of the post-fracture behavior of brittle Al/Cu hybrid foams. First, both compressive and tensile behavior of the core material (i.e., Al for Al/Cu hybrid foams) is assumed to be elastic-perfect plastic. Secondly, since the electrodeposited copper coating fails at a small strain, it is assumed that the electrodeposited copper coating has a brittle behavior in tension. In other words, the strength of copper coating in tension is neglected. Meanwhile, the compressive behavior of copper coating is assumed to be elastic-perfect plastic. Thirdly, it is assumed that the full section (except the coating area in tension) has plastified, or yielded, when equilibrium is achieved in the fractured ligament section.

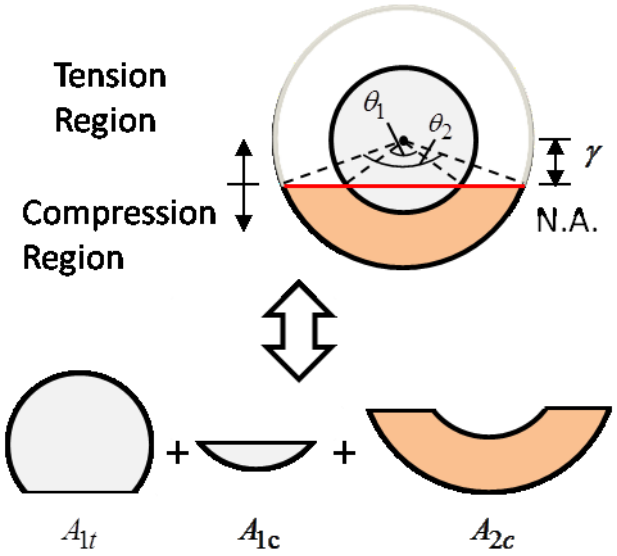

Figure 5-9 Schematic of fractured ligament cross-section of Al/Cu hybrid foam

The fractured cross-section of a brittle Al/Cu hybrid foam ligament can thus be separated as three parts as shown in Figure 5-9. To maintain force equilibrium the resulting tension force from the core area in tension region needs to balance the resulting compressive force from the core and coating areas in the compression region.

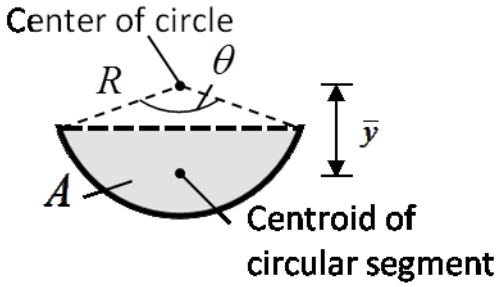

Figure 5-10 Schematic of a circular segment

For a circular segment, the area and the distance of its centroid from the center of the circle (see Figure 5-10) can be calculated using Equation 5-45 and Equation 5-46.

$$A = \frac{R^2}{2}(\phi - \sin\phi) \qquad \text{Equation 5-45}$$

$$\bar{y} = \frac{4R\sin^3\frac{\phi}{2}}{3(\phi - \sin\phi)} \qquad \text{Equation 5-46}$$

The relations in Equation 5-47 to Equation 5-50 can be found for the fractured ligament cross section shown in Figure 5-10, in which γ is the distance from the center of the original ligament cross section to the current neutral axis (fractured section).

$$\cos(\phi_1/2) = \gamma / R_1 \qquad \text{Equation 5-47}$$

or,
$$\phi_1 = 2\arccos(\gamma / R_1) \qquad \text{Equation 5-48}$$

$$\cos(\phi_2/2) = \gamma / R_2 \qquad \text{Equation 5-49}$$

or,
$$\phi_2 = 2\arccos(\gamma / R_2) \qquad \text{Equation 5-50}$$

Thus the areas of core in compression (A_{1c}), core in tension (A_{1t}) and coating in compression (A_{2c}) can be calculated using Equation 5-51, Equation 5-52, and Equation 5-53.

$$A_{1c} = \frac{R_1^2}{2}(\phi_1 - \sin\phi_1) \qquad \text{Equation 5-51}$$

$$A_{1t} = \pi R_1^2 - A_{1c} \qquad \text{Equation 5-52}$$

$$A_{2c} = \frac{R_2^2}{2}(\phi_2 - \sin\phi_2) - A_{1c} \qquad \text{Equation 5-53}$$

To maintain force equilibrium, Equation 5-54 needs to be satisfied, from which γ can be solved.

$$A_{1c}\sigma_1 + A_{2c}\sigma_2 = A_{1t}\sigma_1 \qquad \text{Equation 5-54}$$

The moment capacity of the fractured ligament cross-section can be calculated as the sum of three moment contributions about the neutral axis, as shown in Table 5-2, in which $\bar{y}$ is the distance from centroid of a circular segment to the center of the original ligament cross-section; and d is the distance from the centroid of the circular segment to the neutral axis.

Table 5-2 Contributions for moment capacity of the fractured ligament cross-section

Part	Area	$\bar{y}$	d	stress
a	A_{1t}	$\bar{y}_a = \dfrac{4R_1 \sin^3 \dfrac{(2\pi - \phi_1)}{2}}{3\left[(2\pi - \phi_1) - \sin(2\pi - \phi_1)\right]}$	$d_a = \gamma + \bar{y}_a$	σ_{y1}
b	$A_{1c} + A_{2c}$	$\bar{y}_b = \dfrac{4R_2 \sin^3 \dfrac{\phi_2}{2}}{3\left(\phi_2 - \sin\phi_2\right)}$	$d_b = \bar{y}_b - \gamma$	σ_{y2}
c	A_{1c}	$\bar{y}_c = \dfrac{4R_1 \sin^3 \dfrac{\phi_1}{2}}{3\left(\phi_1 - \sin\phi_1\right)}$	$d_c = \bar{y}_c - \gamma$	$\sigma_{y1} - \sigma_{y2}$

The moment capacity of fractured ligament cross-section can thus be calculated using Equation 5-55.

$$M_{low} = \sigma_{y1} A_{1t} d_a + \sigma_{y2}\left(A_{1c} + A_{2c}\right) d_b + \left(\sigma_{y1} - \sigma_{y2}\right) A_{1c} d_c \qquad \text{Equation 5-55}$$

The lower stress level σ_{low} after the initial peak stress σ_{fr} can be calculated from M_{low} using Equation 5-56.

$$\sigma_{low} = \frac{M_{low}}{2x\left(L\cos\theta\right)^3} \qquad \text{Equation 5-56}$$

5.3.3 Results

The expressions solutions derived in Section 5.3.1 and 5.3.2 were used to predict the response of brittle Al/Cu hybrid foams with different levels of coating thicknesses. All calculations were based on a 40 PPI foam and the ligament diameter and its length were taken as 0.192 mm and 1.04 mm, respectively. The material properties used for the calculations are summarized in Table 5-3. The values for the initial stress peak σ_{fr} and post-peak stress σ_{low} are summarized in Table 5-4.

Table 5-3 Material properties used for analytical model of Al/Cu hybrid foams

Material	Modulus (MPa)	Yielding stress (MPa)	Fracture stress in tension (MPa)
6101-T6 Al (Core)	70000	330	-
Electrodeposited Cu (Coating)	102000	225	225

Figure 5-11 compares the analytical solution and experimental data for the compressive behavior of brittle Al/Cu hybrid foams. The negative slope after the initial stress peak in the analytical solution was assumed to 5% of the initial stiffness. The post-peak behavior was modeled based on the method used by Gibson and Ashby with D = 1.2 and m = 0.8 (Equation 4-42 to Equation 4-44). It can be seen that the analytical model provides a good prediction on the initial peak stresses and the plateau stresses for the compressive behavior of brittle Al/Cu hybrid foams with different coating thicknesses.

Table 5-4 Initial stress peak and post-peak stresses for Al/Cu hybrid foams with different coating thicknesses

Coating (μm)	σ_{fr} (MPa)	σ_{low} (MPa)
30	1.72	1
60	2.37	1.36
90	3.28	1.89

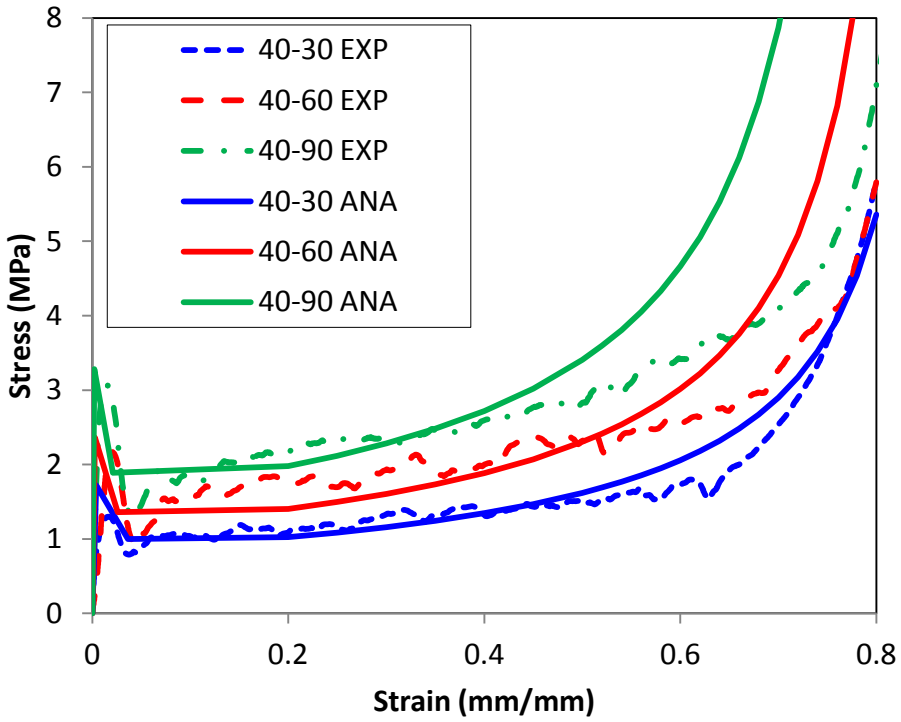

Figure 5-11 Comparison of analytical solution and experimental data on the compressive behavior of brittle Al/Cu hybrid foams

5.4 Conclusions

Analytical solutions for hybrid foams consisting two different materials were derived to predict the uniaxial compressive behavior of hybrid foams. Different solutions were presented considering different coating ductility level. The following conclusions are drawn from this study:

1) The modulus of hybrid foams consisting two materials can be predicted using the obtained analytical solution. It has been shown that the modulus of hybrid foam is directly related to the relative density of the base foam and hybrid foam.

2) The analytical solution derived for hybrid foam with ductile coating provides a good estimation on the plastic stress. The solutions were used to predict the compressive behavior of annealed Al/Cu hybrid foams with different coating levels and the results agree well with experimental data.

3) By considering coating failure in tension, the analytical solutions for hybrid foam with low ductility coating can predict the distinct behavior of as-built electrodeposited hybrid foams with a reasonable accuracy.

CHAPTER 6 CHARACTERIZATION OF DYNAMIC BEHAVIOR OF AL/CU HYBRID FOAMS

6.1 Overview

In this chapter, the mechanical properties of Al/Cu hybrid foams under high stain-rate compression demands were investigated using a split Hopkinson pressure bar. It is hypothesized that the energy absorption capacity of aluminum open-cell foams under high strain rate loading can be effectively enhanced by electrodeposited metal coatings. However, the low ductility capacity of nanocrystalline coatings is detrimental to the performance of the fabricated hybrid foams, and thus the performance of such hybrid foams can be further enhanced by improving the ductility of the coating material. Al/Cu hybrid foams were manufactured by electrodepositing copper on aluminum open-cell foams to investigate the compressive response and failure mechanism of the composite material under high strain rate loading. Compared to the current literature the present work provides an extended experimental evaluation on the dynamic behavior of hybrid foams with different coating thicknesses to provide guidance on the design of functionally graded foam material systems under high-rate compressive strains. In order to study the influence of the ductility capacity of the nano-copper coating, an annealing process was performed on part of the specimens after electrodeposition and their behavior was compared with that of specimens without annealing.

6.2 High Strain Rate Experiments

6.2.1 SHPB Tests

The compressive performance of Al/Cu hybrid foams under high strain rate loading was investigated using a split Hopkinson pressure bar (SHPB). Figure 6-1 shows a schematic of the SHPB set up, which consists of an incident bar, a transmission bar, and a striker. The incident bar and the striker were two solid aluminum bars with a diameter of 19 mm and lengths of 1829 mm and 508 mm, respectively. Due to the low impedance of the foam material studied, a hollow aluminum bar (I.D. = 15 mm, O.D. = 19 mm) with a length of 1829 mm was used as the transmission bar. A 1 mm thick copper plate was used as the pulse shaper. Strain gages were placed at the half length point of both the incident and transmission bars to measure the incident strain $\varepsilon_i(t)$, the transmitted strain $\varepsilon_t(t)$ and the reflected strain $\varepsilon_r(t)$.

To reduce noise in the measured signal, four strain gages were placed on the transmission bar and connected to a full bridge configuration while a half bridge configuration was used for the strain gage on the incident bar. In order to achieve equilibrium during the SHPB experiments the specimen length (L_S) needs to be small, especially for materials with low impedance [106]. However, when evaluating foams it is necessary that the test sample contains several cells in the loading direction. As a result, the SHPB specimens used in this study (see Figure 6-2a) had a diameter of 15.9 mm and a length of 5 mm (about eight times the pore size), which was the same length used in the study by Jung et al. [7].

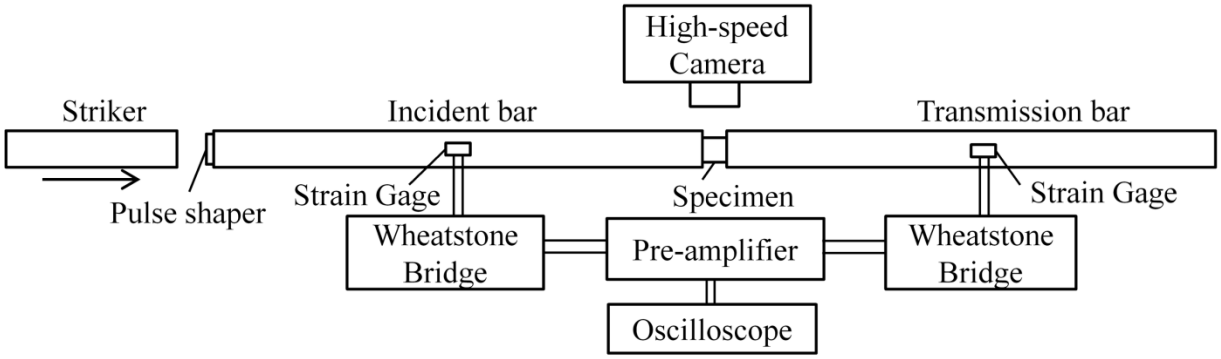

Figure 6-1 Schematic of split Hopkinson pressure bar (SHPB) setup

(a)  (b) 

Figure 6-2 Cross section pictures of (a) uncoated circular-shaped (5 mm thick with a diameter of 15.9 mm) specimen for dynamic experiments and (b) Cu-coated square-shaped specimen (25.4 mm × 25.4 mm × 5 mm) for quasi-static experiments

Figure 6-3 shows an oscilloscope record obtained during one of the SHPB experiments. The flat plateau of the incidence and reflected pulse indicates a constant strain rate of about 180 microseconds for the noted setup. The stress, strain and strain rate of the specimen were reconstructed from the strain-time records using Equation 6-1 to Equation 6-3 [107]:

$$\sigma_s(t) = E_t \frac{A_t}{A_s} \varepsilon_t(t) \qquad \text{Equation 6-1}$$

$$\varepsilon_S(t) = \frac{2C_0}{L_S}\int_0^t \left[\varepsilon_i(t) - \varepsilon_r(t) - \varepsilon_t(t)\right] dt \qquad \text{Equation 6-2}$$

$$\frac{2C_0}{L_S}\left[\varepsilon_i(t) + \varepsilon_r(t) - \varepsilon_t(t)\right] \qquad \text{Equation 6-3}$$

where C_0 is the wave speed within the bar; A_t and A_S are the cross-sectional areas of the specimen and the transmission bar, respectively; and E_t is the Young's modulus of the transmission bar.

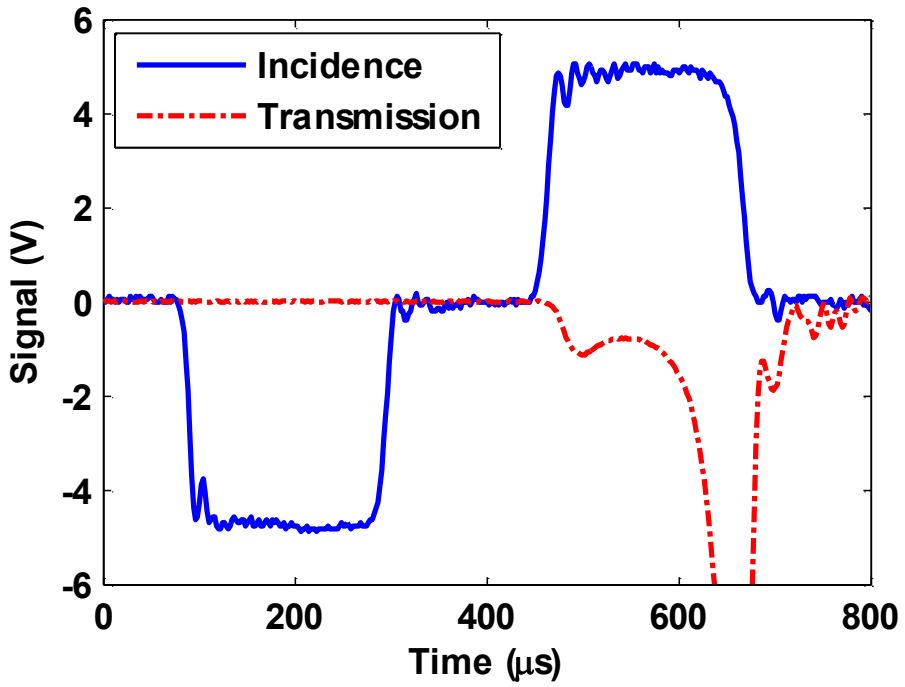

Figure 6-3 Typical oscilloscope records from SHPB experiments

Four different types of specimens were considered: uncoated, and Cu coated with 30 μm, 60 μm, and 120 μm nominal coating thicknesses; and three experiments were conducted for each

specimen type. Two different strain rates were obtained in the SHPB experiments conducted in this study, namely, 2.8×10^3 s^{-1} and 4.9×10^3 s^{-1}.

6.2.2 Quasi-static Experiments

To provide a reference for the high strain rate experiments, quasi-static compressive experiments were also performed with a universal testing frame. It is important to maintain the same specimen length in the loading direction in both the high strain rate and quasi-static experiments as the non-uniform collapse of cells in foam specimens of larger size may lead to a different overall behavior [18]. Thus, the specimens used for the quasi-static experiments (Figure 6-2b) also had a thickness of 5 mm and a cross-section of 25.4 mm by 25.4 mm. The experiments were conducted in a displacement control mode at a strain rate of 3.3×10^{-3} s^{-1}. Three experiments were conducted for each specimen type.

6.2.3 Compressive Behavior of Hybrid Foams

Figure 6-4 shows a typical compressive stress strain curve for the Al/Cu hybrid foams reported in this study. Nominal stress (load divided by original cross-sectional area) and nominal strain (deformation divided by original length) are used throughout the results presented here. Similar to the behavior of a conventional single-material metal foam, the response features an elastic region, a collapse region and a densification region. However, it was observed that the stress level in the collapse region dropped significantly after the initial peak stress σ_P for the hybrid foams, while such difference is usually small in conventional single-material metal foams [13, 18]. Ideally the stress level should remain constant at a nominal level close to the initial peak stress throughout the collapse region to maximize the energy absorbed during plastic deformations under a constant stress level. Thus, the significant drop after the initial peak stress

is considered an unfavorable behavior feature and needs to be considered when evaluating the energy absorption performance of hybrid foams.

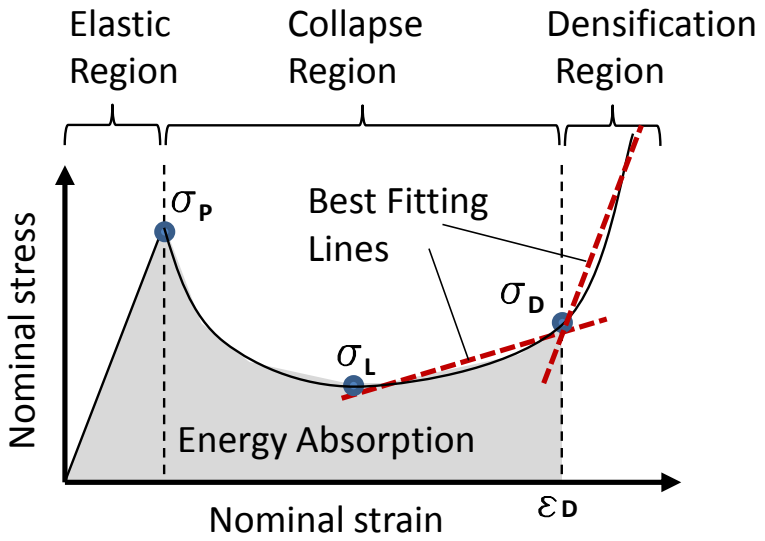

Figure 6-4 Schematic of typical compressive behavior of Al/Cu hybrid foams with peak stress (σ_P), lowest stress in collapse region (σ_L), densification stress (σ_D) and densification strain (ε_D)

In this study, the densification strain ε_D was defined as the strain level at the intersection of the best fitting lines (using a least square fit) of the ascending part in the collapse region and the densification region, respectively, as shown in Figure 6-4. The energy absorption capacity was defined as the area under the stress-strain curve up to the densification strain. In addition, energy absorption efficiency was defined as the ratio of the absorbed energy to an ideal energy absorption level, which was defined as the product of the densification strain ε_D and the initial peak stress σ_P, or the stress at densification strain σ_D, whichever is larger (see Equation 6-4).

The quantitative parameters of all experiments are summarized in Table 6-1, where σ_L is the lowest stress level in the collapse region and $\Delta\sigma$ is the ratio of the stress drop to the initial peak stress calculated using Equation 6-5. The letters "S" and "D" in the sample identification (ID) names represent quasi-static (with strain rate of 3.3×10^{-3} s^{-1}) and dynamic experiments, respectively. The number after letter "C" represents the nominal thickness of the nano-copper coating in μm and the last number indicates the strain rate ("28" and "49" refer to strain rates of 2.8×10^{3} s^{-1} and 4.9×10^{3} s^{-1}, respectively). Sample ID names with an "A" refer to annealed samples. The experimental data summarized in Table 6-1 is based on the average of three repeated experiments for each specimen type. It needs to be noted that at the strain rate of 2.8×10^{3} s^{-1} the densification region in the dynamic response of Al/Cu hybrid foams could not be fully captured with the current setup and thus the densification strain ε_D and the energy absorption capacity could not be determined at such strain rate.

$$Efficiency = \frac{Energy\ Absorption}{\max(\sigma_P, \sigma_D)\cdot\varepsilon_D} \qquad \text{Equation 6-4}$$

$$\Delta\sigma = \frac{\sigma_P - \sigma_L}{\sigma_P}\times 100\% \qquad \text{Equation 6-5}$$

Table 6-1 Summary of results from all experiments

Sample ID	σ_P (MPa)	σ_L (MPa)	$\Delta\sigma$ (%)	ε_D (mm/mm)	Energy Absorption (N·mm)	Ideal Energy (N·mm)	Efficiency (%)
S.C0	0.64	0.63	2	0.68	0.70	2.11	33
S.C30	2.66	1.35	49	0.68	1.28	2.65	48
S.C60	4.21	1.83	57	0.65	1.71	3.79	45
S.C120	10.59	4.32	59	0.62	3.68	6.57	56
D.C0.28	0.67	0.54	19	-	-	-	-
D.C30.28	1.96	0.74	62	-	-	-	-
D.C60.28	4.00	1.14	71	-	-	-	-
D.C120.28	10.82	1.68	85	-	-	-	-
D.C0.49	0.73	0.52	29	0.68	0.69	2.52	27
D.C0.49	2.97	0.73	75	0.65	1.11	2.80	40
D.C60.49	4.39	1.02	77	0.61	1.31	2.68	49
D.C120.49	12.68	1.91	85	0.61	2.79	7.73	36
D.C30.49.A	2.10	1.16	45	0.59	1.22	2.56	48
D.C60.49.A	4.43	2.29	48	0.55	1.93	3.70	52
D.C120.49.A	9.10	5.92	35	0.52	3.94	6.10	65

6.2.4 Effect of Electrodeposited Copper Coating

The stress-strain curves obtained from quasi-static and high-strain rate compression experiments are shown in Figure 6-5 to Figure 6-7. The naming convention for the different experiments can be found in Section 6.2.3. The behavior for each specimen type presented in this paper is the average of three separate experiments. Specimen size was dictated by the high-rate experiment requirements. As the foam response is affected by sample size, the behavior reported here differs from that obtained by Wang et al. [8] with larger specimens. Yet, the objectives of

this work are not thought to be compromised by this fact since the results are used for mutual comparison.

It can be seen from Figure 6-5 to Figure 6-7 that the performance of the aluminum foam under both quasi-static and high strain rate compressive loading was effectively enhanced by the electrodeposited copper coating. In general, the initial peak stress and the plateau stress of the coated foam specimen increased with the coating thickness. This is expected as the moment of inertia of a reinforced ligament section is larger and thus its load bearing capacity (controlled by flexural yielding) is increased. Meanwhile, a slight decrease of the densification strain for specimens with thicker coating was observed in both quasi-static and dynamic experiments, which is attributed to the fact that the densification of a foam is basically a volumetric phenomenon and that specimens with thicker coating have more material.

As mentioned in Section 6.2.3, a significant stress drop in the compressive stress-strain curve was observed in all experiments on coated samples and such drop was more significant for specimens with thicker coatings. A similar behavior was reported in previous studies on open-cell Al foam with nanocrystalline Ni coatings by Bouwhuis et al. [6] and Jung et al. [7] and the study on Al/Cu hybrid foams by Wang et al. [8].

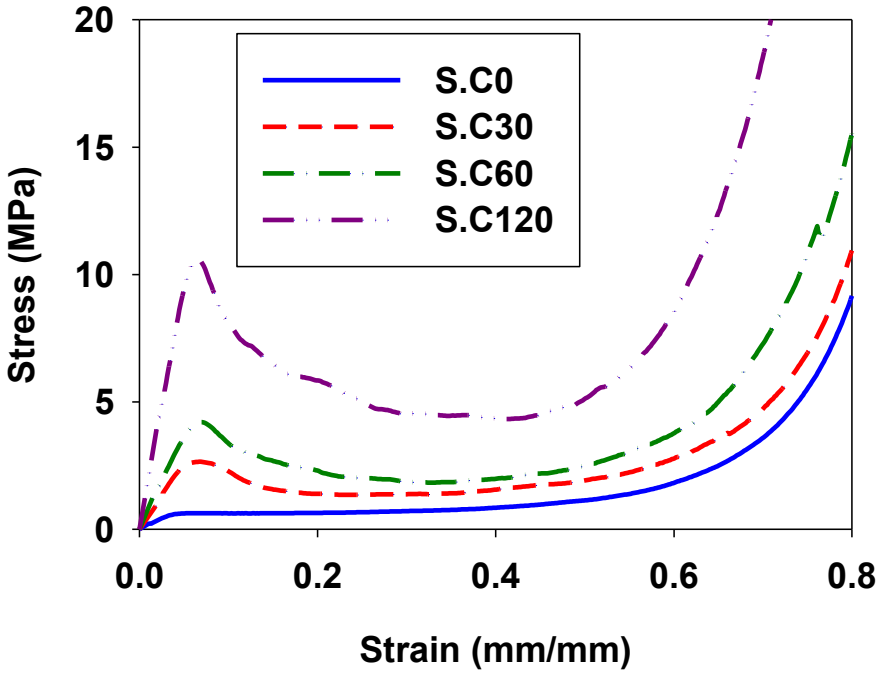

Figure 6-5 Quasi-static compressive behavior of Al/Cu hybrid foams (3.3×10^{-3} s^{-1})

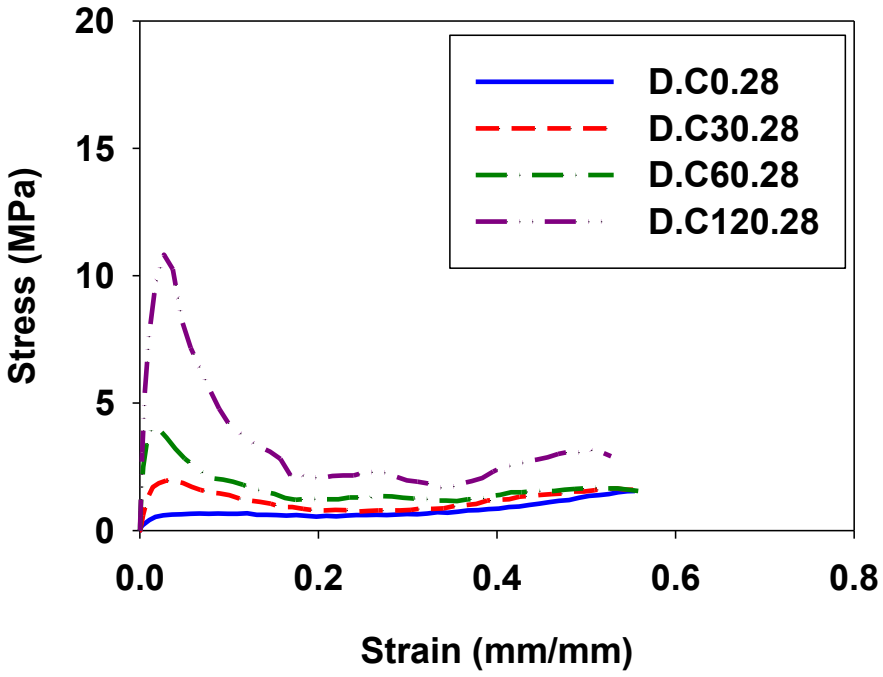

Figure 6-6 High strain rate compressive behavior of Al/Cu hybrid foams (2.8×10^{3} s^{-1})

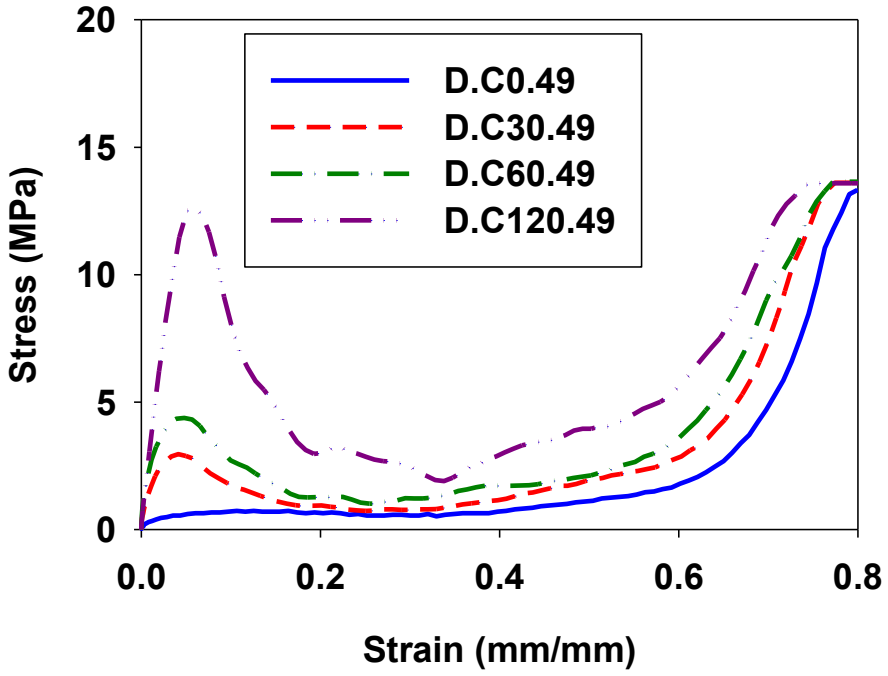

Figure 6-7 High strain rate compressive behavior of Al/Cu hybrid foams (4.9×10^{3} s^{-1})

Considering the previously noted definition of energy absorption capacity, a high peak stress followed by a large drop can significantly reduce the foam's energy absorption efficiency. As demonstrated in the annealing effect evaluation (CHAPTER 4) and numerical studies (CHAPTER 3), the observed stress drop is mainly attributed to the rupture of the electrodeposited coating material, as electrodeposition usually leads to a material with low ductility [66].

The larger stress drop for specimens with thicker coatings is due to the increased capacity loss of the ligament, and the foam, upon brittle failure of the thicker section reinforcement. It was also observed that the stress drop was more significant under high strain rate loading (see Figure 6-5 to Figure 6-7). This may be attributed to the fact that the shattering of foam ligaments and the spalling of coating material was more severe under high strain rate loading. Such

phenomenon also led to a slightly higher densification strain in Al/Cu hybrid foams under high strain rate loading conditions, especially with thicker coatings. It can be seen from Table 6-1 that the lower plateau stress from high strain rate experiments lead to a relatively lower energy absorption capacity and efficiency compared to the quasi-static experiments.

Figure 6-8 compares the performance of foam specimens with different coating thickness under different loading rates. No significant difference on the initial peak stress (see Figure 6-8a) with respect to loading rates was observed for plain Al foams and Al/Cu hybrid foams with nominal copper coating thicknesses less than 120 μm. However, the hybrid foams with 120 μm nominal coating thickness showed slightly higher initial peak stress at a strain rate of 4.9×10^3 s^{-1} compared to that at lower strain rates. Figure 6-8b shows that the lowest stress level in the collapse region of the coated foams was lower in the dynamic experiments, which can again be explained by the more severe specimen shattering and material spalling under high-rate loading. No significant difference in the lowest stress values was observed under strain rates of 2.8×10^3 s^{-1} and 4.9×10^3 s^{-1}.

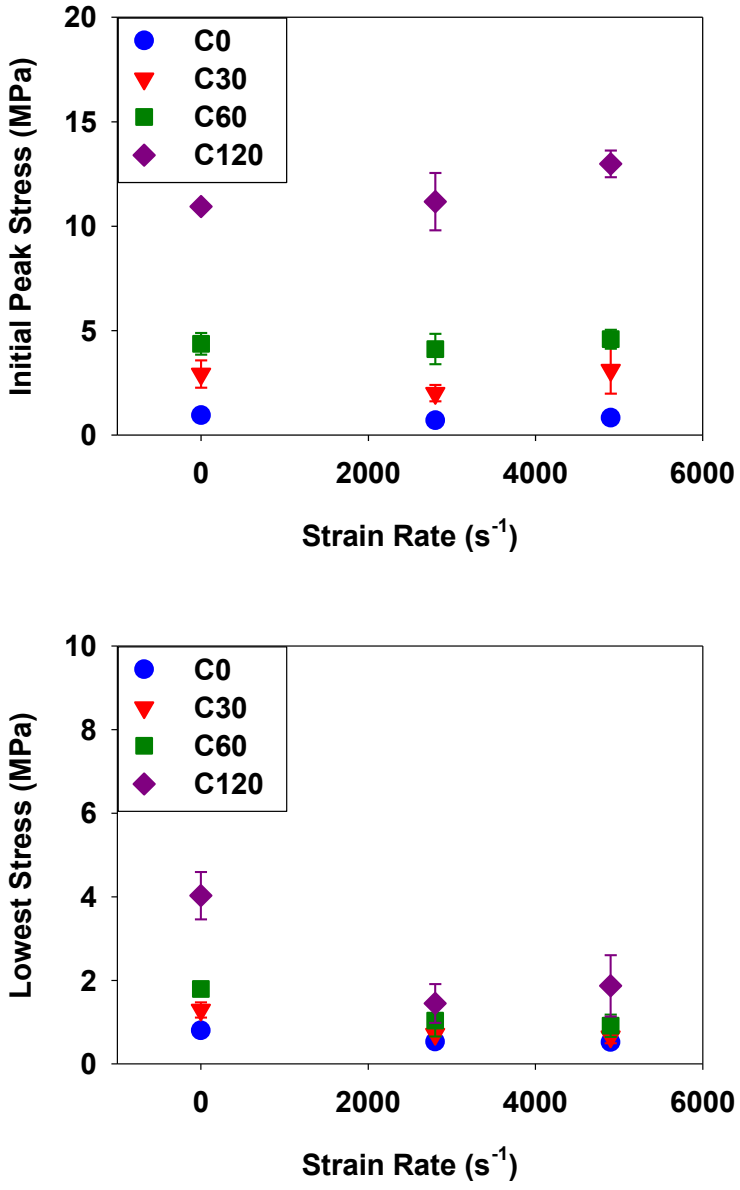

Figure 6-8 Initial peak stress and lowest stress level in the compressive behavior of Al/Cu hybrid foams under different strain rates

6.2.5 Effect of Annealing

The low ductility capacity of the electrodeposited metal coating is considered to be unfavorable for the overall energy absorption performance of hybrid foams as most of the energy

absorbed is due to large plastic deformation of the cell struts. Thus, it is necessary to investigate the effect of ductility capacity of the coating material on the performance of the hybrid foam.

An annealing process was thus added to some of the specimens after the electrodeposition process to investigate the effect of enhanced coating ductility in hybrid foams. Annealing is a well-established heat treatment process for metals to release internal stresses and enhance ductility through recrystallization and grain growth, which also usually results in a lower strength due to the change of crystal structure [46, 58, 89]. Annealing was conducted at a temperature of 400 °C in a vacuum furnace (3×10^{-5} torr) for one hour. The noted temperature was chosen since it is about half of the melting temperature of copper (1084 °C) at which recrystallization can occur [58] and at the same time it is not too close to the melting temperature of aluminum (660 °C). The temperature was increased at a rate of about 10 °C/min and the furnace was cooled down slowly after the annealing process.

6.2.6 Results for Effect of Annealing

The compressive behavior of annealed and un-annealed Cu/Al hybrid foams under high strain rate loading (4.9×10^{3} s^{-1}) is shown in Figure 6-9 to Figure 6-11. For reference purposes, the result of a plain aluminum foam specimen is included in all plots. First, it can be seen from the plots in Figure 6-9 to Figure 6-11 that the annealed specimens generally show a similar or lower peak stress compared to the un-annealed specimens. This is because the recrystallization and grain growth that occurs during annealing changes the crystal structure and leads to a lower yield strength [46, 58, 89].

Secondly, the results in Figure 6-9 to Figure 6-11 also show that the stress plateau after the peak stress was higher for the annealed foam specimens. As a result, the annealing process

reduced the difference between the initial peak stress and the stress level in the collapse region, which is beneficial for energy absorption efficiency. It can also be seen that the effect of annealing was more significant for foam specimens with thicker coatings as the improvement in ductility is mainly on the copper coating.

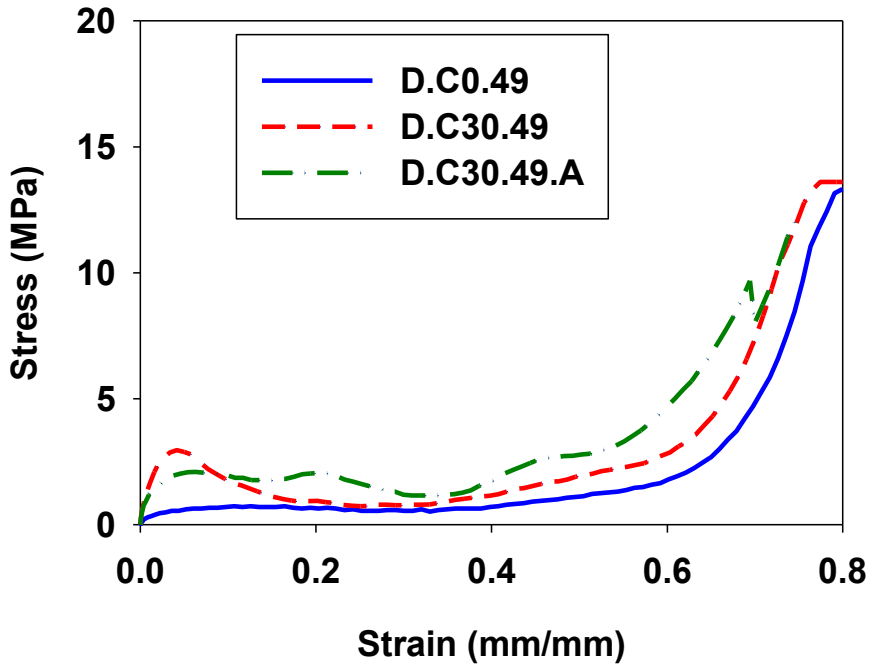

Figure 6-9 Compressive behavior of annealed specimen and un-annealed specimen with nominal copper coating thicknesses of 30 μm under high strain rate loading (4.9×10^3 s^{-1})

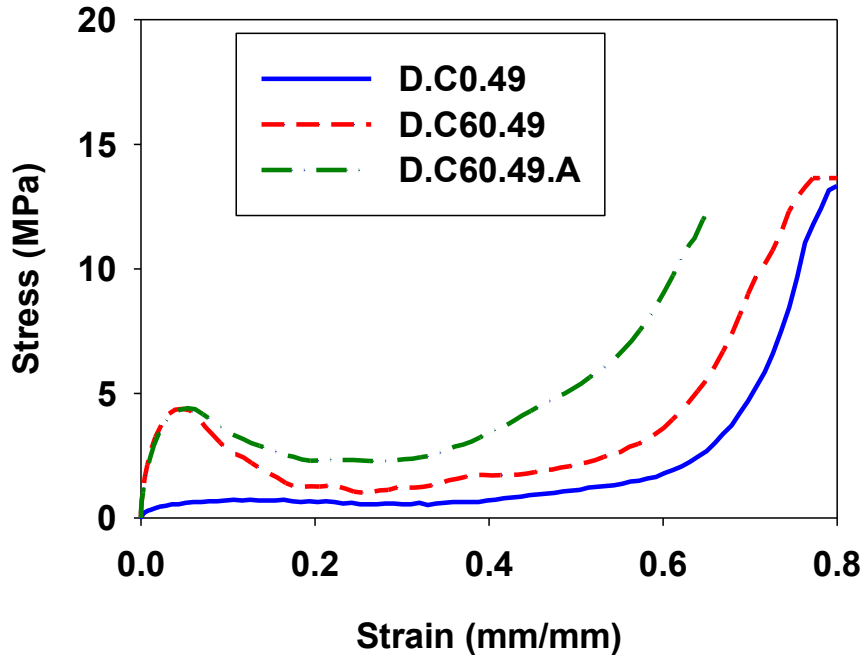

Figure 6-10 Compressive behavior of annealed specimen and un-annealed specimen with nominal copper coating thicknesses of 60 μm under high strain rate loading (4.9×10^3 s^{-1})

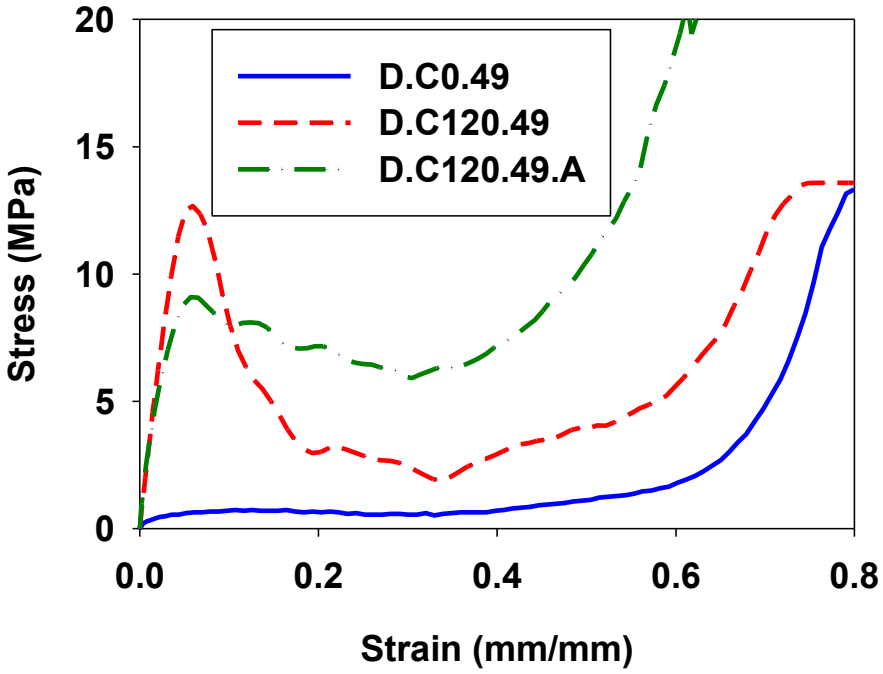

Figure 6-11 Compressive behavior of annealed specimen and un-annealed specimen with nominal copper coating thicknesses of 120 μm under high strain rate loading (4.9×10^3 s^{-1})

Thirdly, it can be observed that the densification onset starts earlier in the annealed specimens, which can also be seen in Table 6-1. The lower densification strain may reduce the improvement in energy absorption capacity. However, it was observed that the annealed specimens stayed intact during the experiments even at high strain loading, while dramatic shattering occurred in the un-annealed specimens (especially the ones with the thickest coating, see Figure 6-12).

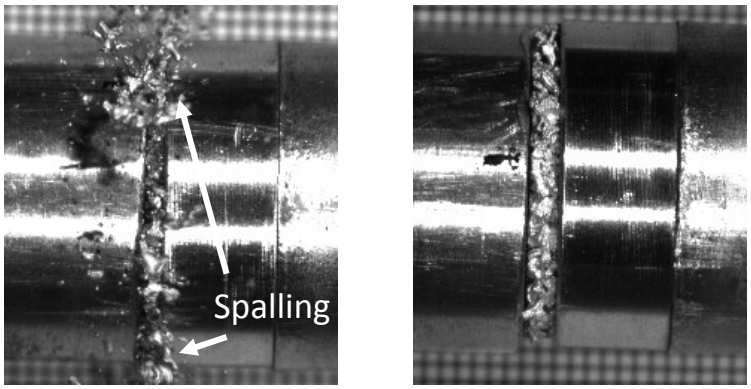

(a) (b)

Figure 6-12 Images of (a) un-annealed and (b) annealed Al/Cu hybrid foam specimens with 120 μm nominal copper coating thickness during high-rate compressive loading

Thus, considering the amount of material broken away from the loaded domain, the densification strain obtained in the plots for the un-annealed specimens may be overestimated. In addition, it is considered that the relatively ductile nature of the annealed hybrid foams under compression is favorable as it may avoid local concentrated damage and thus further improve the energy absorption efficiency of the material.

6.3 Discussion

Figure 6-13 to Figure 6-15 shows the comparison of energy absorption, stress drop ratio and energy absorption efficiency of Al/Cu hybrid foams with different coating thicknesses. The discussion herein is based on the experimental results from the two extreme strain rates in this study, namely, 3.3×10^{-3} s^{-1} (quasi-static) and 4.9×10^{3} s^{-1}. It can be seen that the energy absorption capacity of the Al/Cu hybrid foams increases with coating thickness (see Figure 6-15a).

The energy absorption capacity of the Al/Cu hybrid foams from high strain rate experiments are lower than those from quasi-static experiments due to the specimen shattering and the material breaking away as mentioned earlier. Even though the initial peak stress was lower for the annealed specimens, the energy absorption capacity was significantly higher compared to the specimens without an annealing process. This indicates that ductility is as important as strength for the coating of hybrid metal foams. Compared to plain aluminum foams, specimens with a nominal coating thickness of 120 μm had an energy absorption capacity approximately four times larger under high strain rate loading and more than five times larger under quasi-static loading.

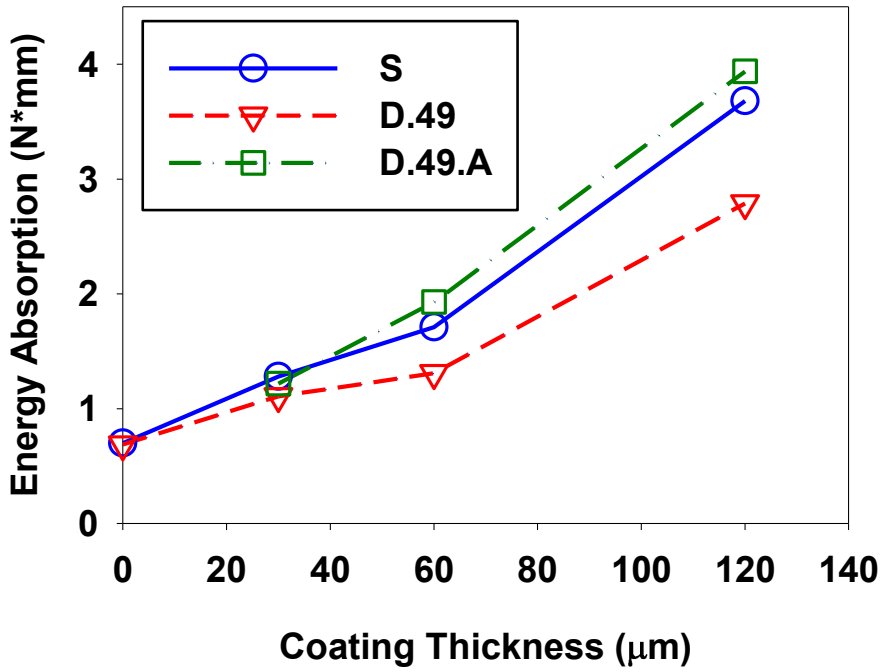

Figure 6-13 Comparison of energy absorption capacity for quasi-static and high strain rate experiments

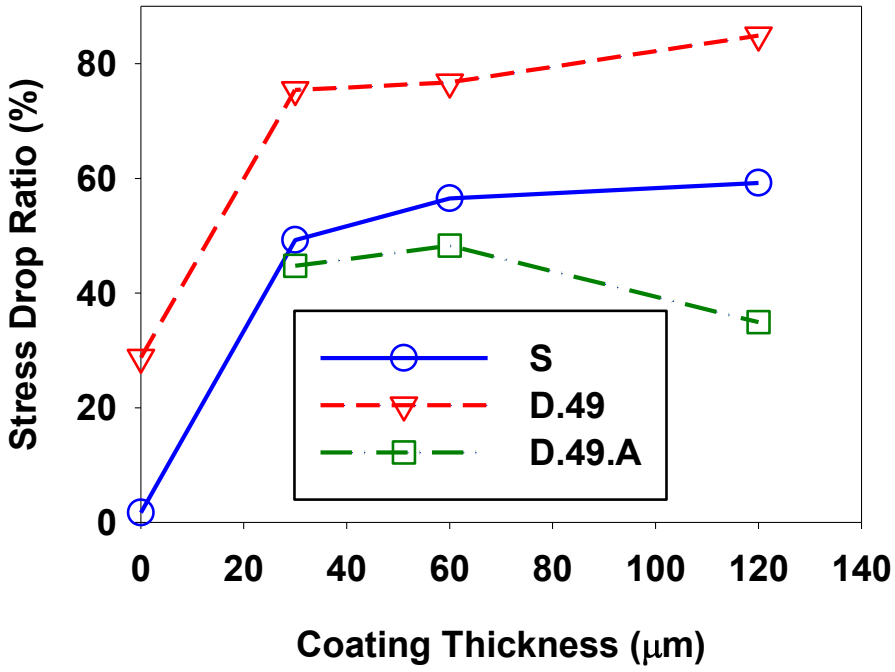

Figure 6-14 Comparison of stress drop ratio for quasi-static and high strain rate experiments

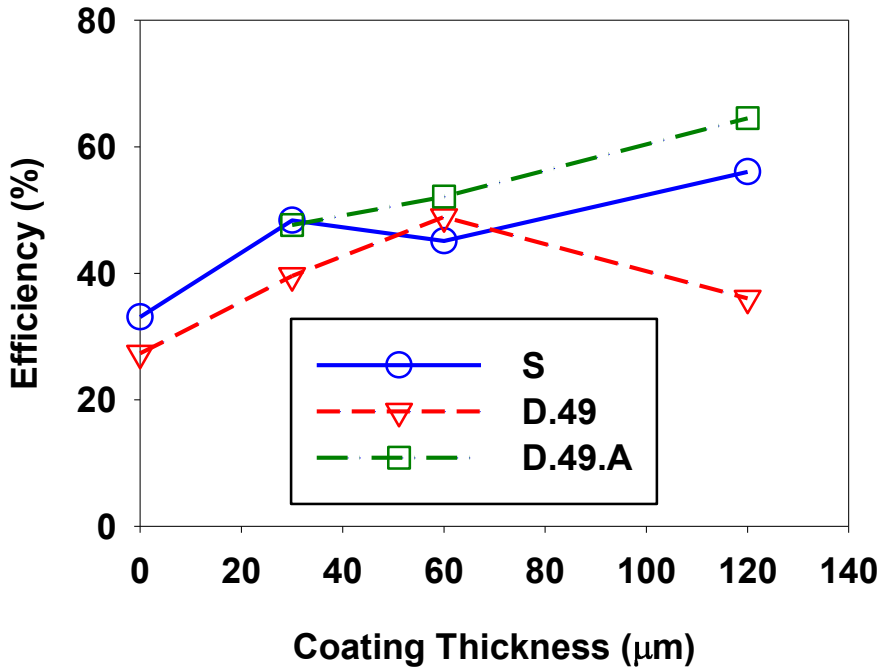

Figure 6-15 Comparison of energy absorption efficiency for quasi-static and high strain rate experiments

The larger stress drop after the initial peak stress for un-annealed specimens with thicker coatings can be seen in Figure 6-15b. Such stress drop significantly limits or even reduces the energy absorption efficiency as shown in Figure 6-15. However, by applying an annealing process the stress drop ratio was significantly reduced, especially for thicker coatings, which lead to a relatively uniform stress level in the collapse region. The enhanced ductility of the copper coating leads to a proportional increase in energy absorption efficiency with coating thickness as shown in Figure 6-15c.

It has thus been shown that Al/Cu hybrid foams manufactured through electrodeposition have a better energy absorption performance that can be effectively modified by controlling the coating thicknesses and processing. Such controllable enhancement indicates the potential to

fabricate functionally graded foams through a designed electrodeposition procedure that provides non-uniform reinforcing coatings.

6.4 Conclusions

The high strain rate compressive behavior of Al/Cu hybrid foams manufactured by electrodepositing nanocrystalline copper onto open-cell aluminum foam was investigated using experimental methods. The effect of ductility enhancement of the coating material on the performance of such hybrid foams was evaluated by introducing an annealing process. It was found that:

1) The energy absorption capacity of aluminum open-cell foams under high strain rate loading can be effectively enhanced by electrodeposited copper coatings and that such enhancement increases with coating thickness.

2) The compressive behavior of Al/Cu hybrid foams with a thick coating (120 μm) had a slightly increased initial peak stress at higher strain rates, while no significant difference in the initial peak stress was observed for hybrid foams with thinner coatings. However, in all cases the stress level in the collapse region was relatively low under high strain rate loading due to specimen shattering and the material breaking away, which lead to a lower energy absorption capacity compared to that under quasi-static loading.

3) A large obvious drop in the stress level following the initial peak stress was observed in the compressive response of Al/Cu hybrid foams. This can be attributed to the rupture of the coating material and the concentration of deformations at weakened critical sections due to the low ductility of the electrodeposited nano-coating. Such phenomenon is more significant in foams with thicker coating and is unfavorable for the energy absorption performance of hybrid metal foams as it limits or even reduces their energy absorption efficiency.

4) The ductility capacity of electrodeposited copper coatings has a great influence on the overall energy absorption efficiency of Al/Cu hybrid foams. Coatings with better ductility (e.g., obtained by adding an annealing process) lead to significant improvements in energy absorption capacity and efficiency, and a more favorable inelastic deformation mechanism. It is believed that such improvement can also be applied to other hybrid foams manufactured using a similar procedure. The more ductile failure mechanism due to the reduction in coating brittleness may be even more beneficial for hybrid foams with larger specimen size since brittle failure mechanisms may cause localized damage and thus reduce their energy absorption efficiency.

CHAPTER 7 STRUCTURAL CHARACTERIZATION AND DESIGN OF FUNCTIONALLY GRADED AL/CU HYBRID FOAMS

7.1 Overview

In this Chapter, functionally graded hybrid foam structures with property gradient in two-dimensions were successfully fabricated by strategically reinforcing conventional open-cell aluminum (Al) foams with nanocrystalline copper (Cu) through electrodeposition. The quasi-static mechanical performance of the fabricated FGHF structural elements were experimentally evaluated under two different bending loading conditions and compared to Al/Cu hybrid foam structure elements with uniform coating. The dynamic behavior of FGHF structural element was investigated using drop weight tower tests considering three-point bending loading conditions.

Functionally graded cellular structures (FGCS) can be used to optimize the mechanical performance of structural elements such as sandwich panels. However, while many studies have been conducted in the development of FGCS, most of the studies are limited to FGCS with property gradients in one-dimension only (usually in the loading direction). And to the author's knowledge, there is no reported experimental effort for the fabrication and investigation of two-dimensional functionally graded foams in public literature. This can be partly attributed to the difficulty in creating gradients with higher dimensions. However, higher dimensional spatial variations in the properties of cellular/foams, in analogy to cortical bone [22], offers a greater opportunity to optimize mechanical performance when foams are used as structural elements.

Wang et al. [35] considered a graded cellular structure in the conceptual design of an acetabular component that changed from solid metal at the liner section to one with high porosity at the implant-bone interface to encourage bone growth upon implantation. Daxner et al. [36]

conducted a numerical study and found that the distribution of foam density can be optimized with respect to structural strength and stiffness for a given loading condition. However, complex designs such as these ones cannot be realized with the manufacturing process of traditional cellular materials. Thus, the development in fabrication and investigation in cellular/foam structures with two-dimensional property gradient is of great interest.

It is hypothesized that the manufacturing process for hybrid foams can be customized to modify and enhance the mechanical performance of open-cell hybrid cellular structural elements by applying reinforcement in a strategic pattern or in critical regions compared to applying the reinforcement uniformly across the domain.

7.2 Behavior of Al/Cu Hybrid Foam

The behavior of Al/Cu hybrid foams have been discussed in previous chapters. Figure 7-1 show the comparison of compressive and tensile behavior of Al plain foam and Al/Cu hybrid foams with different coating thicknesses. It can be seen that hybrid foams have enhanced performance in both compression and tension compared to plain Al foam. As expected, the enhancement in performance is more significant for hybrid foams with thicker coatings. Such controllable behavior serves as the basis for the design of functionally graded foam systems.

The compressive response of plain Al and Al/Cu hybrid foams has a stress plateau after yielding and the compressive stress increases significantly at large deformations due to densification. However, plain Al and hybrid Al/Cu foams have distinct behavior characteristics when under tensile demands. When the foam samples are in tension fracture occurs at a relatively low strain level (less than 10% strain). Al/Cu hybrid foam samples show a higher failure strain (i.e., higher ductility) in tension than plain Al foam samples. The maximum tensile

strength of plain Al and hybrid Al/Cu foams is slightly higher than their respective critical plastic stress in compression. For both plain and coated foams, tensile strength drops sharply after rupture occurs and the samples fail in a brittle form. This constitutive response indicates that when such foam materials are used as structural elements, the global structural level failure mechanism may be governed by tension and material failure will occur in regions where high tensile stress exists. Such tension controlled failure mechanism may be alleviated if the coating material can be strategically distributed to provide more reinforcement on tensile stressed regions.

7.3 Selective Electrodeposition of Nc-Cu

The hybrid foams manufactured using the method discussed in Section 2.4.2 have a uniform coating thickness throughout the sample [8]. While it has been demonstrated that the hybrid foams have enhanced and controllable modulus, strength and energy absorption capacity compared to the base material, it is expected that the deformation and failure mechanisms of the hybrid foams can be modified and improved by reinforcing specific regions in a designed pattern. In addition, the mechanical performance of the hybrid foams can also be further optimized by strategically distributing the coating material according to the loading conditions.

Hybrid foam samples with graded coating thicknesses can be fabricated by controlling the surface of the base foam sample in contact with electrolyte during electrodeposition, which can be achieved using two approaches. The first approach is to immerse only part of the sample into the electrolyte during the electrodeposition process, as shown in Figure 7-2a. In this manner, the coating material is deposited on to the part of the sample immersed in the electrolyte, while the rest of the sample is not coated since there is no direct contact between the surfaces of the foam substrate to the electrolyte. This approach can thus be used to fabricate graded hybrid foams with partially coated regions.

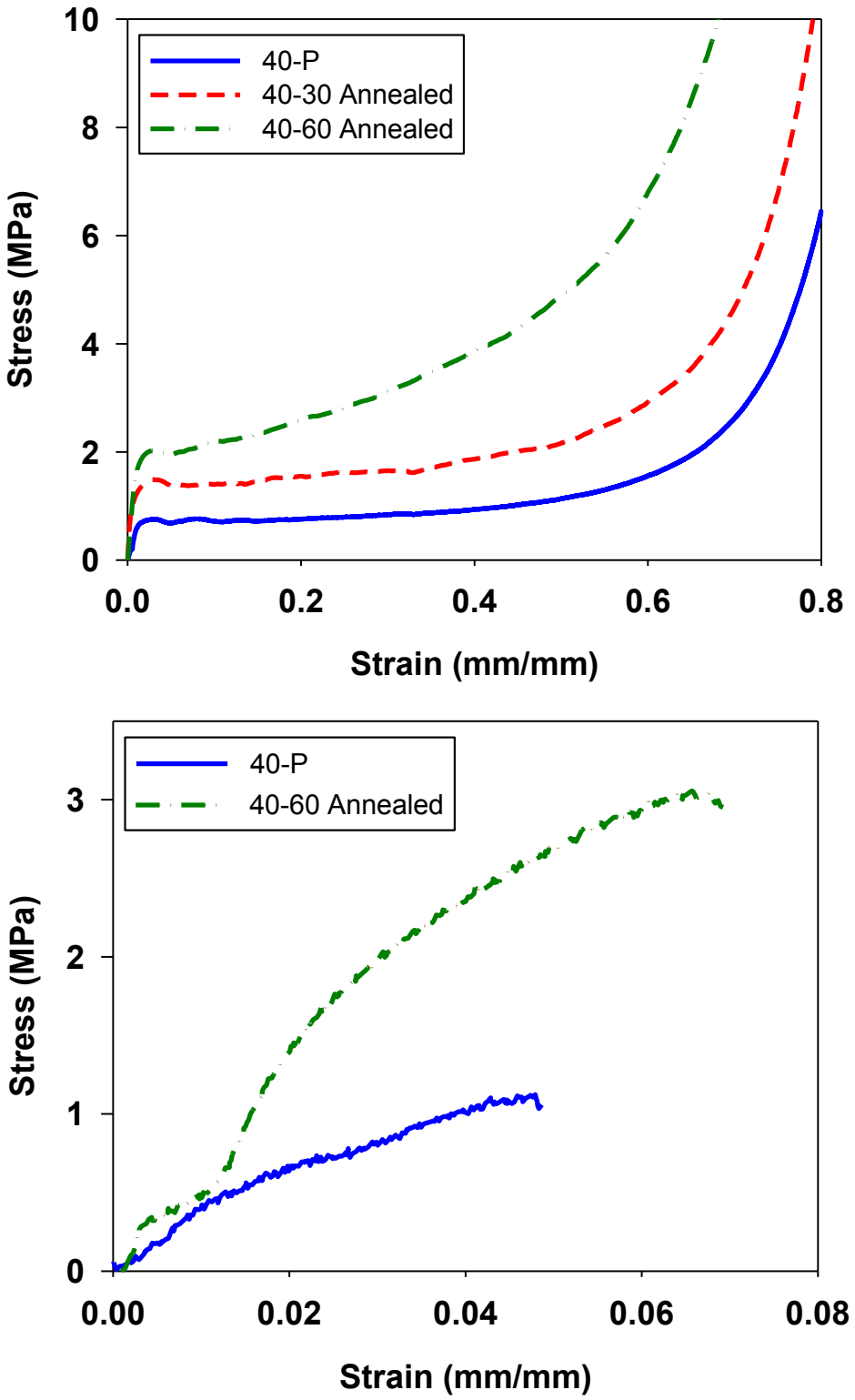

Figure 7-1 Compressive and tensile behavior of plain Al and hybrid Al/Cu foams with uniform coating

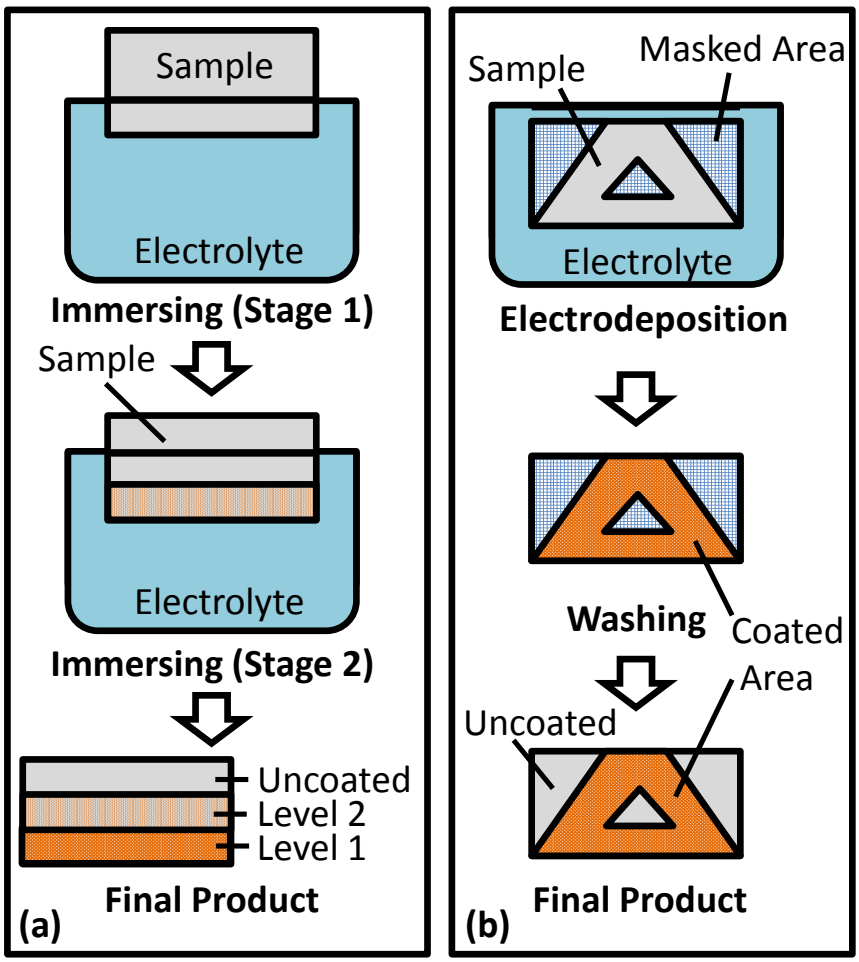

Figure 7-2 Manufacturing of graded hybrid foam using a) Partial immersion method and b) Masking -Washing method

Hybrid foams with graded coating thicknesses can also be fabricated using the noted method of immersing the foam substrate into the electrolyte in several stages. The level of coating thicknesses in different regions can be controlled by the time of electrodeposition for different stages. This method is straight forward and easy to conduct for producing hybrid foams with a simple coating thickness gradient. However, it is difficult to use this method for fabricate hybrid foams with more complicated two–dimensional patterns such as that shown in Figure 7-3.

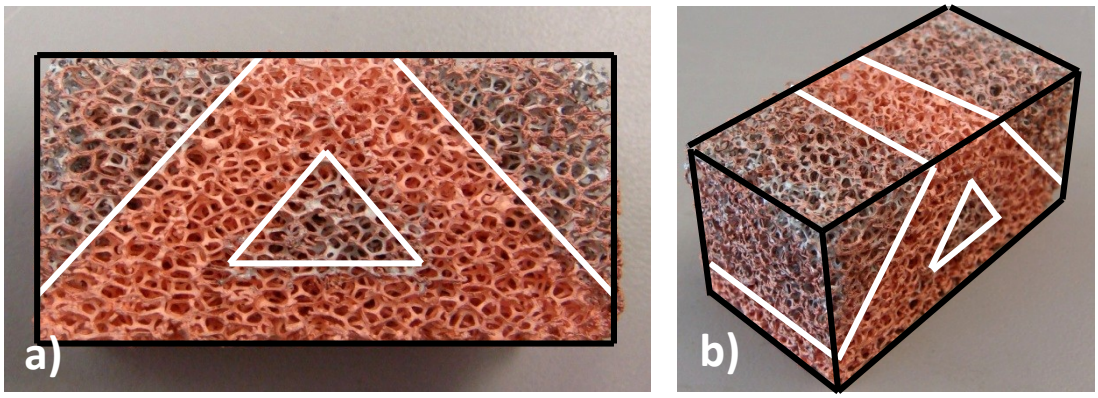

Figure 7-3 Hybrid foams with two dimensional graded coating pattern

Another method to fabricate hybrid foams with graded coating thicknesses is to mask a region of the foam samples using a non-conductive mask agent during the electrodeposition process, as shown in Figure 7-2b. A liquid acrylic laquer conformal coating (419B, M.G. Chemicals, Surrey, BC, Canada) was used in this study as mask agent. The mask agent had service temperature limit of 105 °C and was not reactive to the electrolyte used. In addition, the mask agent can be removed by acetone after the electrodeposition process. The mask agent was applied on to the desired region of the foam sample after surface pretreatment procedure. When the mask agent fully cures after 24 hours, the entire foam sample was immersed into the electrolyte and the electrodeposition procedure was initiated. Once the desired amount of coating material was applied, the sample was washed and then immersed into acetone for about 10 minutes to remove the mask agent. The method just described is able to produce two-dimensional coating patterns such as the one shown in Figure 7-3. It needs to be noted that a small amount of coating was observed in the masked region after electrodeposition. This may be due to the unevenness of the mask agent thickness and some coating material can be deposited on to the foam substrate where the mask agent is too thin. The coating material within the

masked region can be further reduced by enhancing the masking procedure (i.e., by applying a second layer of masking agent after curing of the first layer). However, the amount of coating within the masked region is insignificant compared to the total amount of coating. Thus, it is considered that the performance of the hybrid foam samples will not be affected.

7.4 Quasi-static Behavior of Functionally Graded Al/Cu Hybrid Foams

The performance of hybrid Al/Cu foams as structural elements with graded coating patterns was evaluated under quasi-static loading conditions. Two flexure type loading conditions with linear bending moment and constant shear were considered, namely, a three-point bending beam and a cantilever beam. While both loading conditions have critical sections, the cantilever beam condition has a lower shear to bending moment ratio compared to the three point bending beam tests. For each loading condition, four samples with different coating designs were tested. Foams with pore size of 40 PPI were used for three point bending tests while 20 PPI foams were used for cantilever beam tests. It needs to be noted that all samples tested in this investigation were subjected to an annealing process.

7.4.1 Design of Functionally Graded Hybrid Foam

The functionally graded hybrid foam (FGHF) structural element designs followed two objectives. The first objective was to show that the failure mechanism of foam structures can be modified and less deformation at critical locations can be achieved by applying reinforcement in critical areas of a foam domain. The second objective was to show that the mechanical performance of open-cell foam structural elements, such as stiffness and strength, can be optimized by employing a strategically designed reinforcement pattern.

In order to evaluate the design's performance, plain Al and hybrid Al/Cu foams with different reinforcement patterns were manufactured and tested. The same amount of coating material was applied to all hybrid foam samples. That is, for each test setup, the hybrid foam samples have approximately the same final weight. Information on the samples is summarized in Table 7-1.

It has been shown in Section 7.2 that the plain Al foam and Al/Cu hybrid foams have ductile behavior in compression. In addition, the compressive strength of these foam materials increases at larger strain due to densification. On the other hand, the tensile behavior of both plain Al and hybrid Al/Cu foams are relatively brittle and rupture occurs at low deformation. As a result, when these foam materials are used in a structural element, their tension capacity will govern the element's global response. Thus, a more balanced failure mechanism can be achieved if the tensioned region of the structural element is reinforced. Based on this criterion, samples with graded reinforcement were manufactured for the two bending conditions for study, which are shown in Figure 7-4.

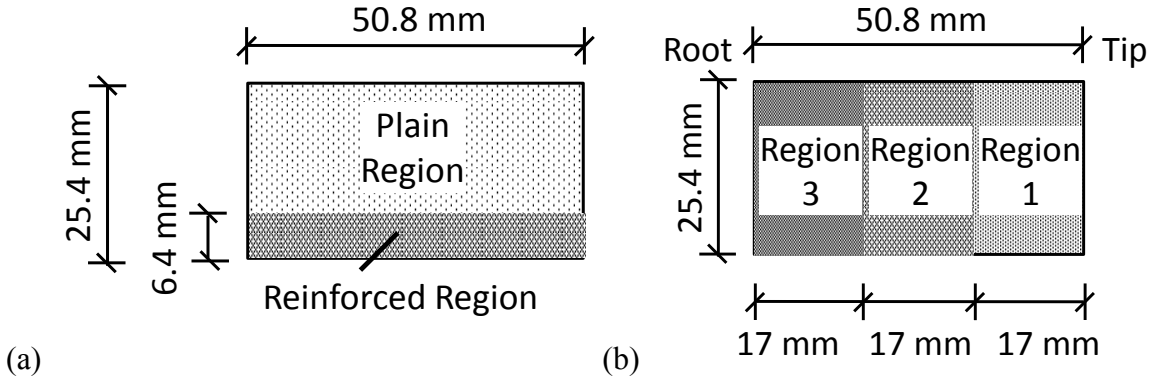

Figure 7-4 Foam samples with graded reinforcement: a) bottom reinforced sample for three-point bending test; b) sample for cantilever beam test with three stepped reinforcement

Table 7-1 Information of Al/Cu hybrid foams for three-point bending and cantilever beam tests

Loading Condition	Sample Name	Description	Weight (g)	Coating Thicknesses (μm)
Three point bending (40 PPI Foams)	T0	Plain Al foam	5.0	0
	T1	Al/Cu hybrid foam with uniform reinforcement	11.0	30
	T2	Al/Cu hybrid foam with bottom region reinforced	11.8	93
	T3	Al/Cu hybrid foam with reinforcement pattern based on topology optimization	11.0	-
Cantilever beam (20 PPI Foams)	C0	Plain Al foam	5.7	0
	C1	Al/Cu hybrid foam with uniform reinforcement	15.9	50
	C2	Al/Cu hybrid foam with three stepped graded reinforcement	16.1	28,50,70
	C3	Al/Cu hybrid foam with reinforcement pattern based on topology optimization	16.3	-

As is well known, the highest tensile stresses occur at the extreme fiber in the tension side of the section with maximum bending moment. For the three-point bending test, the maximum tensile stress is at the bottom of the mid-section and failure at that location will govern the element's load-carrying capacity. A sample with reinforcement applied at the bottom of the sample (T2) was manufactured with the aim of delaying such failure mechanism (see Figure

7-4a). On the other hand, a sample with a three step graded reinforcement (C2) was manufactured for the cantilever beam test. Different reinforcement levels were applied to three regions (see Figure 7-4b) by controlling the amount of coating material at each region. The coating level increased incrementally from region 1 to 3 with the highest coating level at the region (region 3) close to the fixed end where maximum bending occurs. For the 3 step sample tested, the amount of coating material applied to region 1, 2 and 3 was 16.7%, 33.3% and 50% of the total coating.

To achieve the second design objective and demonstrate the potential of optimizing the mechanical performance of open-cell hybrid foam structural elements, samples with a reinforcement design based on topology optimization were manufactured. The optimized reinforcement design was developed through a simple power-law topology optimization approach using the educational program developed by Sigmund [108]. The design optimization objective was to minimize compliance for the two bending configurations in the study. Figure 7-5 shows the optimized design and manufactured samples with optimized coating pattern for both the three-point bending test (T3) and cantilever test (C3).

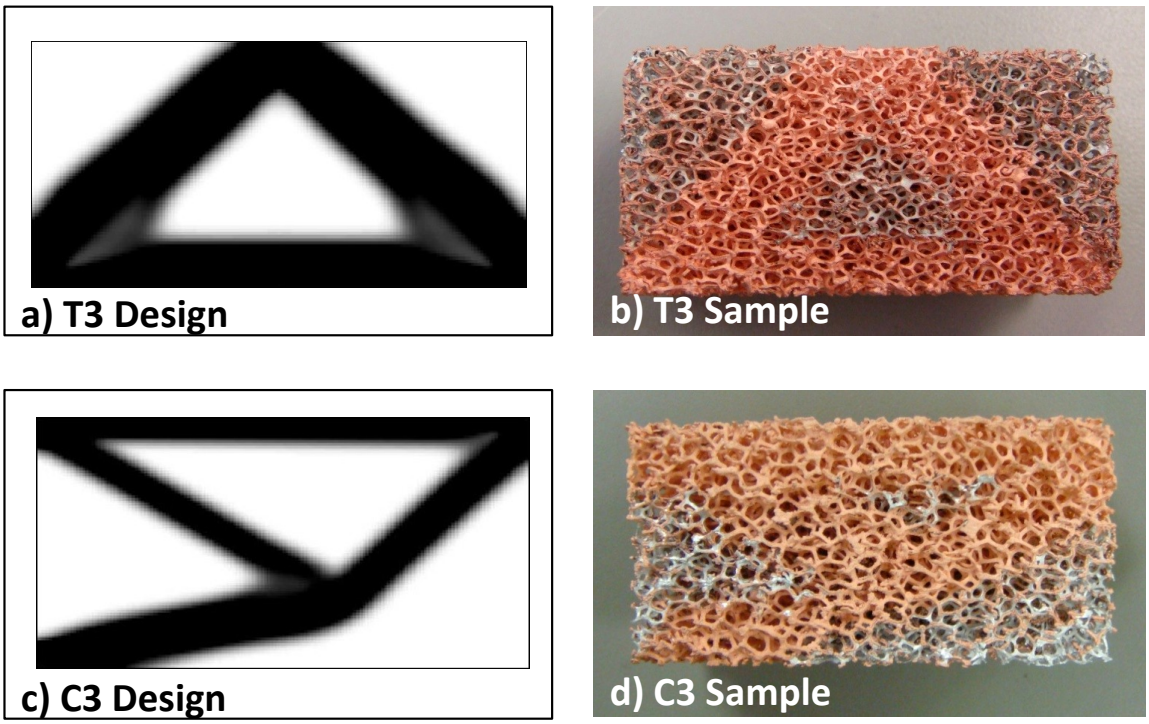

Figure 7-5 Topology optimized reinforcement design: a) For three-point bending test; b) for cantilever beam test

7.4.2 Test Setup (3-point bending and cantilever beam)

The test setup for three-point bending and cantilever beam tests is shown in Figure 7-6. For the three-point bending tests the samples were placed spanning along their long dimensions with 2 mm wide supports on each side. Loading was applied by a universal loading frame through a semi-cylindrical (radius of 5 mm) loading tip that created a line loading condition at the center of the top surface of sample. Two aluminum plates with a width of 12.7 mm and thickness of 0.4 mm were attached to the bottom of the sample at the supports to avoid localized damage during testing. Pilot test trials showed that placing an aluminum plate on the top region in contact with the loading tip reduced the bending type failure. In addition, it was of interest to study the behavior of foam material itself. Thus, no aluminum plate was attached to the top

surface of the sample tested. The tests were carried out with a loading rate of 0.05 mm/second. For the cantilever beam tests, samples were attached to a T-shaped fixture using epoxy, and the fixture was then mounted using bolts to a rigid steel beam to create a fixed boundary condition.

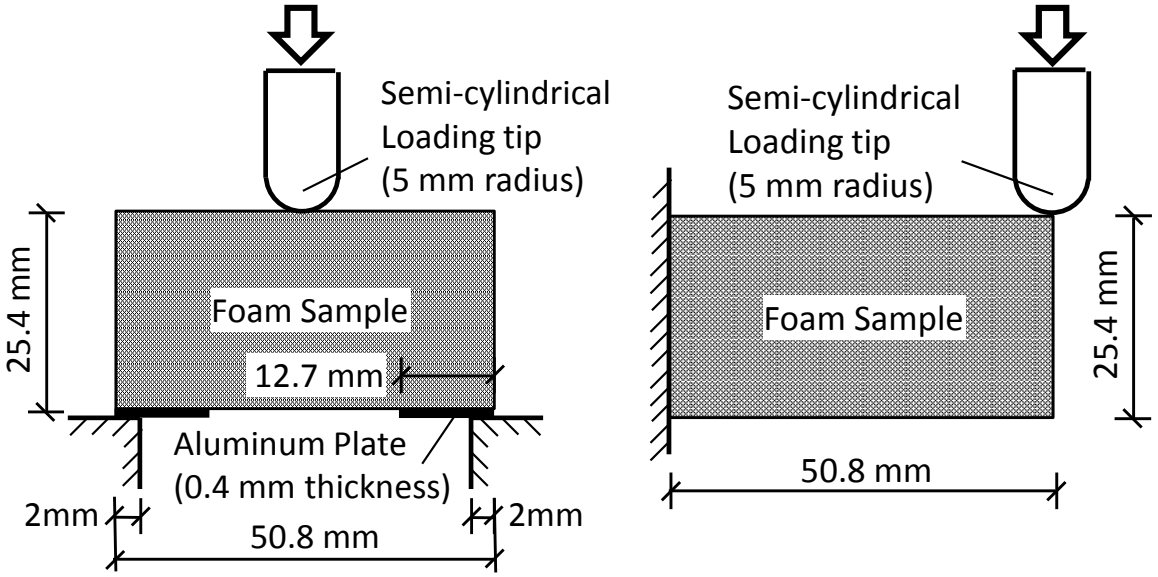

Figure 7-6 Test setup of: a) Three-point bending test; and b) Cantilever beam test.

The cantilever beam tests were conducted using the same loading frame and loading tip as those used for the three-point bending tests were used for the cantilever beam tests. The line loading from the semi-cylindrical loading tip was aligned with the edge of the top surface of the sample (see Figure 7-6b). The cantilever beam tests were also conducted with a loading rate of 0.05 mm/second. Tests were ended when fracture of the sample was observed. The applied force and the displacement of the loading tip were recorded during the tests.

7.4.3 Results

7.4.3.1 Three-point Bending Tests

Figure 7-7 shows the deformation of the three-point bending units at the instance when fracture was observed. In all cases, failure by tensile fracture occurred at the bottom of the mid-section. The force-deformation response was, however, noticeably, different for each design. The displacement history at the center of sample bottom was obtained by using the image processing tool in MATLAB [109] based on images captured from a video recording and shown in Figure 7-7.

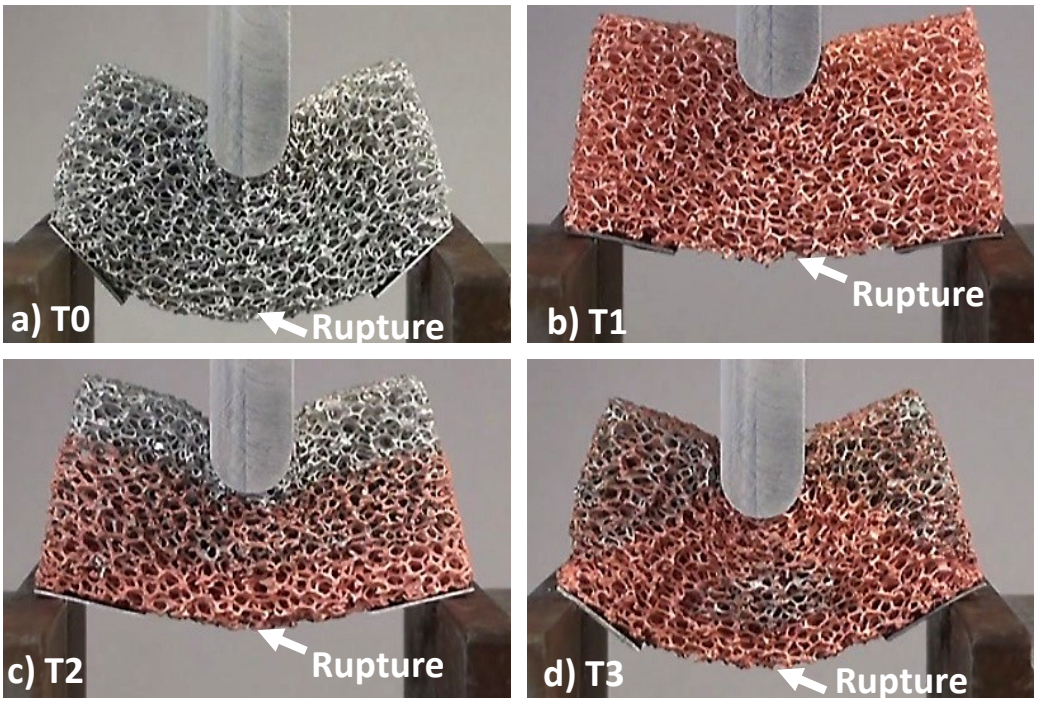

Figure 7-7 Images of foam samples in three point bending tests

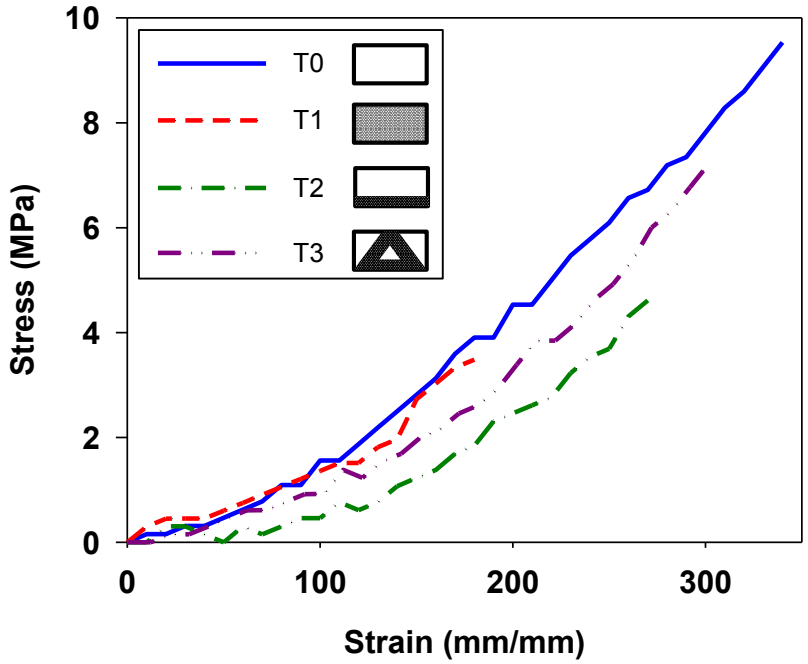

Figure 7-8 Bottom displacement vs. time from three point bending tests

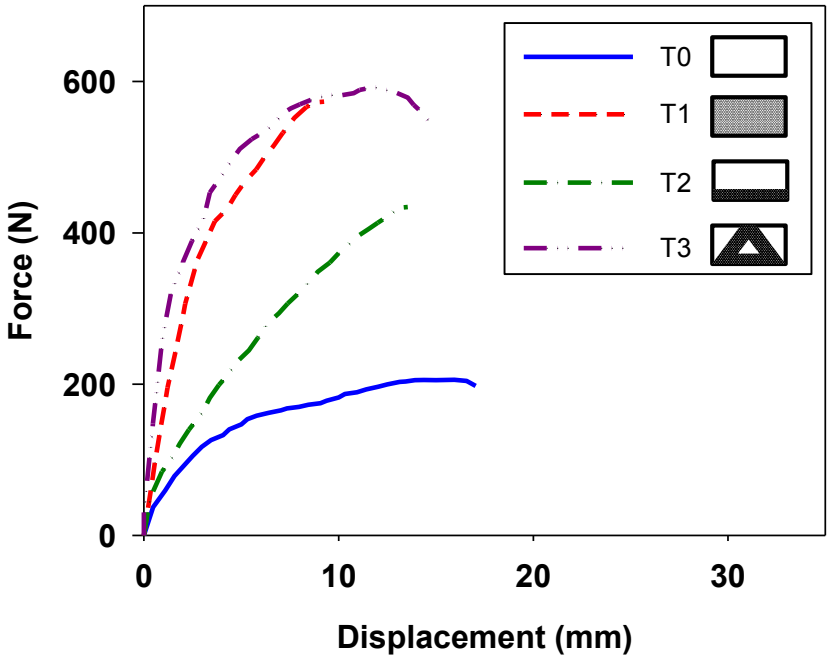

Figure 7-9 Force vs. loading tip displacement from three point bending tests

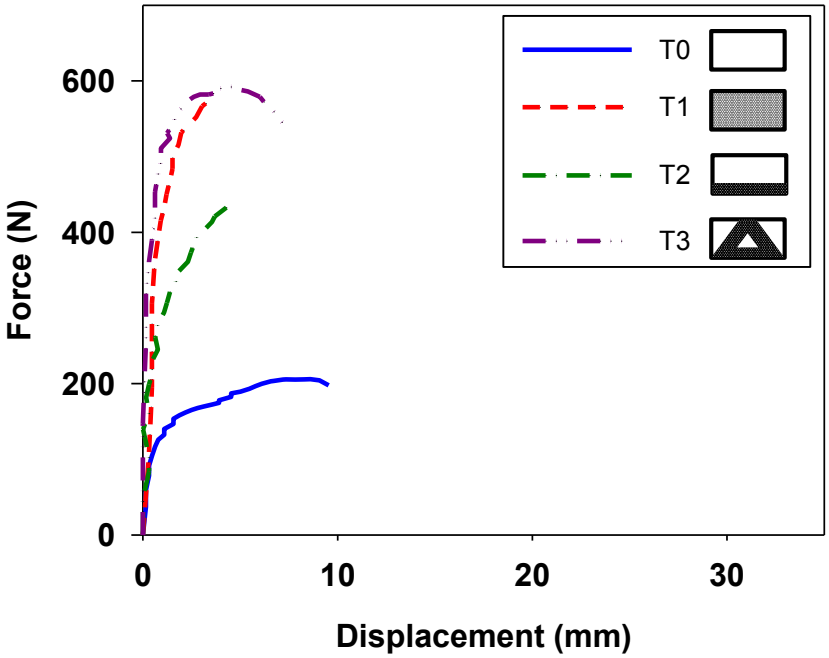

Figure 7-10 Force vs. displacement at sample bottom center from three point bending tests

From Figure 7-8 it can be observed that the bottom mid-span deformation of the uniform coating sample (T1) is close to that of the plain Al foam (T0). Conversely, the bottom deformation for the bottom reinforced (T2) and optimized samples (T3) was "delayed," that is the mid-span deformation did not grow as rapidly. The bottom reinforced sample (T2) had lowest bottom deformation among all hybrid Al/Cu foam samples. This is because the tension region in sample T2 is significantly enhanced in stiffness and strength and thus deformation on the compression region is involved in the deformation mechanism. The sample with optimized coating pattern (T3) maximized the stiffness of the foam structure, which lead to reduced bottom mid-span deformation. It can also be seen that the samples with designed coating pattern (T2 and T3) have a more ductile response as failure occured at larger flexural curvatures (and also bottom deformation). This can be attributed to the enhanced ductility provided to the bottom region with the thicker nc-Cu coating. However, even though the bottom coated sample T2 had a larger

reinforcement amount in tension region, rupture occurred earlier in this sample compared to the optimized design sample T3. This is because the increased compressive deformation in the bottom reinforced sample effectively reduced the size of the mid-span section (i.e., the section modulus is reduced) and thus leads to higher tensile stresses and early failure at the sample bottom. This indicates a compression controlled deformation mechanism.

Figure 7-9 and Figure 7-10 show the force-deformation response at the loading tip and sample bottom center for three point bending tests. Tests results are summarized and shown in Table 7-2. It can be seen that all the hybrid foam samples had enhanced stiffness and strength compared to the plain Al foam sample (T0). The sample with optimized coating pattern (T3) had the highest stiffness and highest strength. In addition, the optimized pattern also led to a higher ductility compared to the sample with uniform reinforcement. It can also be seen that, due to the excessive deformation in the compression zone, the performance of the bottom reinforced sample (T2) was significantly lower compared to the other hybrid foams. This indicates that while the failure and deformation mechanism of the beam element can be modified by reinforcing the tension region, a more strategically distributed coating pattern can lead to improved, and even optimized, structural performance.

Table 7-2 Results summary of tests

Sample		Initial Stiffness (N/mm)	Max Force (N)	Top Displacement at Fracture (mm)	Bottom Displacement at Fracture (mm)	Deformation of Mid-section at Fracture (mm)
Three-point Bending	T0	75	206	17.0	9.5	7.5
	T1	169	574	9.3	3.5	5.8
	T2	114	435	13.5	4.6	8.9
	T3	300	592	15.9	8.3	7.6
Cantilever Beam	C0	67	75	11.5	NA	NA
	C1	115	309	15.9	NA	NA
	C2	90	369	No Fracture	NA	NA
	C3	108	349	20.8	NA	NA

7.4.3.2 Cantilever Beam Tests

Figure 7-11 shows the cantilever samples at maximum deformation response. Tests were ended when rupture was observed in the sample or when a displacement of 24 mm at the loading tip was reached. As for the cantilever beam tests, failure was defined by fracture in tensile stress region as indicated by the arrows in Figure 7-11.

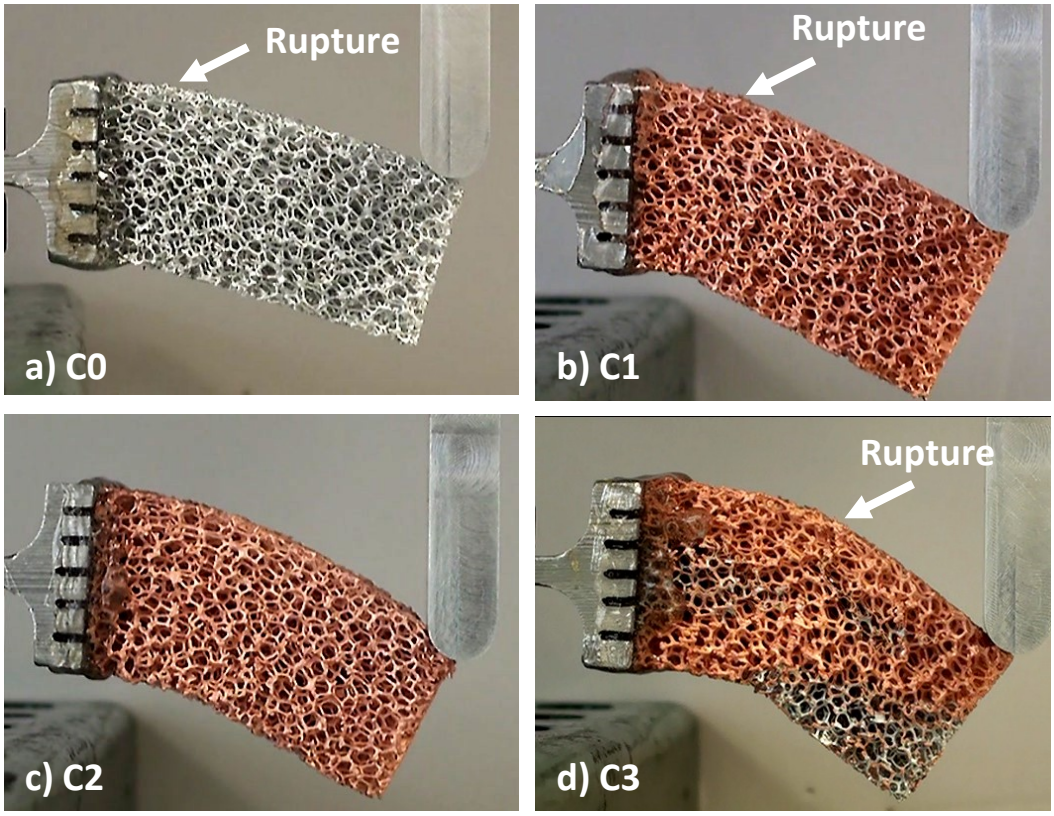

Figure 7-11 Images of foam samples in cantilever beam tests

For the plain Al foam (C0) and Al/Cu hybrid foam with uniform coating (C1) fracture occurred near the fixed end where the bending moment is maximum. On the other hand, no failure was observed in the three step graded foam sample (C2) in which more coating material was provided near the fixed end. In the sample with optimized coating pattern (C3) fracture happened at relatively large tip deformation (see Table 7-2) and the location was shifted close to the center of the sample. This demonstrates that by strategically applying the coating material, the location of material failure in the foam structure can be shifted or even avoided.

Figure 7-12 shows the force deformation response at the cantilever tip for all samples and relevant test data is summarized in Table 7-2. It can be seen that the hybrid foams had

significantly better performance (i.e., increased stiffness, strength and deformation capacity) compared to the plain foam. Compared to the uniformly reinforced foam sample (C1), the three stepped graded foam (C2) and the optimized coating pattern foam (C3) had a 19% and 13% larger strength, respectively. The elastic stiffness of the optimized coating pattern foam (C3) was close to the uniformly reinforced foam sample (C1) while the stiffness of the three stepped graded foam (C2) was slightly lower.

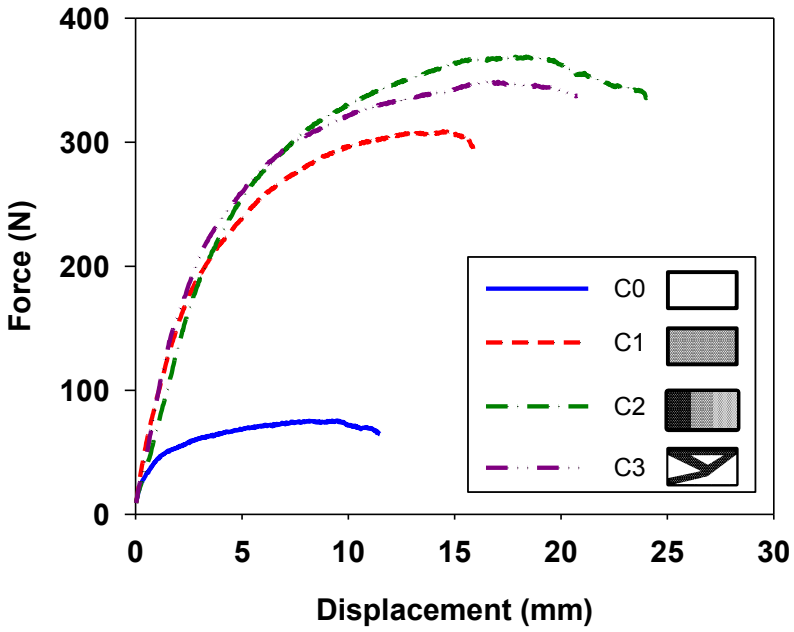

Figure 7-12 Results from cantilever beam tests

It needs to be noted that the stiffness of the optimized coating pattern foam (C3) may be further enhanced by improving the coating pattern. (Notice there is some difference between the design of the coating pattern and the actual pattern on cantilever beam samples shown in Figure 7-5.) It can also be seen that higher ductility was achieved in the samples with strategically distributed coatings compared to the one with uniform reinforcement. The efficiency in enhancing structural performance by adopting a strategically distributed coating design is thus demonstrated.

7.5 Dynamic Behavior of Functionally Graded Al/Cu Hybrid Foams

When metal foams are used for impact resistance or energy absorption, they are usually subjected to high-strain-rate loading. Due to its unique feature, the short-duration incident pulse can be delayed and lead to a relatively long-duration transmitted pulse. It has been shown in Section 6.4 that by adopting a strategically designed coating pattern, the failure mechanisms of Al/Cu hybrid foam can be modified and the mechanical properties can be optimized under quasi-static conditions. On the other hand, it is of interest to investigate the dynamic behavior of functionally graded hybrid foams with designed reinforcements to control the stress wave propagation through the material. The dynamic performance of Al/Cu hybrid foam structural elements with graded coating patterns were evaluated using drop weight tower tests under a three-point bending loading condition.

7.5.1 Design of Coating Pattern

Many studies have been conducted to investigate the performance of functionally graded foam structures under dynamic loading conditions. Cui et al. [1, 33] investigated the behavior of functionally graded foam materials under impact loading using finite element analyses and found functionally graded foams can reduce the duration of the high acceleration during an impact and had superior energy absorption performance over equivalent uniform foams under low energy impacts. They also found that convex gradients perform better than concave gradients and a better performance can be achieved by increasing the density range. Zeng et al. [29, 79] found that placing the hardest layer as the first impacted layer and the weakest layer on the remote side had some benefits to maximize energy absorption with a minimum force level transmitted to the protected structures. However, placing the weakest layer at the impacted end is preferable to avoid the breakage of the face sheet for sandwich panels subjected to localized impact.

Ajdari et al. [34] studied the in-plane crushing of regular, irregular and functionally graded honeycombs using numerical methods and found that a density gradient could significantly change the deformation mode and energy absorption of cellular structures under both low and high crushing velocities. Wang et al. [30] and Gardner et al. [31, 32] conducted shock tube experiments to study the dynamic response of sandwich panels with graded styrene foam cores. They found that the overall blast performance and structural integrity can be improved by increasing the number of monotonically graded foam core layers and applying polyurea between foam core and the back face sheet. Zhou et al. [78] studied low velocity impact response on sandwich structures with foam core that has graded densities using experimental and numerical method and found a better performance of graded core structures over the monolithic cores. In a parallel study with the current research,

Ohlsson [110] investigated and optimized the performance of a simplify supported structural panel with Al/Cu hybrid foams core subjected to blast loading. Figure 7-13 shows the optimized design found by Ohlsson with the object to minimize the displacement of the center of the bottom plate. In this figure, the darker elements have more reinforcement (thicker coating). It can be seen that the optimized design basically indicates an arch-shaped strengthened region that "guides" the loading from the impacted surface to the supports. It needs to be noted that the loading condition considered by Ohlsson was a uniform compressive loading on the top surface of the panel. In addition, an isotropic material definition was assumed for the Al/Cu hybrid foam. However, it has been shown in Section 6.1 that the tensile performance of Al/Cu hybrid foam is quite different compared to its compressive performance, especially in terms of ductility.

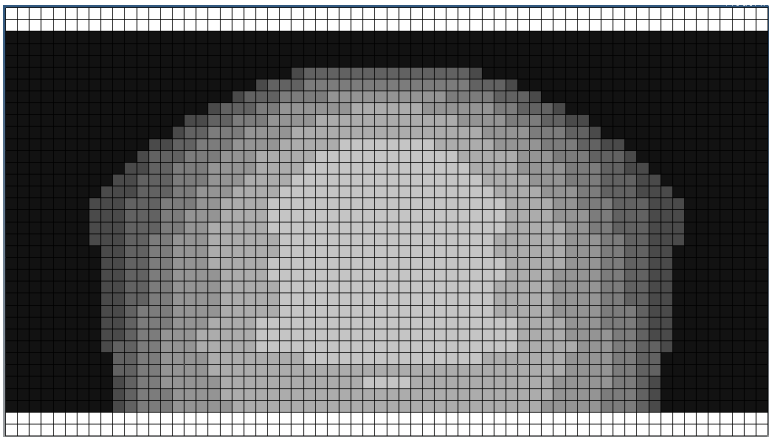

Figure 7-13 Optimized design of structural panel with Al/Cu hybrid foam core [110]

The design of coating patterns for the drop tower tests were based the criteria discussed in Section 6.4.1. The dynamic performance of Al/Cu hybrid foam was evaluated using drop weight tower tests with a three-point bending condition. Similar to the quasi-static testing, plain Al foam and Al/Cu hybrid foam samples with uniform coating thicknesses were also included in the test matrix for comparison purposes. Besides these samples, Al/Cu hybrid foam samples with two different coating patterns were fabricated and tested, as shown in Figure 7-14.

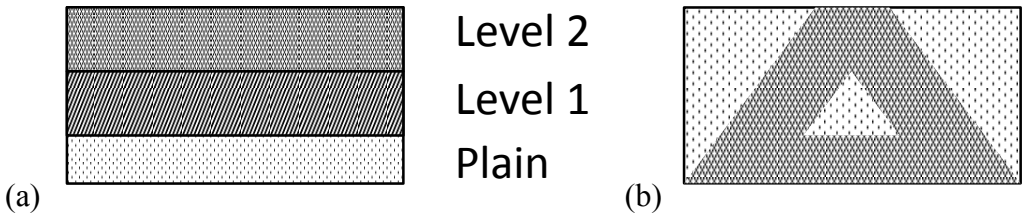

Figure 7-14 Design of Al/Cu hybrid foams for drop tower tests

The first sample (see Figure 7-14a) had a three-step graded coating pattern. The coating thicknesses increased in the upward direction. In other words, the top layer has the thickest coating while the bottom layer is not coated at all. Such design is based on the conclusion from the work by Zeng et al. [29], which indicates that such design is beneficial for energy absorption and also leads to lower magnitude for transmitted stress.

The second design (see Figure 7-14b) is a modified version of the optimized design of Al/Cu hybrid foam core in the study by Ohlsson [110]. Compared to the design found by Ohlsson, the current design does not have reinforced region for the two top corner regions. This is because the loading is only applied to the center region of the top surface of the sample in the drop tower tests. Meanwhile, the current design still provides a "guide" from the loading to the supports. The second difference is that coating was introduced to the bottom of the sample with the purpose to reinforce the tension region in the bottom. The final coating pattern for the second design in the dynamic test samples is the same as optimized coating pattern in the quasi-static tests.

Table 7-3 shows the test matrix for the drop tower impact tests. Six types of specimens were considered. Three plain Al foams with different relative densities were considered. The first plain Al foam had the same relative density (6%) as the base foam for all Al/Cu hybrid foam specimens. The second plain Al foam had a similar relative density (8%) as the Al/Cu hybrid foam with uniform coating thickness. And the third plain foam specimen had a similar weight to the hybrid foam tested. For the Al/Cu hybrid foam specimens, the first one had a uniform copper coating throughout the sample. The second and third Al/Cu hybrid foam samples are the two designs shown in Figure 7-14. All Al/Cu hybrid foams were designed to have a similar weight. It also needs to be noted that all hybrid foam samples were annealed (400 ^{o}C for 5 min.) after the

eletrodeposition process as it has been shown that annealed hybrid foams have improved performance. As a result, all plain Al foams were treated under the same annealing conditions to eliminate the influence of material properties due to different processing.

Table 7-3 Sample design for drop tower tests

Loading Condition	Sample Name	Description	Weight (g)	Coating Thicknesses (μm)
Three-point bending (40 PPI Foams)	D-T0	Plain Al foam (Nominal RD=6%)	5.6	0
	D-T0-RD8	Plain Al foam (Nominal RD=8%)	6.8	
	D-T0-RD12	Plain Al foam (Nominal RD=12%)	10.5	
	D-T1	Al/Cu hybrid foam with uniform reinforcement	11.7	30
	D-T2	Al/Cu hybrid foam with graded coating thickness (thicker coating on impact side)	11.1	N/A
	D-T3	Al/Cu hybrid foam with reinforcement pattern based on topology optimization	11.8	N/A

7.5.2 Test Setup (Drop Tower)

An INSTRON Dynatup 9250HV drop tower impact tester was used for the dynamic investigation. In a drop tower impact test, a drop weight is raised to a specific height above the specimen and then dropped onto the specimen. Figure 7-15 shows the setup for the drop tower tests conducted in this study. The setup basically consists of two components: the drop tower

impact tester system and high speed camera system. In the current study, the drop weight and specified impact velocity was same for all tests. Before each test, the tower system drives the drop weight to an automatically calculated height to achieve the specified impact velocity. The data acquisition system connected to the drop tower impact tester captures the load and displacement data at a high frequency as the specimen deforms and fails under impact.

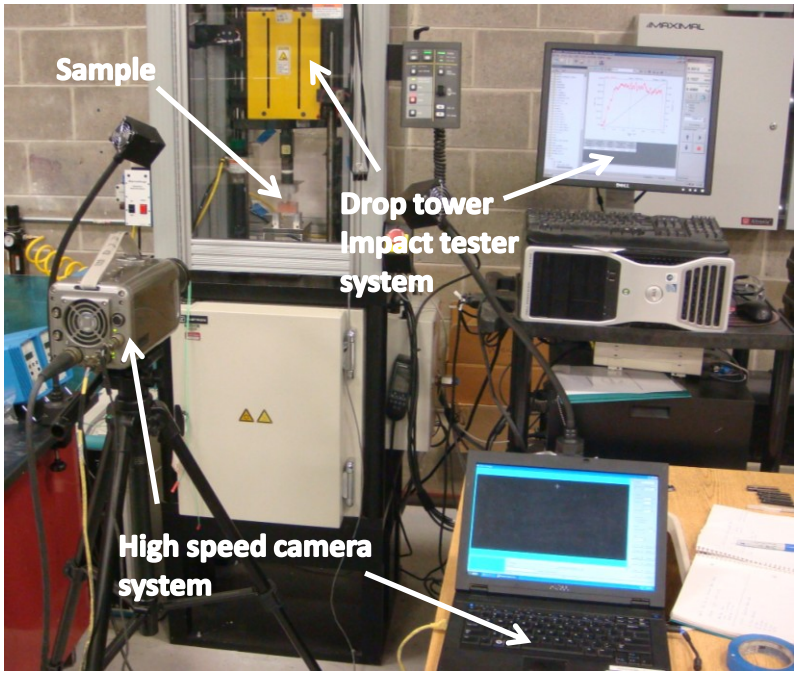

Figure 7-15 Test setup for drop tower test

The specimens used for the drop tower tests had the same size as those for the quasi-static tests (25.4 mm by 25.4 mm by 50.8 mm) and the setup was similar to the three point bending tests in the quasi-static tests conducted in previous section (see Figure 7-16). The specimen was supported by two blocks with 5 mm sitting on the block on each side. Two small plates were attached to the bottom of the specimen at the supports to avoid localized damage during testing.

An indenter with semi-cylindrical loading tip (similar to the one used for quasi-static testing) was aligned with the center of the specimen. As a result, a line loading is applied to the top surface of specimen at the impact. The speed at impact used was 10 m/s and the drop weight was 6.56 kg for all tests.

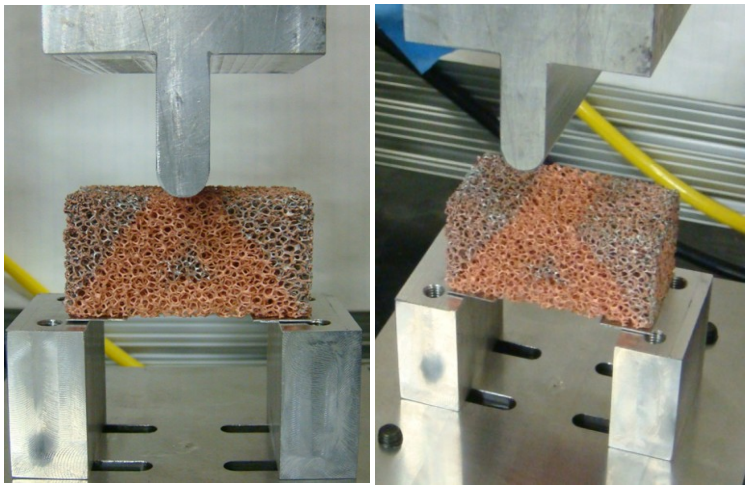

Figure 7-16 Sample loading setup for drop tower test

7.5.3 Results and Discussion

The results from drop weight tower tests are discussed in this section. The comparisons are based on force-displacement curves and energy input. Figure 7-17 shows the force-displacement results from drop tower tests for plain Al foam with a relative density of 6% and all Al/Cu hybrid foams fabricated on similar base plain Al foams.

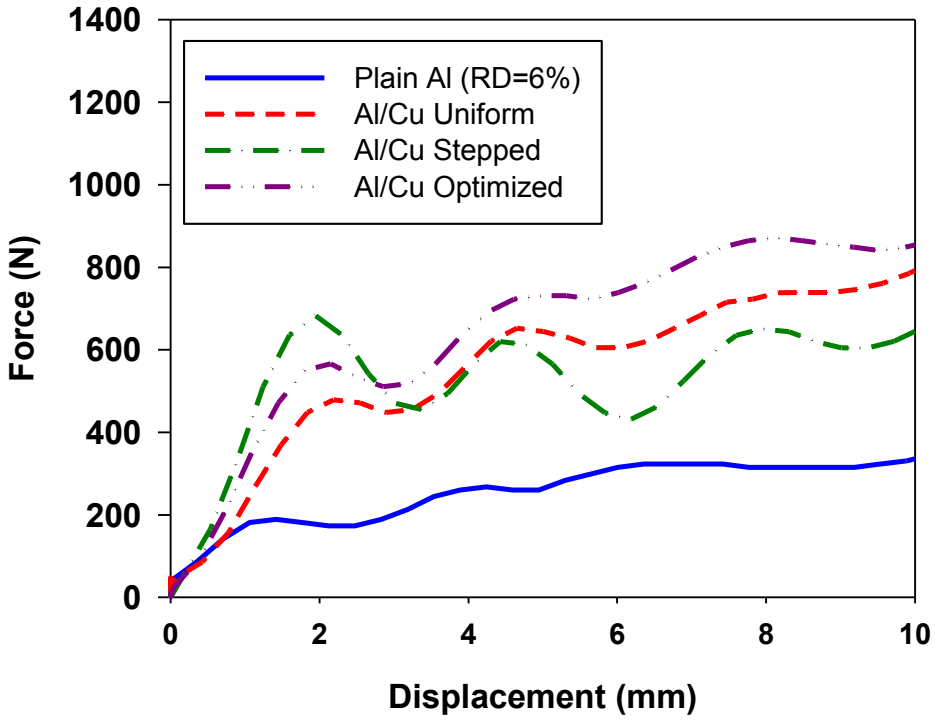

Figure 7-17 Force-displacement curves for samples in drop tower tests

The fluctuations observed in the force-deformation response for all tests (Figure 7-17) can be attributed to the wave propagation through the sample while the loading is applied. In spite of this effect, it can be seen that generally the Al/Cu hybrid foam had enhanced stiffness as well as strength compared with the plain Al foam due to the additional copper coating. The specimen with graded coating showed stiffer behavior at low deformations compared to other Al/Cu hybrid foam samples. This is because the hardest layer is on the impact side of the sample. Once the loading tip hits the sample, the loaded region in the top layer collapses first and distributes the load more evenly to the remaining material, thus leading to a stiffer response. A similar behavior was reported by Zeng et al [29] by putting stiffer material on the impact face. However, at larger deformations the strength of the graded foam was lower compared to the uniformly coated hybrid foam and the one with topology optimized coating pattern. Compared to

the uniformly coated hybrid foam specimen, the optimized coating pattern led to a higher stiffness and higher strength. This may be attributed to that in the optimized design the coating material is more efficiently distributed to the highly stressed regions, which leads to a higher strength.

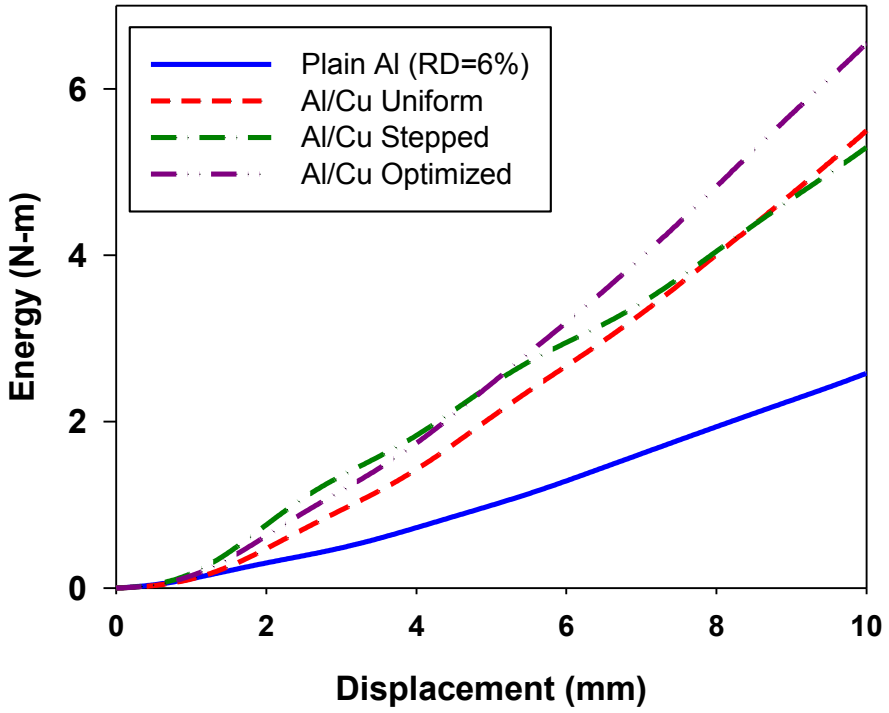

Figure 7-18 Energy versus time curves for samples in drop tower tests

Figure 7-18 shows the plot of input energy with respect to the loading tip displacement. It can be seen that the Al/Cu hybrid foams had a significantly higher level of energy absorption compared to the plain Al foam. Among the Al/Cu hybrid foams, the specimen with stepped density gradient had higher energy absorption at low deformations compared to other hybrid foams. This can be attributed to the high initial stiffness and strength of specimen D-T2 at low deformations. However, the energy absorbed by foams D-T1 and D-T3 surpassed that of specimen D-T2 as these two specimens has higher strength at larger deformation. Among all

hybrid foams, the specimen with a topology optimized design pattern had largest amount of energy absorption after 5 mm of tip displacement.

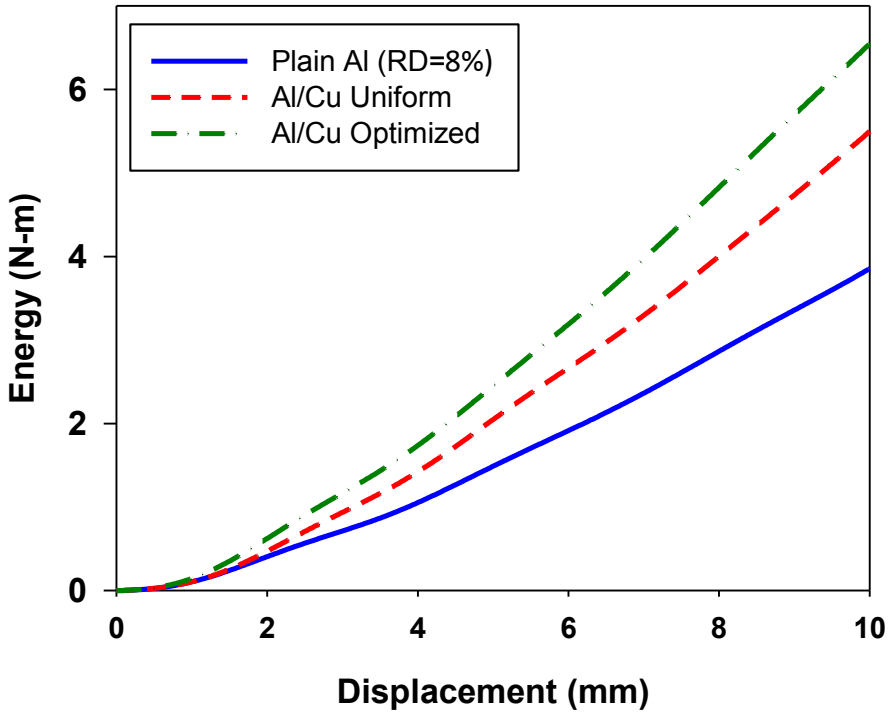

Figure 7-19 Comparison of energy absorption capacity of foams with similar solid volumn

Figure 7-19 compares the energy absorption capacity of the hybrid foams with uniform and optimized coating pattern compared to a plain Al foam with a relative density of 8%. As mentioned earlier, the uniformly coated sample in the dynamic tests had a relative density of 8.1%. In other words, the hybrid foam specimens tested had approximately the same solid volume as the plain Al foam with relative density of 8%. From this comparison, it can be seen that with the same amount of solid volume, the hybrid foam had much higher energy absorption compared to the plain Al foam with 8% relative density. The enhancement in energy absorption capacity seen in Figure 7-19 for the Al/Cu hybrid foam with optimized designs comes from two

sources: i) the coating material (annealed copper) is stronger compared to the base material (annealed aluminum); and 2) the optimized pattern further enhanced the energy absorption capacity by more efficiently redistributing the coating material.

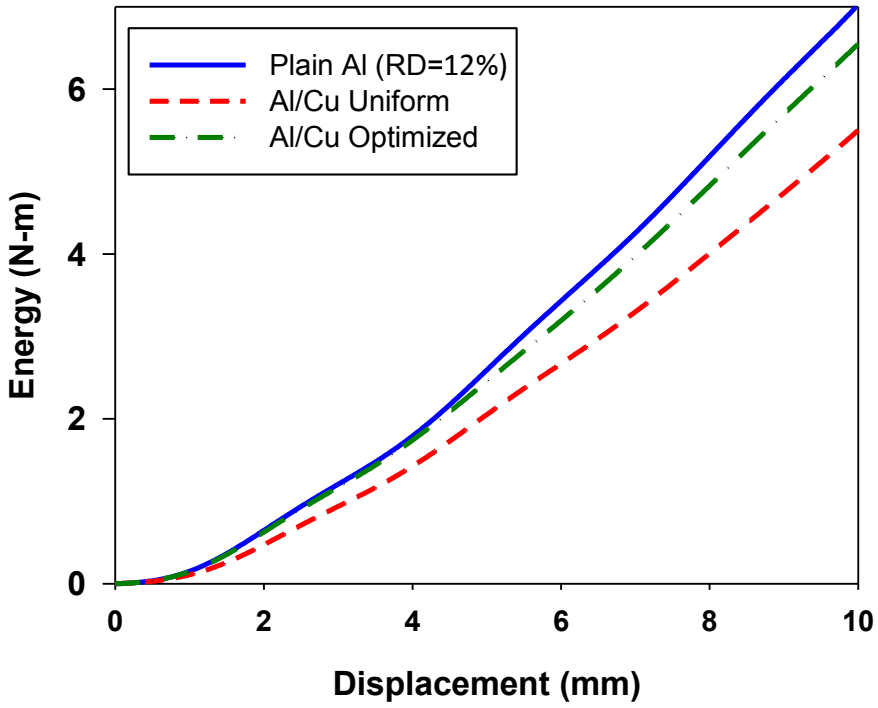

Figure 7-20 Comparison of energy absorption capacity of foams with similar weight

Figure 7-20 shows a comparison of the energy absorption of the hybrid foams with uniform and optimized coating patterns compared to a plain Al foam with a relative density of 12%. The plain Al foam with 12% relative density had similar specimen weight compared to the hybrid foams. As the density of copper is much higher (more than three times higher) compared to aluminum, the hybrid foam with uniform coating had a much lower energy absorption compared to the plain Al foam with similar weight. Meanwhile, due to the enhancement of the designed coating pattern, specimen D-T3 had a similar energy absorption capacity compared to

the plain Al foam with similar weight. This comparison indicates that, compared to a plain Al foam, the use of Al/Cu hybrid foams may not be efficient in weigh-sensitive applications, even with a strategically designed coating pattern. However, certain measures can be adopted to enhance the performance of hybrid foams. For example, the amount of coating can be increased in which case the advantage of adopting a functionally graded foam may be more significant. Nonetheless, the choice of coating material can be optimized by choosing a stronger material (e.g., Nickel).

7.6 Discussion

The Al/Cu hybrid foam samples tested in this study had approximately the same weight as a 40 PPI Al foam sample with a uniform 30 μm coating and a 20 PPI foam sample with uniform 50 μm Cu coating for the three-point bending and cantilever beam tests, respectively. The advantage of using strategically distributed reinforcement on the open-cell foam structural elements was demonstrated. The samples with designed coating pattern were shown to have superior performance, namely reduced deformations and damage, enhanced stiffness, higher strength and larger ductility. The enhancements and advantages of using functionally graded coating patterns will likely be more significant compared to uniform reinforcement for cases with thicker coatings. The proposed manufacturing approach of open-cell foam structures with two dimensional property gradient can also be applied to other material systems of recent research interest such as Al/Ni hybrid foams [6, 7, 40, 111].

7.7 Conclusions

Functionally graded open-cell hybrid Al/Cu foam structural elements manufactured through electrodeposition of nano crystalline Cu onto an open-cell Al foam were manufactured

and their performance was evaluated under different types of flexure loading conditions and loading rate. The performance of functionally graded Al/Cu hybrid foams were compared with plain foam with different relative density and Al/Cu hybrid foams with uniform coating thickness. The following conclusions were reached:

1) An approach to manufacture open-cell cellular structures with two-dimensional property gradients was presented and demonstrated. The approach allows for strategic reinforcement across the domain of an open-cell metal foam, in the form of nanocrystalline metal coatings, for the provision of functionally graded properties.

2) The tension-controlled deformation and failure mechanism of open-cell foam structural elements under flexural demands can be controlled by reinforcing the tension region. However, when the tension region is highly reinforced, the increased demands and possible large in the compression region need to be considered, as the reinforcement strategy can reduce the sectional flexural performance.

3) The location of failure and damage in open-cell foam structural elements can be shifted or eliminated by employing functionally graded coating patterns. This can be used to avoid damage at critical regions within the foam structural elements.

4) Under flexure-type loading conditions at different loading rates, the stiffness, strength and ductility of open-cell foam structural elements can be optimized by implementing strategically designed coating patterns.

5) The energy absorption capacity of hybrid foam material under high strain rate loading conditions can be optimized by implementing strategic coating pattern.

CHAPTER 8 CONCLUSIONS

8.1 Research Significance

This research provided new understanding on the micro- and macro-scale behavior of hybrid metal foams created through electrodeposition. In addition, the manufacturing process for such material was improved by introducing an annealing process that enhanced the ductility of the nanocrystalline structured electrodeposited coating. The experimental characterization under high strain rate condition provided useful information on the dynamic behavior of hybrid metal foams. Finally, functionally graded hybrid metal foam systems with strategically designed nanostrured coating through electrodeposition, which can be designed to achieve optimized mechanical performances according to different loading conditions, were also developed. The findings from this research provide essential information on the development of structural components incorporating functionally graded cellular materials under both quasi-static and high strain rate loadings.

8.2 Conclusions

Based on the discussions in previous chapters, the following general conclusions can be provided:

1) Rupture of the electrodeposited Cu coating is a prevailing failure mechanism in Al/Cu hybrid foams and fracture of the ligaments can occur under quasi-static as well as high-strain rate loading conditions. Such behavior is due to the low ductility of the electrodeposited nanocrystalline coating and is proportional to the coating thickness. This detrimental effect can jeopardize the the overall performance of hybrid foam systems fabricated through electrodeposition, such as their energy absorption capacity.

2) Beam-element based macro-scale simulations created using multiple Kelvin cells were established and were shown to adequately capture the unique quasi-static behavior of Al/Cu hybrid foams. It was shown damage and fracture of the coating and core materials need to be considered in the simulation of hybrid foams.
3) ,The ductility of the electrodeposited copper coating in Al/Cu hybrid foams can be enhanced with proper amount of annealing. This improvement in coating material of hybrid foams leads to an enhanced compressive and tensile behavior and a better overall energy absorption performance under quasi-static and high-strain-rate conditions. Such effect is more significant in hybrid foams with thick coatings.
4) Analytical solutions to predict the compressive and tensile response of annealed Al/Cu hybrid foams were derived. With input on basic properties for base and coating materials and the relative densities of base and hybrid foams, the analytical models were shown to have an adequate predictive ability.
5) Hybrid open-cell foams with two-dimensional property gradient were successfully fabricated and it was shown that the deformation, failure mechanism, and region of damage of open-cell foam structural elements can be modified or controlled by reinforcing specific regions. It was also demonstrated that the mechanical properties of hybrid open-cell foam structural element, such as stiffness, strength and ductility, under quasi-static and dynamic loading conditions can be optimized by implementing strategically designed coating patterns.

8.3 Future Research

8.3.1 Optimized Material System

This study and investigation was based on Al/Cu hybrid foams systems manufactured by introducing nanocrystalline copper coating onto plain aluminum foam through electrodeposition. Copper was chosen as the coating material mainly due to the well-established knowledge in its electrodeposition process, ease in availability and relatively low cost. However, many other metals and alloys can also be electrodeposited. Furthermore, with other electroplating techniques (i.e., electroless deposition), the choice of core and coating materials can be extended to nonmetal materials such as polymers and ceramics. Using similar techniques and concept as those presented in this study, it can be of great interest to identify other material systems that lead to hybrid foams with optimized performance.

8.3.2 Multi-scale Modeling

The evaluation of functionally graded hybrid foam systems at the structural scale using numerical methods can offer insight and guidance in the design of structural components consisting of functionally graded foams. This requires proper definition of the macroscopic behavior of hybrid foams. However, the behavior of hybrid foams is highly anisotropic and thus defining a representative constitutive response for them through analytical or experimental approaches can be complicated. On the other hand, to capture the unique behavior of hybrid foams using a numerical approach requires detailed modeling of the microstructure and to account for failure mechanisms in the ligaments, such as inelastic buckling, fracture and contact. Such complicated mechanisms make it almost impossible to establish a macroscopic analysis that explicitly models the microstructure due to the large computational expense. An alternative

way is to establish a micro-to-macro scale analysis, i.e., a multi-scale analysis). Multi-scale analysis is based on the homogenization approach and can be implemented into the framework of the finite element method in which a local periodicity is assumed and the macroscopic behavior at certain integration point is determined through detailed modeling of the microstructure assigned to that point [112-117]. As a result, there is no need to specify the homogenized constitutive behavior at the macroscopic integration points. This approach is thus considered to be preferable in the simulation of hybrid foams in order to capture the micro-scale mechanisms while maintaining realistic computational demands.

8.3.3 Ductility Enhancement

It has been shown that rupture of the electrodeposited nanocrystalline coating can jeopardize the overall performance of hybrid metal foams. This is due to the low ductility of the electrodeposited metal material. In this study an annealing process was applied to hybrid metal foams as an approach to enhance the coating ductility by modifying its grain structure and eventually improving the performance of hybrid metal foams. However, the grain size also depends on the electrochemical condition during the electrodeposition process and thus a better understanding of the relationship between the parameters in the electrodeposition process and the performance of hybrid metal foams may help improve the manufacturing of hybrid metal foams..

8.3.4 Wave Propagation through Functionally Grade Metal Foams

The behavior of Al/Cu hybrid foams under high-strain-rate conditions was characterized in this study. However, one-dimensional propagation of stress wave through functionally graded hybrid foams has not been fully investigated. A detailed investigation on stress wave propagation through functionally graded foam structural elements with two dimensional properties gradient

also requires further understanding to better design functionally graded metal foams for use in high-strain-rate condition.

REFERENCES

REFERENCES

[1] L. Cui, S. Kiernan, and M. D. Gilchrist, "Designing the energy absorption capacity of funcationally graded foam materials," *Materials science and engineering A,* vol. 507, pp. 215-225, 2009.

[2] A. H. Brothers and D. C. Dunand, "Mechanical properties of a density-graded replicated aluminum foam," *Materials Science and Engineering: A,* vol. 489, pp. 439-443, 2008.

[3] S. Kieman, L. Cui, and M. D. Gilchrist, "Propagation of a stress wave through a virtual functionally graded foam," *International Journal of Non-linear Mechanics,* vol. 44, pp. 456-468, 2009.

[4] A. H. Brothers and D. C. Dunand, "Density-Graded Cellular Aluminum," *Advanced Engineering Materials,* vol. 8, pp. 805-809, 2006.

[5] Y. Hangai, K. Takahashi, T. Utsunomiya, S. Kitahara, O. Kuwazuru, and N. Yoshikawa, "Fabrication of functionally graded aluminum foam using aluminum alloy die castings by friction stir processing," *Materials Science and Engineering: A,* vol. 534, pp. 716-719, 2012.

[6] B. A. Bouwhuis, J. L. McCrea, G. Palumbo, and G. D. Hibbard, "Mechanical properties of hybrid nanocrystalline metal foams," *Acta Materialia,* vol. 57, pp. 4046-4053, Aug 2009.

[7] A. Jung, H. Natter, S. Diebels, E. Lach, and R. Hempelmann, "Nanonickel Coated Aluminum Foam for Enhanced Impact Energy Absorption," *Advanced Engineering Materials,* vol. 13, pp. 23-28, 2010.

[8] W. Wang, R. Burgueño, J.-W. Hong, and I. Lee, "Nano-deposition on 3D open-cell aluminum foam materials for improved energy absorption capacity," *Materials Science and Engineering A,* vol. 572, pp. 75-82, 2013.

[9] T. Ngo, P. Mendis, A. Gupta, and J. Ramsay, "Blast Loading and Blast Effects on Structures - An Overview," *EEJSE Special Issue: Loading on Structures,* 2007.

[10] H. Draganic and V. Sigmund, "Blast Loading on Structures," *Tehnicki Vjesnik-Technical Gazette,* vol. 19, pp. 643-652, Sep 2012.

[11] R. W. Prugh, "The Effects of Explosive Blast on Structures and Personnel," *Process Safety Progress,* vol. 18, pp. 5-16, 1999.

[12] G. C. Mays and P. D. Smith, *Blast Effects on Buildings - Design of Buildings to Optimize Resistance to Blast Loading*: Tomas Telford, 2000.

[13] L. J. Gibson and M. F. Ashby, *Cellular solids: Structure and properties, second edition*: Cambridge University Press, 1999.

[14] L. Gong and S. Kyriakides, "Compressive response of open-cell foams Part II: Initiation and evolution of crushing," *International journal of solids and structures,* vol. 42, pp. 1381-1399, 2005.

[15] L. Gong, S. Kyriakides, and W. Y. Jang, "Compressive response of open-cell foams. Part I: Morphology and elastic properties," *International journal of solids and structures,* vol. 42, pp. 1355-1379, Mar 2005.

[16] H. Yu, Z. Guo, B. Li, G. Yao, H. Luo, and Y. Liu, "Research into the effect of cell diameter of aluminum foam on its compressive and energy absorption properties," *Materials Science and Engineering: A,* vol. 454–455, pp. 542-546, 2007.

[17] W. Y. Jang, A. M. Kraynik, and S. Kyriakides, "On the microstructure of open-cell foams and its effect on elastic properties," *International journal of solids and structures,* vol. 45, pp. 1845-1875, Apr 2008.

[18] W. Y. Jang and S. Kyriakides, "On the crushing of aluminum open-cell foams: Part I. Experiments," *International journal of solids and structures,* vol. 46, pp. 617-634, Feb 2009.

[19] N. J. Reynolds, *Functionally Graded Materials*: Nova Science Publishers, Inc., 2012.

[20] S. Suresh and A. Mortensen, *Fundamentals of Functionally Graded Materials*: The University Press, Cambridge, 1998.

[21] S. Amada, Y. Ichikawa, T. Munekata, Y. Nagase, and H. Shimizu, "Fiber texture and mechanical graded structure of bamboo," *Composites Part B: Engineering,* vol. 28, pp. 13-20, 1997.

[22] T. J. Reiter, *Functional adaptation of bone and application in optimal structural design*: VDI-Verlag Düsseldorf, GFR, 1996.

[23] M. F. Ashby, E. A, N. A. Fleck, L. J. Gibson, J. W. Hutchinson, and H. N. G. Wadley, *Metal foams: a design guide.* Boston: Butterworth-Heinemann, 2000.

[24] A. Neubrand, "Electrochemical processing of porosity gradients for the production of functionally graded materials," *Journal of Applied Electrochemistry,* vol. 28, pp. 1179-1188, 1998/11/01 1998.

[25] Y. Matsumoto, A. H. Brothers, S. R. Stock, and D. C. Dunand, "Uniform and graded chemical milling of aluminum foams," *Materials Science and Engineering: A,* vol. 447, pp. 150-157, 2007.

[26] A. Pollien, Y. Conde, L. Pambaguian, and A. Mortensen, "Graded open-cell aluminium foam core sandwich beams," *Materials Science and Engineering a-Structural Materials Properties Microstructure and Processing,* vol. 404, pp. 9-18, Sep 15 2005.

[27] Y. Hangai, H. Kato, T. Utsunomiya, and S. Kitahara, "Effect of the Amount of Gases on the Foaming Efficiency of Porous Aluminum Using Die Castings Fabricated by Friction Stir Processing," *Metallurgical and Materials Transactions A,* vol. 41, pp. 1883-1886, 2010/08/01 2010.

[28] N. Gupta, "A functionally graded syntactic foam material for high energy absorption under compression," *Materials Letters,* vol. 61, pp. 979-982, Feb 2007.

[29] H. B. Zeng, S. Pattofatto, H. Zhao, Y. Girard, and V. Fascio, "Impact behaviour of hollow sphere agglomerates with density gradient," *International journal of mechanical sciences,* vol. 52, pp. 680-688, May 2010.

[30] E. H. Wang, N. Gardner, and A. Shukla, "The blast resistance of sandwich composites with stepwise graded cores," *International journal of solids and structures,* vol. 46, pp. 3492-3502, Sep 2009.

[31] N. Gardner, E. Wang, P. Kumar, and A. Shukla, "Blast Mitigation in a Sandwich Composite Using Graded Core and Polyurea Interlayer," *Experimental Mechanics,* vol. 52, pp. 119-133, 2012/02/01 2012.

[32] N. Gardner, E. Wang, and A. Shukla, "Performance of functionally graded sandwich composite beams under shock wave loading," *Composite Structures,* vol. 94, pp. 1755-1770, 2012.

[33] L. Cui, M. A. F. Rueda, and M. D. Gilchrist, "Optimisation of energy absorbing liner for equestrian helmets. Part II: Functionally graded foam liner," *Materials & Design,* vol. 30, pp. 3414-3419, Oct 2009.

[34] A. Ajdari, H. Nayeb-Hashemi, and A. Vaziri, "Dynamic crushing and energy absorption of regular, irregular and functionally graded cellular structures," *International journal of solids and structures,* vol. 48, pp. 506-516, Feb 2011.

[35] H. Wang, S. R. Johnston, and D. W. Rosen, "Design of a graded cellular structure for an acetabular hip replacement component," in *The Seventeeth Solid Freeform Fabrication Symposium*, Austin, TX, 2006.

[36] T. Daxner, F. G. Rammerstorfer, and H. J. Böhm, "Adaptation of density distributions for optimising aluminium foam structures," *Materials Science and Technology,* vol. 16, pp. 935-939, 2000.

[37] Y. D. Gamburg and G. Zangari, *Theory and Practice of Metal Electrodeposition*: Springer Science & Business Media, 2011.

[38] W. H. Safranek, *The Properties of Electrodeposited Metals and Alloys*, Second ed.: American Electroplaters & Surface Finishers Society, 1986.

[39] J. C. M. Li, *Mechanical Properties of Nanocrystalline Materials*: Pan Stanford Publishing, 2011.

[40] Y. Boonyongmaneerat, C. A. Schuh, and D. C. Dunand, "Mechanical properties of reticulated aluminium foams with electrodeposited Ni-W coatings," *Scripta Materialia,* vol. 59, pp. 336-339, Aug 2008.

[41] Y. Sun, R. Burgueño, A. J. Vanderklok, S. A. Tekalur, W. Wang, and I. Lee, "Compressive behavior of aluminum/copper hybrid foams under high strain rate loading," *Materials Science and Engineering: A,* vol. 592, pp. 111-120, 2014.

[42] Y. S. Lee and D. N. Lee, "Characterization of dislocations in copper electrodeposits," *Journal of Materials Science,* vol. 35, pp. 6161-6168, 2000.

[43] W. Rolf, "Material Science of Electrodeposits," *Plating & Surface Finishing,* vol. 69, pp. 46-51, 1982.

[44] D. A. Hardwick, "The Mechanical-Properties of Thin-Films - a Review," *Thin Solid Films,* vol. 154, pp. 109-124, Nov 12 1987.

[45] H. D. Merchant, "Annealing Kinetics and Embrittlement of Electrodeposited Copper," *Journal of Electronic Materials,* vol. 22, pp. 631-638, Jun 1993.

[46] Y. Xiang, T. Y. Tsui, and J. J. Vlassak, "The mechanical properties of freestanding electroplated Cu thin films," *Journal of Materials Research,* vol. 21, pp. 1607-1618, Jun 2006.

[47] F. J. Humphreys and M. Hatherly, *Recrystallization and Related Annealing Phenomena*, Second ed.: Elsevier, 2004.

[48] B. J., "Manufacture characterization and application of cellular metals and metal foams.," *Prog Mater Sci,* pp. 46-559, 2001.

[49] K. Lord, "On the Division of Space with Minimum Partitional Area," *Philosophical Magazine,* vol. 24, p. 503, 1887.

[50] D. Weaire and R. Phelan, "A Counter-example to Kelvin's Conjecture on Minimal Surfaces," *Philosophical Magazine Letters,* vol. 69, pp. 107-110, 1994.

[51] A. M. Kraynik, "The Structure of Random Foam," *Advanced Engineering Materials,* vol. 8, pp. 900-906, 2006.

[52] V. S. Deshpande and N. A. Fleck, "Isotropic constitutive models for metallic foams," *Journal of the Mechanics and Physics of Solids,* vol. 48, pp. 1253-1283, Jun-Jul 2000.

[53] H. X. Zhu, J. F. Knott, and N. J. Mills, "Analysis of the elastic properties of open-cell foams with tetrakaidecahedral cells," *Journal of the Mechanics and Physics of Solids,* vol. 45, pp. 319-343, 1997.

[54] A. Jung, h. Natter, and R. Hempelmann, "Nanocrystalline alumina dispersed in nanocrystalline nickel: enhanced mechanical properties," *Journal of Material Science,* vol. 44, pp. 2725-2735, 2009.

[55] C. A. Harper, *Electronic Materials and Processes Handbook*: McGraw Hill Professional, 2003.

[56] E. Rosemary Gene and I. Aaron, "Faraday's Electrochemical Laws and the Determination of Equivalent Weights," *Journal of Chemical Education,* vol. 31, pp. 226-232, 1954.

[57] K. S. Kumar, S. Suresh, M. F. Chisholm, J. A. Horton, and P. Wang, "Deformation of electrodeposited nanocrystalline nickel," *Acta Materialia,* vol. 51, pp. 387-405, 2003.

[58] J. F. Shackelford, *Introduction to materials science for engineers*: Prentice Hall, 2008.

[59] S. Nakahara, "Direct Observations of Inclusions in Electrodeposited Films by Transmission Electron Microscopy," *Journal of Electrochemical Society,* vol. 129, p. 201C, 1982.

[60] D. J.W. and H. R. Johnson, "Influence of Carbon on the Properties of Sulfamate Nickel Electrodeposits," *Surface Technology,* vol. 4, p. 217, 1976.

[61] R. R. Vandervoort, E. L. Raymond, H. J. Wiesner, and W. P. Frey, "Strengthening of Electrodeposited Lead and Lead Alloys, II-Mechanical Properties," *Plating,* vol. 7, p. 362, 1970.

[62] N. J. Petch, "The Cleavage Strength of Polycrystals," *Journal of the Iron and Steel Institute,* vol. 174, pp. 25-28, 1953.

[63] E. O. Hall, "The deformation and ageing of mild steel: III Discussion of Results," *Proceedings of the Physical Society. Section B,* vol. 64, pp. 747-753, 1951.

[64] M. Paunovic and M. Schlesinger, *Fundamentals of Electrochemical Deposition*, Second ed.: Wiley - Interscience, 2006.

[65] M. Klein, A. Hadrboletz, B. Weiss, and G. Khatibi, "The 'size effect' on the stress-strain, fatigue and fracture properties of thin metallic foils," *Materials Science and Engineering A,* vol. 319, pp. 924-928, Dec 2001.

[66] S. Zhang, M. Sakane, T. Nagasawa, and K. Kobayashi, "Mechanical Properties of Copper Thin Films Used in Electronic Devices," *Procedia Engineering,* vol. 10, pp. 1497-1502, 2011.

[67] Y. W. Cheng, D. T. Read, J. D. McColskey, and J. E. Wright, "A tensile-testing technique for micrometer-sized free-standing thin films," *Thin Solid Films,* vol. 484, pp. 426-432, Jul 22 2005.

[68] D. S. Gianola, S. Van Petegem, M. Legros, S. Brandstetter, H. Van Swygenhoven, and K. J. Hemker, "Stress-assisted discontinuous grain growth and its effect on the deformation behavior of nanocrystalline aluminum thin films," *Acta Materialia,* vol. 54, pp. 2253-2263, May 2006.

[69] D. E. Sherlin and L. K. Bjelland, "Relationship of Corner Cracking in Multilayer Board Holes to Pyrophosphate Copper Plate," *Circuit World,* vol. 4, p. 22, 1977.

[70] M. Laroussi, K. Sab, and A. Alaoui, "Foam mechanics: nonlinear response of an elastic 3D-periodic microstructure," *International journal of solids and structures,* vol. 39, pp. 3599-3623, 2002.

[71] W. Y. Jang and S. Kyriakides, "On the crushing of aluminum open-cell foams: Part II analysis," *International journal of solids and structures,* vol. 46, pp. 635-650, Feb 2009.

[72] S. Gaitanaros, S. Kyriakides, and A. M. Kraynik, "On the crushing response of random open-cell foams," *International journal of solids and structures,* vol. 49, pp. 2733-2743, 2012.

[73] A. M. Kraynik, *Microrheology of Random Soap Foams*: University of Wisconsin--Madison, College of Engineering, Rheology Research Center, 2001.

[74] S. M. Allameh, J. Lou, F. Kavishe, T. Buchheit, and W. O. Soboyejo, "An investigation of fatigue in LIGA Ni MEMS thin films," *Materials Science and Engineering a-Structural Materials Properties Microstructure and Processing,* vol. 371, pp. 256-266, Apr 25 2004.

[75] M. A. Meyers, *Dynamic Behavior of Materials*: John Wiley & Sons, 1994.

[76] A. Hassani, A. Habibolahzadeh, and H. Bafti, "Production of graded aluminum foams via powder space holder technique," *Materials & Design,* vol. 40, pp. 510-515, 2012.

[77] M. S. Kirugulige, R. Kitey, and H. V. Tippur, "Dynamic fracture behavior of model sandwich structures with functionally graded core: a feasibility study," *Composites Science and Technology,* vol. 65, pp. 1052-1068, 2005.

[78] J. Zhou, Z. W. Guan, and W. J. Cantwell, "The impact response of graded foam sandwich structures," *Composite Structures,* vol. 97, pp. 370-377, Mar 2013.

[79] H. B. Zeng, S. Pattofatto, H. Zhao, Y. Girard, and V. Fascio, "Perforation of sandwich plates with graded hollow sphere cores under impact loading," *International journal of impact engineering,* vol. 37, pp. 1083-1091, 2010.

[80] J. Zhou, Z. Gao, S. Allameh, E. Akpan, A. M. Cuitino, and W. O. Soboyejo, "Multiscale deformation of open cell aluminum foams," *Mechanics of advanced materials and structures,* vol. 12, pp. 201-216, May-Jun 2005.

[81] "Abaqus Documentation 6.11," ed: Dassault Systemes Simulia Corp, 2011.

[82] N. J. Mills, "The high strain mechanical response of the wet Kelvin model for open-cell foams," *International journal of solids and structures,* vol. 44, pp. 51-65, 2006.

[83] Y. Takahashi, D. Okumura, and N. Ohno, "Yield and buckling behavior of Kelvin open-cell foams subjected to uniaxial compression," *International journal of mechanical sciences,* vol. 52, pp. 377-385, Feb 2010.

[84] R. Harb, E. Taciroglu, and N. Ghoniem, "Partitioning of elastic energy in open-cell foams under finite deformations," *Acta Materialia,* vol. 61, pp. 1454-1468, 2013.

[85] J. L. Grenestedt, "Influence of cell shape variations on elastic stiffness of closed cell cellular slids," *Scripta Materialia,* vol. 40, pp. 71-77, 1999.

[86] H. S. Cho, K. J. Hemker, K. Lian, J. Goettert, and G. Dirras, "Measured mechanical properties of LIGA Ni structures," *Sensors and Actuators a-Physical,* vol. 103, pp. 59-63, Jan 15 2003.

[87] A. A. Volinsky, J. Vella, I. S. Adhihetty, V. Sarihan, L. Mercado, B. H. Yeung, and W. W. Gerberich, "Microstructure and mechanical properties of electroplated Cu thin films," *Materials Research Society Symposium,* vol. 649, 2001.

[88] Y. Sun, R. Burgueno, W. Wang, and I. Lee, "Modeling and Simulation of the Quasi-static Compressive Behavior of Al/Cu Hybrid Open-cell Foams," *international journal of solids and structures,* In Review.

[89] M. T. Perez-Prado and J. J. Vlassak, "Microstructural Evolution in Electroplated Cu Thin Films," *Scripta Materialia,* vol. 47, pp. 817-823, 2002.

[90] G. K. Williamson and W. H. Hall, "X-ray line broadening from filed aluminium and wolfram," *Acta Metallurgica,* vol. 1, pp. 22-31, 1953.

[91] H. E. Swanson, *Standard x-ray diffraction powder patterns.* vol. 1: Washington, DC : U.S. Dept. of Commerce, National Bureau of Standards, 1953.

[92] Y. Sun, R. Burgueño, A. Vanderklok, and S. A. Tekalur, "Compressive Behavior of Aluminum/Copper Hybrid Foams under High Strain Rate Loading," *Materials science & engineering A,* In Review.

[93] H. G. Jiang, J. Y. Dai, H. Y. Tong, B. Z. Ding, Q. H. Song, and Z. Q. Hu, "Interfacial reactions on annealing Cu/Al multilayer thin films," *Jounral of Applied Physics,* vol. 74, 1993.

[94] M. Braunovic and N. Alexandrov, "Intermetallic Compounds at Aluminum-to-Copper Electrical Interfaces: Effect of Temperature and Electric Current," *IEEE Transactions on Componentds, Packaging, and Manufacturing Technology - Part A,* vol. 17, pp. 78-85, 1994.

[95] M. Abbasi, A. K. Taheri, and M. T. Salehi, "Growth rate of intermetallic compounds in Al/Cu bimetal produced by cold roll welding process," *Journal of Alloys and Compounds,* vol. 319, pp. 233-241, 2001.

[96] H.-J. Kim, J. Y. Lee, K.-W. Paik, K.-W. Koh, J. Won, S. Choe, J. Lee, J.-T. Moon, and Y.-J. Park, "Effects of Cu/Al Intermetallic Compound (IMC) on Copper Wire and Aluminum Pad Bondability," *IEEE Transactions on Componentds, Packaging, and Manufacturing Technology,* vol. 26, pp. 367-374, 2003.

[97] W.-B. Lee, K.-S. Bang, and S.-B. Jung, "Effects of intermetallic compound on the electrical and mechanical properties of friction welded Cu/Al bimetallic joints during annealing," *Jounral of Alloys and Compounds,* vol. 390, pp. 212-219, 2005.

[98] C.-Y. Chen, H.-L. Chen, and W.-S. Hwang, "Influence of Interfacial Structure Development on the Fracture Mechanism and Bond Strenght of Aluminum/Copper Bimetal Plate," *Materials Transactions,* vol. 47, pp. 1232-1239, 2006.

[99] P. Xue, B. L. Xiao, D. R. DNi, and Z. Y. Ma, "Enhanced mechanical properties of friction stir welded dissimilar Al-Cu joint by intermetallic compounds," *Materials science & engineering A,* vol. 527, pp. 5723-5727, 2010.

[100] L. y. Sheng, F. Yang, T. F. Xi, C. CLai, and H. Q. Ye, "Influence of heat treatment on interface of Cu/Al bimetal composite fabricated by cold rolling," *Composites: Part B,* vol. 42, pp. 1468-1473, 2011.

[101] A. International, *ASM handbook*. Materials Park, Ohio: ASM International, 1990.

[102] J. Zhang, N. Kikuchi, V. Li, A. Yee, and G. Nusholtz, "Constitutive modeling of polymeric foam material subjected to dynamic crash loading," *International journal of impact engineering,* vol. 21, pp. 369-386, 1998.

[103] M. W. Schraad and F. H. Harlow, "A stochastic constitutive model for disordered cellular materials: Finite-strain uni-axial compression," *International journal of solids and structures,* vol. 43, pp. 3542-3568, 2006.

[104] Park R and P. T., *Reinforced concrete structures*: John Wiley & Sons, 1975.

[105] H. E.B., *Atlas of Stress-Strain Curves.*: ISM International, Metals Park, OH, 2000.

[106] W. Chen, F. Lu, D. J. Frew, and M. J. Forrestal, "Dynamic compression testing of soft materials," *Journal of Applied Mechanics,* vol. 69, pp. 214-223, May 2002.

[107] U. S. Lindholm, "Some Experiments with the Split Hopkinson Pressure Bar," *Journal of the Mechanics and Physics of Solids,* vol. 12, pp. 317-335, 1964.

[108] O. Sigmund, "A 99 line topology optimization code written in Matlab," *Structural and Multidisciplinary Optimization,* vol. 21, pp. 120-127, 2001.

[109] "MATLAB Documentation," vol. 2010, ed. Matick, Massachusetss: Math Works, 2011.

[110] E. N. Ohlsson, "Tailored Stress Wave Propagation and Topology Optimization of Composite Metal Foams," M.S., Michigan State University, 2012.

[111] A. Jung, H. Natter, R. Hempelmann, and E. Lach, "Metal Foams," US Patent, 2010.

[112] V. Kouznetsova, W. A. M. Brekelmans, and F. P. T. Baaijens, "An approach to micro-macro modeling of heterogeneous materials," *Computational Mechanics,* vol. 27, pp. 37-48, 2001.

[113] R. J. M. Smit, W. A. M. Brekelmans, and H. E. H. Meijer, "Prediction of the mechanical behavior of nonlinear heterogeneous systems by multi-level finite element modeling," *Computer methods in applied mechanics and engineering,* vol. 155, pp. 181-192, Mar 16 1998.

[114] R. G. Breuls, B. G. Sengers, C. W. Oomens, C. V. Bouten, and F. P. Baaijens, "Predicting local cell deformations in engineered tissue constructs: a multilevel finite element approach," *J Biomech Eng,* vol. 124, pp. 198-207, Apr 2002.

[115] O. van der Sluis, P. J. G. Schreurs, W. A. M. Brekelmans, and H. E. H. Meijer, "Overall behaviour of heterogeneous elastoviscoplastic materials: effect of microstructural modelling," *Mechanics of Materials,* vol. 32, pp. 449-462, Aug 2000.

[116] E. W. C. Coenen, V. G. Kouznetsova, E. Bosco, and M. G. D. Geers, "A multi-scale approach to bridge microscale damage and macroscale failure: a nested computational homogenization-localization framework," *International Journal of Fracture,* vol. 178, pp. 157-178, 2012/11/01 2012.

[117] V. G. Kouznetsova, M. G. D. Geers, and W. A. M. Brekelmans, "Multi-scale second-order computational homogenization of multi-phase materials: a nested finite element solution strategy," *Computer methods in applied mechanics and engineering,* vol. 193, pp. 5525-5550, 2004.